Spine development and activity-dependent plasticity in the hippocampus of a mouse model of the fragile X syndrome

Von der Fakultät für Lebenswissenschaften

der Technischen Universität Carolo-Wilhelmina zu Braunschweig

zur Erlangung des Grades

einer Doktorin der Naturwissenschaften

(Dr. rer. nat.)

genehmigte

D i s s e r t a t i o n

von Franziska Scharkowski
aus Beckendorf-Neindorf

1. Referent: Professor Dr. Martin Korte
2. Referent: Professor Dr. Reinhard Köster
eingereicht am: 12.10.2016
mündliche Prüfung (Disputation) am: 08.12.2016

Druckjahr 2016

Vorveröffentlichungen der Dissertation

Teilergebnisse aus dieser Arbeit wurden mit Genehmigung der Fakultät für Lebenswissenschaften, vertreten durch den Mentor der Arbeit, in den folgenden Beiträgen vorab veröffentlicht:

Publikationen

Michaelsen-Preusse K., Zessin S., Grigoryan G., Scharkowski F., Feuge J., Remus A., Korte M. (2016): Neuronal profilins in health and disease: Relevance for spine plasticity and Fragile X syndrome. *Proceedings of the National Acadamy of Science of the United States of America 113:33365-3370.*

Tagungsbeiträge

Scharkowski F., Michaelsen-Preusse K.; Rostosky C., Herrmann U., Rottner K., Korte M.: The actin-binding protein Cortactin in processes of neuronal plasticity and memory formation, *9th FENS Forum of Neuroscience, Mailand (2014)*

Scharkowski F., Korte M., Michaelsen-Preusse K.: Crucial function of FMRP in the development of the hippocampal mossy fiber pathway, *11th Meeting of the German Neuroscience Society, Göttingen (2015)*

Scharkowski F., Korte M., Michaelsen-Preusse K.: Altered connectivity and synapse maturation of the hippocampal mossy fiber pathway in the fragile X syndrome, *EMBO Conference – Imaging the Brain, Warsaw (2016)*

Scharkowski F., Frotscher M., Korte M., Michaelsen-Preusse K.: Altered connectivity and synapse maturation of the hippocampal mossy fiber pathway in the fragile X syndrome, *10th FENS Forum of Neuroscience, Copenhagen (2016)*

Du gegen mein Verlorengehn'
Deine Lässigkeit lässt mein 'Kaputt' alt aussehen

Du jubelst Orkane in den dichten Staub
Trittst Türen ein, reißt Fenster auf

(‚Dein Hurra' – BOSSE)

Weil ihr genau das für mich seid. Danke Mama, Papa, Opa und Steffen.

Table of Contents

Zusammenfassung

Der Gyrus Dentatus (DG) ist der Hauptinformationszugang in den Hippocampus und daher entscheidend beteiligt an der Gedächtnisbildung. Die Körnerzellen des DG bilden spezialisierte Moosfaser-Endigungen, welche hochkomplexe postsynaptische Fortsätze an CA3 Pyramidalneuronen kontaktieren, die sogenannten *Thorny excrescences* (TEs). Das *fragile X mental retardation protein* (FMRP), ein RNA-bindendes Protein, ist angereichert im Hippocampus und hier insbesondere durch sognannten *fragile x syndrome granules* (FXG) im *stratum lucidum*, in dem die Mossy fiber-TE Synapse gebildet wird. Die Lokalisation und Funktion von FMRP deutet dabei auf seine wichtige Rolle in der Proteinsynthese in diesen Strukturen hin. Diese ist jedoch besonders in der Entwicklung und Funktionalität des Moosfasersignalweges weitgehend unbekannt.

In dieser Arbeit wurde der Einfluss von FMRP auf prä- und postsynaptische Strukturen im Hippocampus untersucht, wobei ein besonderer Fokus auf die Moosfaser-TE Synapse gelegt wurde. Hierzu wurden *fmr1* Knockout-Mäuse verwendet. Die Ergebnisse zeigen, dass es in *fmr1* KO Tieren abhängig vom Entwicklungszeitpunkt und von der Subregion innerhalb von CA3 zu einer Veränderung der Morphologie der TEs kommt, zusammen mit einem abnormalen Verhalten im *marble burying* Test. Zusätzlich konnte gezeigt werden, dass TEs in *fmr1* KO Tieren frühreif und verstärkt mit Körnerzellen des DG verbunden sind, während die Moosfaserenden eine verkleinerte Fläche aufweisen. Darüber hinaus weisen, dendritische *spines* im *stratum radiatum* eine unreife Struktur auf. In Kombination wirkt sich dies vermutlich besonders nachteilig auf die Informationsverarbeitung der CA3 Neurone aus. In weiteren Experimenten konnte zusätzlich gezeigt werden, dass die Aktivitäts-abhängige strukturelle Plastizität in CA1 Neuronen gestört ist. Dieser Phänotyp wurde von einer veränderten Gedächtnisbildung im *Morris water maze* Test begleitet.

Zusammenfassend wurde eine entscheidende Rolle von FMRP in der streng regulierten Entwicklung von neuronalen Verbindungen festgestellt. Daher könnten Fehlregulierungen, besonders in der Entwicklung des DG-CA3 Signalweges und in der Aktivitäts-abhängigen strukturellen Plastizität, entscheidend zu einigen der markanten Symptome des fragilen X Syndroms, wie etwa kognitiven Defiziten und stereotypem Verhalten, beitragen.

Abstract

The dentate gyrus (DG) is the main input region into the hippocampus and therefore crucial for processes of memory formation. Granule cells of the DG form specialized large mossy fiber terminals (LMT) which contact highly complex postsynaptic protrusions – so called thorny excrescences (TE) - on CA3 pyramidal neurons in the *stratum lucidum*. The RNA-binding protein fragile X mental retardation protein (FMRP) is enriched in the hippocampus and especially via fragile x syndrome granules (FXG) in the *stratum lucidum*, the area of mossy fiber-TE synapse formation. This is indicating the crucial importance of protein synthesis for these structures. The role of FMRP for development and function of the mossy fiber pathway remains elusive.

In this thesis, the influence of FMRP on the pre- and post-synaptic structures throughout the hippocampus were investigated with focusing on the LMT/ TE synapse by taking advantage of a *fmr1* knockout mouse model. The results indicate that indeed, along with an increased activity in the marble burying task TEs display an exaggerated phenotype in a subregion and age-dependent manner in *fmr1* knockout animals compared to WT littermates. Furthermore, the findings point towards a critical period of thorny excrescence morphogenesis that is affected in the course of the fragile X syndrome. Additionally, TEs in *fmr1* knockout animals are premature and hyperconnected to DG granule cells, while LMTs are decreased in size. Although the TEs, the synaptic structure located in the *stratum lucidum* displays a premature phenotype, dendritic spines of CA3 neurons in the *stratum radiatum* show an immature spine morphology, a fact most likely detrimental for information processing in CA3 pyramidal neurons. Moreover, activity-dependent structural plasticity was found to be impaired in spines of *fmr1* KO CA1 neurons accompanied by altered memory consolidation in the Morris water maze paradigm.

Taken together the results suggest a crucial role of FMRP for the tightly balanced development of neuronal connections. Therefore, dysregulation especially during early development of the DG-CA3 mossy fiber pathway together with altered activity-dependent structural plasticity in CA1 could indeed represent key features responsible for prominent symptoms of FXS as compromised hippocampal network function, as well as behavioral and cognitive deficits.

1. Introduction

1.1 The fragile X syndrome – From one gene to cognitive dysfunction

‘Simon is weird and wonderful. He’s friendly and curious and talks non-stop. He often repeats sentences. When his mom reprimands him for something, he’ll say, ‘Well I have Fragile X.’ His next sentence is often, ‘I want to get rid of it’. He would like to drive but understands that he needs to learn to read first. ‘That’s too hard,’ he says’. This description of a fragile X syndrome (FXS) patient, provided by FRAXA, displays some of the common cognitive deficits of the disorder. Together with its high prevalence of 1 man affected out of 2500 (Hagerman and Hagerman, 2002), the reason why FXS is such an extensively investigated neurological disorder is to find treatments that can help the patients to live an independent life.

As partially described by Simon, patients with FXS can display autism-like behavior, a drastically reduced IQ, problems with working and short-term memory, hyperactivity and hypersensitivity (Melinda B. Kemper, 1988; Merenstein et al., 1996; Tsiouris and Brown, 2004). In comparison to many other genetic or chromosomal syndromes FXS patients have none or only mild physical characteristics as a long, narrow face and enlarged ear size. Most males develop macroorchidism which is an enlargement of the testes (Tsiouris and Brown, 2004). Due to these phenotypes and its X chromosome linked heredity the disease could be classified in 1943 (Martin and Bell, 1943). Since then, studies found FXS to be the most common monogenetic inherited form of mental retardation (Hagerman and Hagerman, 2002). It took almost 50 years until the origin could be found which is an expansion of a CGG repeat that is located in the 5’ untranslated region of exon 1 on the X chromosomal *fmr1* gene (Verkerk et al., 1991). Healthy individuals harbor 5-50 CGG repeats which are stably transmitted to the offspring while in some cases the CGG repeats can become unstable and get extended. The latter can cause a full mutation with more than 200 repeats which causes a hypermethylation of the entire *fmr1* CpG island, so that the gene product the fragile X mental retardation protein (FMRP) cannot be expressed (Bagni and Oostra, 2013).

1.2 The fragile X mental retardation protein

The dramatic consequences of the lack of the fragile X mental retardation protein (FMRP) point to its important role, especially in cognitive functions. Indeed, FMRP is

predominantly expressed in testes and brain, in the latter especially in hippocampus and cerebellum (Devys et al., 1993; Christie et al., 2009). The structure of FMRP reveals four RNA-binding motifs which includes two heterogeneous nuclear ribonucleoprotein K homology (KH) domains and one RGG box *in vitro* (figure 1 A; Ashley et al., 1993; Siomi et al., 1993). The functionality of the RNA-binding capacity could be illustrated by a severe phenotype of a FXS patient with a point-mutation in the second KH domain resulting in reduced RNA-binding (De Boulle et al., 1993; Siomi et al., 1994; Verhelj et al., 1995). Besides that, FMRP could be shown to associate with the ribosomal 60S subunit of free and membrane-bound ribosomes via RNA (Eberhart et al., 1996; Khandjian et al., 1996; Siomi et al., 1996; Tamanini et al., 1996; Willemsen et al., 1996). Supporting these findings, it could be shown that a missense mutation in the 2nd RNA binding domain (I304N) prevents FMRP polyribosome association which led to a FXS phenotype in mice and humans (De Boulle et al., 1993; Feng et al., 1997a; Zang et al., 2009). Moreover, I304N mice were documented to have a number of defects in synaptic plasticity (Zang et al., 2009). Indeed, FMRP was found to interact with approximately 4% of mRNA in the mouse brain transcriptome (Ashley et al., 1993; Darnell et al., 2011).

The FMRP structure also includes a nucleolus location signal as well as a nuclear export signal (Derek E. Eberhart, 1996; Fridell et al., 1996; Liu et al., 1996). Taken all together (figure 1 A), FMRP is able to regulate mRNA translation as well as transport and stability (Bassell and Warren, 2008; De Rubeis and Bagni, 2010; Bagni et al., 2012). As it can be expected many mRNAs that are targeted by FMRP are linked to neurological disorders that can be correlated to aspects of the FXS phenotypes. The mRNAs are translated into proteins that are essential for neuronal function as proteins involved in synaptic activity, cell adhesion and the regulation of the cytoskeleton (Pasciuto and Bagni, 2014). This suggests that the dysregulation of these mRNAs is responsible for the neurological phenotypes found in FXS.

Especially some characteristics can be correlated to malfunction of hippocampal circuits, since pattern separation and completion are impaired leading to stereotypic behavior and excessive adherence to patterns in patients (Cohen et al., 1988; Hernandez et al., 2009). In fact, FMRP is predominantly expressed in the hippocampus, a structure which is essential for learning processes and memory formation (Scoville and Milner, 1957; O'keefe and Nadel, 1978). In neurons, FMRP is found in the cell body, dendrites and at the base of dendritic spines (Feng et al., 1997b; Antar et al., 2004; Ferrari et al., 2007), as well as in growth cones and mature axons (Antar et al., 2006).

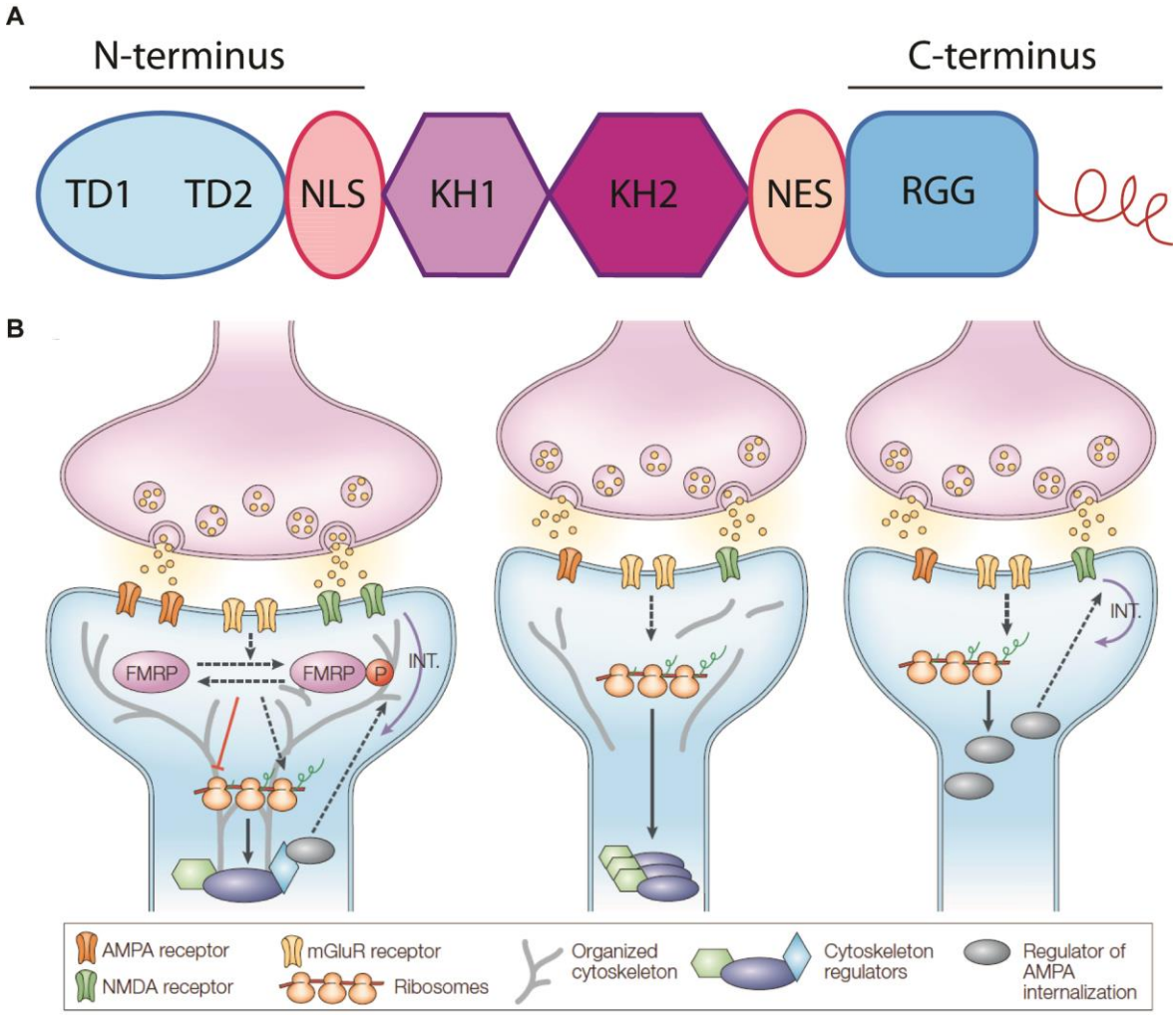

Figure 1: FMRP structure and function at neuronal synapses (**A**) Scheme of the fragile X mental retardation protein. The structure displays two tudor domains (TD1 & TD2), nuclear localization signal (NLS), two K homology domains (KH1 & KH2), one nuclear export signal and a RGG box (Bagni and Oostra, 2013). (**B**) Model of FMRP function in synapses displaying in the left a wildtype spine. FMRP negatively regulates the translation of proteins that are involved in long-term depression & remodeling of the actin cytoskeleton. FMRP is phosphorylated & is therefore releasing specific mRNAs. The middle panel displays a spine of a patient or mouse of the FXS. The absence of FMRP causes altered expression of proteins that are regulators of the actin cytoskeleton. As a consequence spine structure is changed in the FXS. The right panel shows the hypothesis that the deletion of FMRP causes the internalization of AMPA receptors and NMDA receptors leading to the weakening of the synapse (Bagni and Greenough, 2005).

Thereby, FMRP is concentrated in both large messenger ribonucleoprotein particles (mRNPs) and in fragile X granules (FXG). MRNPs contain numerous protein partners, specific mRNAs and non-coding RNAs. It is suggested that mRNPs are translationally silent since they travel from the soma to synapses along dendrites. FMRP-containing mRNPs are composed dynamically, so interacting proteins undergo a series of rearrangements (Bagni and Greenough, 2005). Therefore, reaching the synapse the FMRP granules release the containing mRNAs that are able to be translated (Bramham, 2008;

Costa-Mattioli et al., 2009). Just recently a study could show that FMRP is not only repressing but also might promote the translation of distinct mRNAs, as it could be found for profilin1, an important actin-binding protein (Michaelsen-Preusse et al., 2016). While mRNPs appear mainly on the post-synaptic site, FXG are located pre-synaptically. FXG are endogenous structures that contain fragile X proteins which include FMRP and its homologs FXR1P and FXS2P. Their localization in axons and presynaptic compartments is highly dependent on the developmental time point (Christie et al., 2009; Akins et al., 2012). Interestingly, FXGs are predominantly found in mossy fiber projections and terminals while they are absent in Schaffer collaterals (Akins et al., 2012). It is interesting to note that both pathways are responsible for different functions of the hippocampus. While the dentate gyrus (DG) granule cells and their connection to CA3 pyramidal neurons could be shown to be essential for pattern separation and completion (Kesner et al., 2000; Bakker et al., 2008), the Schaffer collaterals formed between CA3 and CA1 pyramidal neurons (figure 2 A) are curtail for the formation of a spatial map as it is needed in the Morris water maze paradigm (Aou et al., 2003)

Since FMRP has important functions, it has to be tightly regulated as well. Throughout the last two decades the 'mGluR theory of fragile X mental retardation' was raised (Bear et al., 2004). Hebbian synaptic plasticity as long-term potentiation (LTP) and depression (LTD), represent cellular mechanisms for driving experience-dependent changes in synaptic circuits (Nicoll and Schmitz, 2005; Kessels and Malinow, 2009; Collingridge et al., 2010). The induction of LTP which is thought to be the molecular mechanism underlying learning and memory formation causes enlargement of spine heads (Matsuzaki et al., 2004; Holtmaat and Svoboda, 2009). The increased spine area goes along with an increase in synaptic receptors as the glutamate receptors N-methyl-D-aspartate receptors (NMDARs) and α-amino-3-hydroxy-5-methyl-4-isoxazolepropionic acid receptors (AMPARs) which leads to a strengthening of the synapse (Park et al., 2004; Park et al., 2006). It is suggested that changes in dendritic spine morphology are crucial for memory formation and learning processes (Yuste and Bonhoeffer, 2001; Kasai et al., 2003; Hotulainen et al., 2009). LTD mechanisms seem to be essential for activity guided synapse elimination, to prevent information over-storage in the brain (Bear, 1998). There exist two types of LTD. 1st NMDA receptor dependent LTD which is in the early phase protein-synthesis independent (Huber et al., 2000; Sajikumar and Frey, 2003). 2nd metabotropic glutamate receptor (mGluR) dependent LTD which requires rapid translation of preexisting mRNAs in postsynaptic dendritic compartments (Huber et al., 2000). In hippocampal CA1 pyramidal

neurons it is suggested that via the activation of mGluR5 by LTD a cascade is initialized that includes a G_q family of g-proteins, extracellular signal-regulated kinase (ERK) and mitogen-activated protein kinases (MAPK) (Huber et al., 2001; Kleppisch et al., 2001). Additionally, it could be shown that mGluR activation stimulates the synthesis of proteins that are involved in the stabilization of LTD and FMRP. It is suggested that FMRP is inhibiting further synthesis of these proteins which causes a break in LTD (Bear et al., 2004). This is supported by an enhanced mGluR dependent LTD in *fmr1* KO mice where FMRP is depleted, compared to wildtype (WT) littermates, while NMDA receptor dependent LTD is not altered (Huber et al., 2002). Additionally, in *fmr1* KO mice the exaggerated LTD is accompanied by a loss of NMDA receptors and AMPA receptors (Snyder et al., 2001). Together, this points to a weakening of synaptic strength in the hippocampus of FXS patients and the mouse model.

1.3 Synaptic phenotypes in patients and the mouse model of the fragile X syndrome

As described above, FXS patients display cognitive impairments. Surprisingly, the brains of individuals with FXS have a normal appearance at least in routine neuroimaging and gross inspection at autopsy. In fact, abnormalities in microscopic neuronal structures seem to be the reason for the neuropathology of the FXS. Dendritic spines were found to be altered in several brain regions of FXS patients. Especially pyramidal neurons are covered with dendritic spines which are membrane extensions that contain the postsynaptic site of most excitatory synapses. The basic spine structure is relatively conserved throughout several brain regions, including the hippocampus. A recent study revealed the importance of the structure, a thin neck and big head, for biochemical and electrical compartmentalization (Tonnesen et al., 2014, figure 2 C).

To study the cause of the FXS spine phenotype in greater detail and the functional consequences, mouse models were developed shortly after the genetic cause of the FXS was found in 1991. In the majority of studies a mouse model with a deletion of the *fmr1* gene was used and it shared several FXS phenotypes that could be found in patients as well (The-Dutch-Belgian-Fragile-X-Consortium, 1994). Investigating the physiology of FXS patients and the mouse model of FXS both showed no differences in general organ morphology in comparison to healthy individuals. In both human and mice the reduction or deletion of FMRP causes macroorchidism. Besides that, body functions as circadian

activity, feeding and mating were found to be comparable between *fmr1* KO mice and WT littermates. The investigation of locomotion capability as gait and swimming could not reveal differences between both genotypes in mice. In human patients body functions were found to be normal as well, or displayed only slight effects as clumsy gait und slight hypotonia (Rudelli et al., 1985; Wisniewski et al., 1985).

The most pronounced phenotypes of the disease are the cognitive disabilities which can be found in mice as well. Patients show deficits in visual short-term memory and visual-spatial learning (Cianchetti et al., 1991; Maes et al., 1994) which could be partially found in the mouse model as well, tested by the Morris water maze task. Here, *fmr1* KO mice displayed a less precise performance in the first trials and in the reversal experiment suggesting a reduced memory acquisition (The-Dutch-Belgian-Fragile-X-Consortium, 1994; D'Hooge et al., 1997; Paradee et al., 1999).

The FXS can also cause autistic like behavior which includes excessive adherence to patterns and impairments in the recognition of facial expression, pointing towards deficits in pattern separation and completion (Cohen et al., 1988; Merenstein et al., 1996; Tsiouris and Brown, 2004; Garber et al., 2008). The same impairments could be observed in mice lacking FMRP, displayed by increased repetitive behavior compared to WT littermates, tested by the marble burying task or analyzing grooming behavior (Pietropaolo et al., 2011; Spencer et al., 2011). Considering the cognitive deficits in both patients and the mouse model of FXS it is surprising that brain weight and the expansion of the brain regions are not altered in both. Several of the behavioral phenotypes found point towards an impairment in hippocampal function, a brain region that is extensively investigated in FXS. However, the gross architecture and morphology of the *cornu ammonis* (CA) region in the hippocampus was found to be normal (The-Dutch-Belgian-Fragile-X-Consortium, 1994).

The focus of FXS research was and still is put on dendritic spines along neurons. Therefore, fixed tissue from FXS patient autopsy was stained using the Golgi method which was used for mouse brain staining as well. Investigating the spine density of cortical layer 2/3 and 5 neurons in patients revealed an increased spine density, as well as in the FXS mouse model even during development (Comery et al., 1997; Irwin et al., 2001; Galvez and Greenough, 2005; McKinney et al., 2005; Su et al., 2011). Alterations in dendritic spine density in both FXS patients and the mouse model could deliver the first explanation for the cognitive deficits found, since it could be shown that an altered spine density results in altered neuronal connections which causes changes in the computational

power of the network (Yuste, 2010). Since altered spine number is a common defect in the cortex of both FXS patients and the mouse model of FXS, a failure in synaptic pruning due to the absence of stabilizing proteins by the deletion of FMRP is suggested by several studies (Irwin et al., 2000; Bagni and Greenough, 2005; He and Portera-Cailliau, 2013). Strikingly, more recent reports failed to detect differences in spine density using 2-photon imaging in the cortex of *fmr1* KO mice compared to Golgi stained tissue as it was performed in earlier studies of FXS patients and the mouse model of the FXS (Meredith et al., 2007; Ruan et al., 2009; Cruz-Martin et al., 2010; Harlow et al., 2010; Pan et al., 2010). Neurons of other brain regions as the olfactory bulb, amygdala and hippocampus displayed increased spine numbers as well (Antar et al., 2006; Grossman et al., 2006; Levenga et al., 2011; Qin et al., 2011; Scotto-Lomassese et al., 2011; Swanger et al., 2011). However, the findings about spine density in the hippocampus are controversial as well. Despite an increased spine density almost the same number of studies could reveal either no alterations (Pfeiffer and Huber, 2007; de Vrij et al., 2008; Levenga et al., 2011; Su et al., 2011), or even reduced spine numbers (Braun and Segal, 2000; Segal et al., 2003). This might be again explained by different staining and analyzing methods used.

Besides a possible alteration in the spine number an overabundance of long and thin dendritic spines was found in cortex layer 3-5 of patients and mice lacking FMRP (figure 1 B; Rudelli et al., 1985; Hinton et al., 1991; He and Portera-Cailliau, 2013). This kind of phenotype is normally displayed by dendritic spines during early development (Yuste and Bonhoeffer, 2001; Portera-Cailliau et al., 2003) which renders the FXS spine phenotype immature. This immature spine phenotype could be found throughout the cortex of mice lacking FMRP as well (Comery et al., 1997; Irwin et al., 2002; Meredith et al., 2007; He and Portera-Cailliau, 2013), while recent *in vivo* studies found no alterations in spine maturity (Cruz-Martin et al., 2010; Pan et al., 2010). A relatively immature spine phenotype could be found in pyramidal neurons and DG granule cells in the hippocampus as well (Antar et al., 2006; Grossman et al., 2006; de Vrij et al., 2008; Bilousova et al., 2009; Grossman et al., 2010). Interestingly, one study in *fmr1* KO mice could reveal an immature spine phenotype along CA1 pyramidal neurons while the dendritic spines of CA3 cells were found to be indistinguishable from WT littermates, pointing to a subregion specific function of FMRP (Levenga et al., 2011). The immaturity of dendritic spines is supported by an increased spine turn-over rate at pyramidal neurons of the cortex (Cruz-Martin et al., 2010), these rapid changes in size and morphology are characteristic during early brain development (Yuste and Bonhoeffer, 2001). The mossy fiber projections of

hippocampal DG granule cells are until now the only presynaptic compartments found to be altered in the mouse model of the FXS. A study could show that the infrapyramidal mossy fiber projection is decreased in size, while the intrapyramidal projection was not affected by the deletion of FMRP in adult mice, compared to WT littermates (Mineur et al., 2002). This shows that there are still several hippocampal synapses that are not studied in the aspect of a FMRP deletion. Most notably, the effect on the synapse crucial for pattern separation and completion (Gold and Kesner, 2005; Bakker et al., 2008) which are impaired in FXS patients and the mouse model of FXS characterized by excessive adherence to patterns and impairments in the recognition of facial expression (Cohen et al., 1988; Merenstein et al., 1996; Tsiouris and Brown, 2004; Garber et al., 2008) remains elusive.

1.4 Excurse: The Mossy fiber synapse

Both CA3 and CA2 excitatory neurons display in addition to regular spines big complex structures in the *stratum lucidum* (figure 2 A & C), the so called thorny excrescences (TE). However, TEs are more complex at CA3 pyramidal neurons. Ultrastructural studies revealed that TEs consist of a slender neck connecting from 1 to 16 bulbous-shaped heads to the dendritic shaft (Blackstad and Kjaerheim, 1961; Amaral and Dent, 1981). Most TEs aggregate in clusters which made it impossible to investigate them in greater detail by light microscopy (Represa et al., 1991; Buckmaster et al., 1993; Gonzales et al., 2001). It could be shown that each TE consists of multiple postsynaptic densities, rendering this synapse especially strong (Amaral and Dent, 1981; Chierzi et al., 2012). TEs are located close to the soma which enables them to drive the firing of CA3 neurons just by the activation of a few TEs (Siegel et al., 1992). This is supported by reports showing that depleting the activation of TEs results in a 80% decrease of synaptic activity (Nicoll and Schmitz, 2005).

Not only the postsynaptic site but also the presynaptic site of this synapse is morphologically unique in the mammalian brain. Large mossy fiber terminals (LMTs) of DG granule cells form the presynaptic site, in detail the boutons of LMTs (figure 2 C, mossy fiber synapse). The mossy fiber projection in CA3 could be shown to be lamellar with respect to the hippocampal long axis. Interestingly, it exhibits simple relationships with respect to the number of postsynaptic partners, since in most cases a single TE is contacted by only one mossy fiber bouton, while a single bouton can contact more than one TE (Chicurel and Harris, 1992; Acsády et al., 1998). Along one mossy fiber projection are

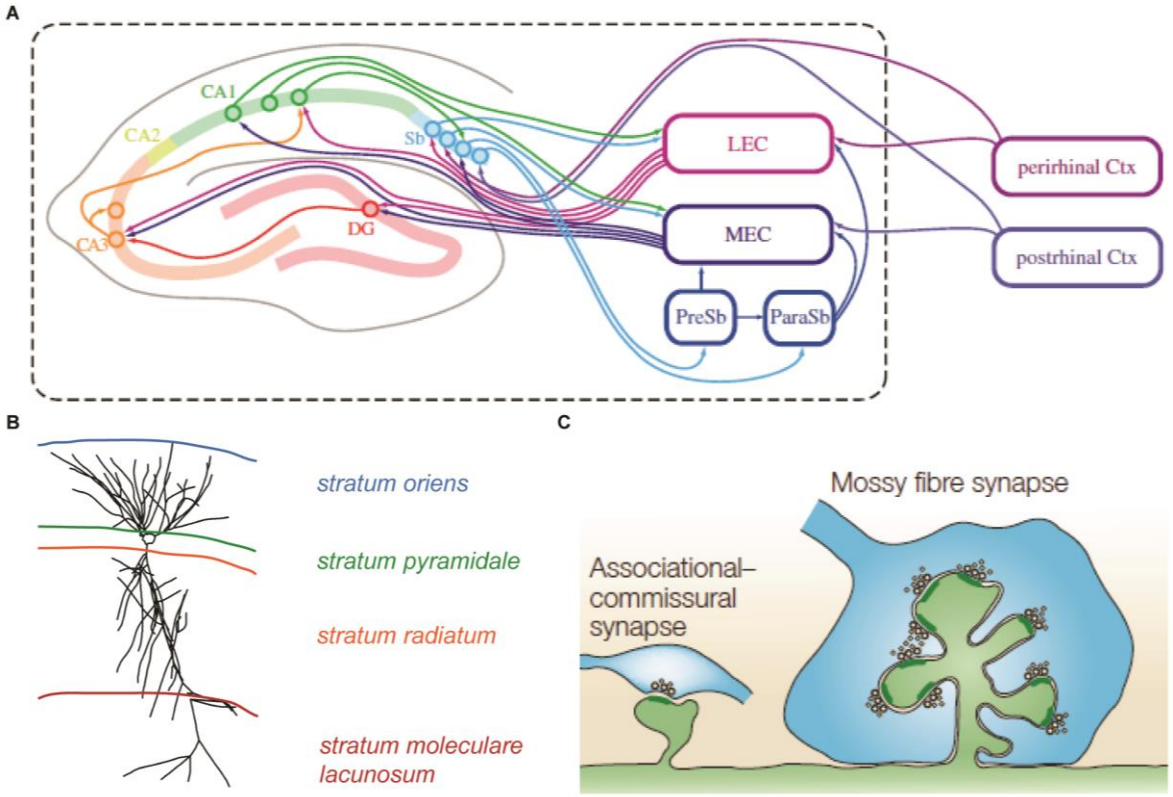

Figure 2: Hippocampal formation and synapse diversity (**A**) Schematic overview of major anatomical pathways in the hippocampal formation. Classic trisynaptic pathway with projections from entorhinal cortex (LEC: lateral entorhinal cortex; MEC medial entorhinal cortex) to dentate gyrus (DG) to CA3 and from CA3 to CA1. Also direct input of LEC & MEC to CA3, CA1 and subiculum (Sb) & parasubiculum (ParaSb). Arrows indicate direction of projection (Hartley et al., 2014). (**B**) A tracing of a CA1 pyramidal neuron showing basal dendrites in the *stratum oriens*, the cell body in *stratum pyramidale*, apical dendrites in the *stratum radiatum* and distal apical dendrites in the *stratum moleculare lacunosum*. (**C**) Schematic drawings of dendritic spines (associational-commissural synapse) and the mossy fiber synapse composed of a large mossy fiber terminal (blue) and a thorny excrescence (green) (Nicoll and Schmitz, 2005).

10-15 LMTs distributed in 80-150 µm intervals (Amaral and Dent, 1981) in which LMTs contact one CA3 pyramidal neuron (Henze et al., 2000). Together with the fact that TEs contain numerous synapses their proximity to the soma renders the synapse very powerful and a detonator directing the storage of information in the CA3 network (Urban et al., 2001).

Besides the core bouton LMTs display filopodia as well which could be shown to form connections with inhibitory interneurons (Acsády et al., 1998; Henze et al., 2002; Nicoll and Schmitz, 2005). These special morphological features allow LMT mediated excitation of CA3 pyramidal neurons firing at higher frequencies and on the other hand feed forward inhibition when firing at low frequencies (Geiger and Jonas, 2000; Henze et al., 2002; Lawrence and McBain, 2003; Mori et al., 2004).

As mentioned previously the stimuli responsive nature of regular dendritic spines is driven

by Hebbian synaptic plasticity. Besides this, homeostatic synaptic plasticity could be found as a mechanism that restrains neuronal activity within physiological boundaries (Turrigiano, 2008). Just recently a key role of the mossy fiber synapse in mediating homeostatic synaptic plasticity could be reported and was shown to be the main loci of homeostatic synaptic plasticity in mature hippocampal neurons (Lee et al., 2013). Behavioral phenotypes appearing in autism spectrum disorders (ASD), as hyperactivity and hypersensitivity, point towards an impaired homeostatic synaptic plasticity which therefore renders the mossy fiber synapse especially interesting in investigating these disorders.

1.5 Aim of study

The fragile X syndrome (FXS) is a developmental neurological disorder which can include autistic-like behavior and cognitive deficits. While the gross brain architecture is not altered in FXS patients as well as in the suitable mouse model an overabundance of immature spine morphology could be found which is thought to be correlated to the behavioral deficits.

The effects of an FMRP deletion on spine formation and potential functional consequences in different hippocampal subregions were investigated in this thesis. Specifically the following questions were addressed:

1st Does the deletion of FMRP have functional consequences on the mossy fiber synapse and is this accompanied by alterations in the formation of the presynaptic (large mossy fiber terminals) or postsynaptic (thorny excrescences) compartment?

2nd Can the developmental character of the FXS found as well in synapse formation and hippocampus dependent memory formation?

3rd What are the underlying mechanism of the investigated structural phenotypes found throughout the hippocampus? How are actin dynamics and their regulators altered in *fmr1* KO mice?

2. Materials and Methods

2.1 Reagents

Chemicals were obtained by AppliChem, Hoechst, Invitrogen, PAA, Roth, Sigma or Merk Millipore if not cited otherwise. Enzymes used were distributed by Fermentas or New England BioLaps.

2.2 Solution and Media

Lysogeny Broth (LB)-Medium

diluted Trypton	10 g/L
NaCl	10 g/L
Yeast extract	5 g/L
Agar	15 g/L
If needed:	
Ampicillin	100 µg/mL
Kanamycin	50 µg/mL

GBSS

$CaCl_2*2H_2O$	1.5 mM
KCl	5 mM
KH_2PO_4	0.22 mM
$MgCl*6H_2O$	1 mM
$MgSO_{4*}7H_2O$	0.28 mM
NaCl	137 mM
$NaHCO_3$	2.7 mM
NaH_2PO_4	0.86 mM
D-Glucose	5.5 mM

Dilute in dH_2O sterile filtrate (store at 4°C)

50 % Glucose solution

Glucose	50 g
H_2O	50 mL

Glucose in H_2O to dilute solution is heat up, directly sterile filtrated and aliquot (storage at -20°C).

Kynurenic acid solution

Kynurenic acid (Sigma)	946 mg
1 M NaOH	5 mL
dH_2O	45 mL

Kynuric acid is diluted in 1 M NaOH & dH_2O, sterile filtrated & stored at -20°C.

Solution for hippocampus preparation

GBSS	98 mL
Kynurenic acid	1 mL
50 % glucose solution	1 mL

pH 7,2 (adjusted 0,5 M HCl) & storage at 4°C.

artificial Cerebrospinal Fluid (aCSF)

$CaCl_2*2H_2O$	2.0 mM
KCl	2.5 mM
NaH_2PO_4	1.25 mM
NaCl	125.0 mM
$MgCl_{2*}6H_2O$	1.0 mM
$NaHCO_3$	26.0 mM
D-Glucose	25.0 mM

pH 7,3 adjusted by

Internal solution for whole cell patch clamp recordings

K-gluconate	126 mM
HEPES	10 mM
KCl	4 mM
MgATP	4 mM
Phosphocreatin Na^+	10 mM
Na GTP	0.3 mM
pH 7.3 – 290 mOsm	

Müller-Kultur-Medium (medium for organotypic hippocampal cultures)

BME medium (Invitrogen)	100 mL
HBSS (Invitrogen)	50 mL
Horse serum (Hyclone)	50 mL
L-Glutamin (200 mM, Sigma)	1 mL
50 % Glucose solution	2 mL
Storage at 4°C	

Mitosis inhibitor

Uridin (Sigma)	1 M
Cytosin-ß-D-Arabinofuranosid-Hydrochlorid	1 M
5-Fluoro-2‘-Deoxyuridin	1 M
Diluted in dH_2O, sterile filtrated and stored at -20°C.	

Hank’s balanced salt solution (HBSS)

10x HBSS (Gibco/life technologies)	50 ml
$NaHCO_3$	175 mg
$CaCl_2*2H_2O$	147 mg
Glucose	1351 mg
Filled up to 500 mL with H_2O (MilliQ)	

Phosphate buffer (PB, 0.2 M)

$NaH_2PO_4*2H_2O$	0.04 M

$Na_2HPO_4*2H_2O$	0.17 M

Diluted in dH_2O, pH 7.4

Phosphate buffered saline (PBS)

$KH_2PO_4*2H_2O$	1.5 mM
KCl	2.7 mM
NaCl	137 mM
$Na_2HPO_4*2H_2O$	10.4 mM

Diluted in dH_2O, pH 7.4

Lyses buffer

Tris/HCl (pH 8)	100 mM
EDTA	5 mM
NaCl	200 mM
SDS	0.2 %
Proteinase K	100 µg/mL

Diluted in dH_2O

4x SDS protein sample buffer

Tris/HCl (pH 7.6)	375 mM
Glycerol 87 %	12 %
Bromphenol blue	0.05 %
SDS	2.0 %
B-Mercaptoethanol	10 %

Diluted in dH_2O

Blocking solution for immunohistochemistry

Triton-X (2 %)	0.2 %
Goat serum	10 %
BSA	1 %

Diluted in PBS

Blocking solution for immunohistochemistry

Triton-X (2 %)	0.2 %
Goat serum	10 %
BSA	1 %
Diluted in PBS	

2.3 Mouse strains

All experiments performed were authorized by the animal welfare representative of the TU Braunschweig and the LAVES (Oldenburg, Germany, Az. §4 (02.05) TSchB TU BS). Animals were kept in standard conditioned cages, exposed to a 12 h dark/light cycle. *Fmr1* knockout mice in a FVB129 background (The-Dutch-Belgian-Fragile-X-Consortium, 1994) obtained from the Jackson laboratory (Strain number 004624) were used. The *fmr1* gene is located on the X chromosome; therefore $fmr1^{+/-}$ females and $fmr1^{y/-}$ males were bred to obtain offspring with both *fmr1* wild type (WT) and knockout (KO) genotype. Additionally, *fmr1* WT and KO mice in a Bl6 background were achieved upon several generation back crossing. The progeny and Thy-1 GFP line M (Feng et al., 2000) mice in a Bl6 background were bred, to obtain *fmr1* WT and KO mice that express the enhanced green fluorescent protein (EGFP) under the control of a modified Thy1 promotor. The genotype was determined by genotyping and tissue obtained by tail biopsy. Mice were used at different ages as mentioned in the respective result parts.

2.4 Genotyping of transgenic mice

Tissue obtained by tail biopsy was used for DNA isolation. A single tail tip was digested in 500 µL lysis buffer with freshly added proteinase K at 55°C over night, followed by 13.000 x g centrifugation at 4°C, to exclude cellular debris. The supernatant was transferred into 500 µL isopropanol, several times inverted and centrifuged at 13.000 x g at 4°C for 15 min. The supernatant was discarded and 1 mL ethanol was added for washing, followed by centrifugation at 13.000 x g at 4°C for 15 min. Afterwards, the supernatant was removed and the DNA-pellet dried and rehydrated with 50 µL Tris/HCl at 37°C for 1 h (afterwards stored at 4°C). The amplification of the alleles was performed according to distributor instructions, using suggested primer sequences (table 1) and PCR reactions (for *fmr1* table 2, for GFP table 3).

Table 1: Primer for genotyping

Primer	Target	Sequence (5' → 3')	Primer type
oIMR2060	*Fmr1* KO (400 bp)	TGT GAT AGA ACT AGT GAG ACG TG	Mutant forward
oIMR6734	*Fmr1 WT* (131 bp)	TGT GAT AGA ATA TGC AGC ATG TGA	Wild-type forward
oIMR6735	*Fmr1 WT* (131 bp)	CTT CTG GCA CCT CCA GCT T	common
G113	GFP	CGG TGG TGC AGA TGA ACT T	Transgene reverse
G114	GFP	ACA GAC ACA CAC CCA GGA CA	Transgene forward
oIMR7338		CTA GGC CAC AGA ATT GAA AGA TCT	Internal positive control forward
oIMR7339		GTA GGT GGA AAT TCT AGC ATC ATC C	Internal positive control reverse

Table 2: PCR reaction for *fmr1*

Component	Concentration	Temperature [°C]	Time
PCR buffer	10 mM	94	3 min
dNTPs	10 nM	94	30 s
Forward primer	100 nM	62	30 s
Reverse primer	100 nM	72	1 min
GoTaq polymerase	1 unit	72	2 min
DNA	1 µL	10	hold
		Steps 2-4 repeated 34 cycles	

Table 3: PCR reaction for GFP

Component	Concentration	Temperature [°C]	Time
5x Kapa 2G HS buffer	1 x	94	2 min
$MgCl_2$	2.00 mM	94	20 s
dNTP KAPA	0.20 mM	65	15 s
oIMR7338	0.50 µM	68	10 s
oIMR7339	0.50 µM	Steps 2-4 repeated 10 cycles	
G113	0.50 µM	94	15 s
G114	0.50 µM	60	15 s
Kapa 2G HS taq polymerase	0.01 U/µL	72	10 s
20x EvaGreen	1 x	72	2 min
DNA	2 µL	10	hold
Filled up with ddH_2O		Steps 5-7 repeated 28 cycles	

The amplified fragments were separated by gel electrophoresis using a 1.5 % agarose gel.

2.5 RNA immunoprecipitation

FMRP is a RNA binding protein. In this thesis the ability of FMRP to bind mRNAs of actin-binding proteins like profilin and cofilin was analyzed. Therefore, a RNA immunoprecipitation was performed by applying the MagnaRIP-Kit (Merk Millipore). The procedure was performed following the distributers instructions, except of some corrections that will be mentioned in the following. All solutions were included in the kit, exceptions are mentioned if otherwise.

2.5.1 Preparation of hippocampus lysate

To reveal the mRNA binding ability of FMRP to profilin1, profilin2a and cofilin1 in the hippocampus, first hippocampus lysate was produced. Therefore, 4 hippocampi of 2 *fmr1* WT mice were prepared (at least 0.1 g tissue). The hippocampi were transferred into ice-cold PBS and washed by 3 times transfer into fresh ice-cold PBS. A dounce homogenizer was used to apart the tissue until a single-cell suspension is obtained, followed by a

centrifugation at 1500 rpm for 5 min at 4°C. The supernatant was discarded and the pellet resuspended in 403 µL complete RIP lysis buffer (400 µL RIP lysis buffer, 2 µL protease inhibitor cocktail, 1 µL RNase inhibitor), afterwards the lysate was frozen by 200 µL each at -80°C.

2.5.2 Immunoprecipitation of Protein-mRNA complexes

The procedure relies on the usage of protein A/G magnetic beads that were resuspended and 50 µL of the suspension was transferred into an Eppendorf tube for one reaction. The beads were washed with 500 µL of RIP wash buffer, shortly vortexed and placed on a magnet separator. Afterwards, the supernatant was carefully removed and the washing procedure was repeated twice. 100 µL RIP wash buffer was added as well as 14 µL of anti-FMRP (MAB2160, Merk Millopore). Three more reaction tubes were needed for a protein positive control (16 µL, anti-SNRNP70), a negative control (17 µL, rabbit IgG) and a control to investigate unspecific binding (15 µL, mouse IgG). All 4 reaction tubes were incubated rotating for 30 min at RT, followed by a shortly centrifugation and placement on the magnet separator. The supernatant was removed and 500 µL of RIP wash buffer added, vortexed, centrifuged and the supernatant removed on the magnet separator. These washing steps were repeated one more time and the antibody coated beads stored in wash buffer on ice.

2.5.3 Purification of RNA

The reaction tubes containing the antibody coated beads were placed on the magnetic separator, the supernatant discarded and 900 µL RIP immunoprecipitation buffer (860 µL RIP wash buffer, 35 µL 0.5 M EDTA, 5 µL RNase inhibitor) was added to each. After the lysate was thaw quickly and centrifuged at 13.000 rpm for 10 min at 4°C, 100 µL of its supernatant was add to the antibody coated beads. The tubes were incubated rotating over night at 4°C, followed by a short centrifugation, placement on the magnet separator, removal of the supernatant and adding of 500 µL RIP wash buffer. These steps were repeated 8 times, to fully remove unspecific bound material. The immunoprecipitates were resuspended in 150 µL proteinase K buffer (117 µL RIP wash buffer, 15 µL 10% SDS, 18 µL proteinase K) and incubated at 55°C for 30 min shaking to digest the protein. Afterwards the suspension was briefly centrifuged, placed on a magnetic separator and the

supernatant was transferred into 250 µL RIP wash buffer. As a next step 400 µL of phenol-chloroform-isoamyl alcohol was added to each tube and vortexed for 15 s, followed by centrifugation at 13.000 rpm for 10 min at RT. 350 µL of the aqueous phase was removed and add to 400 µL of chloroform and again centrifuged. 300 µL of the aqueous phase was removed and add to 920 µL salt solution (50 µL salt solution I, 15 µL salt solution II, 5 µL precipitate enhancer, 850 µL absolute ethanol), mixed and kept at -80°C over night. The next day the precipitate was centrifuged at 13.000 rpm at 4°C for 30 min und the supernatant carefully discarded. The pellet was once washed with 80% ethanol, centrifuged, the supernatant discarded and after drying of the pellet resuspended in 20 µL RNase-free water.

2.5.4 Analysis of immunprecipitated RNA

To show whether FMRP binds one of the mRNAs of interest, a RT-PCR had to be applied. Therefore, 10 µL of RNA solution was added to 1 µL anchored Oligo$(dT)_{16}$ primer and 7.9 µL filtrated RNase free water. This reaction was incubated for 10 min at 65°C in a PCR cycler (PTC-200, MJ Research) and cooled down on ice. Afterwards the reaction was added to the transcriptase solution (table 4), mixed and placed in the PCR cycler for 30 min at 55°C, followed by 8 min at 85°C and afterwards cooled down on ice.

Table 4: RT-PCR reaction

Component	Amount [µL]
5x Transcriptor high fidelity RT reaction buffer	4
Protect RNase inhibitor (40 U/µL)	0.5
dNTP-Mix (10 mM)	2
DTT (100 mM)	1
Transcriptor high fidelity reverse transcriptase (20 U/µL)	1.1

The obtained cDNA from the RT-PCR reaction it was amplified by PCR (table 5). Primer were specially designed for profilin1, profilin2a, cofilin1 and arc (table 6). It was previously shown that arc mRNA is bound by FMRP (Zalfa et al., 2007) that is why it is serving as a positive control in this thesis.

Table 5: PCR reaction for cDNA amplification

Component	Concentration	Temperature [°C]	Time
PCR buffer 10x	2 µL	94	2 min
dNTPs	2 µL	94	30 s
Forward primer	1.8 µL (45 pmol)	52 (54 for pfn1 & pfn2a)	30 s
Reverse primer	1.8 µL (45 pmol)	72	45 s
Taq one polymerase	0.5 µL	72	3 min
cDNA	5 µL	10	hold
Filled up to 20 µL with H_20		Steps 2-4 repeated 35 cycles	

Table 6: Primer used for cDNA amplification

Primer	Target	Sequence (5' → 3')	Primer type
pCfl1-Exon34-F	Cofilin 1, in exon 3	TGC ACC CCT CAA GAG CAA AA	forward
pCfl1-Exon34-R	& 4, in 3' UTR	CCT AGG ACG GGA CTT GGT CT	reverse
pPfn1-Exon3- F	Profilin 1, exon 3	CAC TTG GGG GCC AGA AAT GT	forward
pPfn1-Exon3-R	& 3' UTR	ATG GAA AGA AGG GGG TGC AA	reverse
pPfn2a-Exon3-F	Profilin 2a, exon 3	TGT CCA CGC AGG CAC AAT TA	forward
pPfn2a-Exon3-R	& 3' UTR	GGA GGG GTG AGA AAG GTG TG	reverse
pArc/Arg3.1-3UTR-F	Arc/Arg3.1, 3' UTR (Zalfa et al., 2007)	TGA GAC CAG TTC CAC TGA TG	forward
pArc/Arg3.1-3UTR-R		CTC CAG GGT CTC CCT AGT CC	reverse

The PCR products were run on an agarose gel (2 % in TAE, 6 µL RotiSafe), by adding 2.5 µL DNA sample buffer to 10 µL DNA sample.

2.6 Cellular biology

2.6.1 Preparation of hippocampal organotypic slice cultures

In this study organotypic hippocampal slice cultures (OHC) were used as an *in vitro* model. OHCs display a useful tool to investigate neuronal structures as well as neuronal connection since the hippocampal network is still intact and functional. Another advantage

is the large range of approaches since the cells are diversely manipulable. Here, OHCs were prepared from mice in the age of 5 days (postnatal day 5, P5) as previously described (Stoppini et al., 1991; Michaelsen-Preusse et al., 2014). Briefly, mice were rapidly decapitated and the brain transferred into ice-cold GBSS. The hippocampi were removed and cut with a McIllwain tissue chopper in 400 µm transversal slices. After 15-20 min incubation in GBSS at 4°C the slices were transferred onto a membrane insert (Millicell®, pore size 0.4 µm) and cultivated in Müller Kultur Medium at 37°C and 5 % CO_2. 72 h after slice preparation, antimitotic drugs were added to the medium and removed after additional 24 h by a 100% medium exchange, to reduce glia cell division. Once a week 50% of the medium was exchanged.

2.6.2 Transfection

2.6.2.1 DNA preparation

Different plasmid DNAs (table 7) were used to manipulate the expression of distinct proteins. Therefore, 1µL DNA was added to 30 µL of competent *Escherichia Coli* (*E. coli*) cells and the solution was transferred into 42°C for 30 s. After incubation in LB medium for 30 min, the solution was distributed on an agar-plate containing the respective antibiotic and incubated over night at 37°C. The next day a single colony was transferred into 3 mL LB-medium containing the respective antibiotics and incubated at 37°C for 6-8 h. The solution was transferred into 200 mL LB medium (containing antibiotics) and incubated over night at 37°C, followed by centrifugation at 6000 x g at 4°C to collect the cells. Preparation and Purification of the plasmid DNA was performed using the Qiagen Plasmid Midi Kit (Qiagen GmbH, Hilden) following the distributers instructions. Using a Qiagen column, the final lysate was purified and the DNA purity and concentration analyzed by a photometer, calculating the UV absorption.

Table 7: Plasmids used in this thesis

Plasmid	Discription	Reference
peGFP-f	farnesylated enhanced green fluorescent protein (CMV promoter)	Clontech
pMApple-N1	Fluorescent protein mApple (CMV promotor)	Michael W. Davidson

pEGFP-β-actin	B-actin fuced to enhanded green fluorescent protein	C.A. Schönenberger
pEF-tWGA	Truncated wheat germ agglutinin	(Yoshihara et al., 1999)
pCl-SEP-GluR1	Super-ecliptic pHluorin, pH sensitive GFP N-terminal to GluR1 cDNA (CMV promotor)	(Kopec et al., 2006)
pET28-mPFN1	Mouse profilin1	M. Rothkegel

2.6.2.2 Single cell DNA & dye electroporation

For dye labeling and genetic manipulation of single cells, single cell electroporation was used. Therefore culture inserts with OHCs were transferred into HBSS at room temperature (RT). The electroporation solution composed of 150 ng DNA in 30 µL HBSS. For analyzing neuronal morphology either a farnesylated eGFP (Clonetec) or mApple (Shaner et al., 2008; Michaelsen et al., 2010a; Michaelsen et al., 2010b) were electroporated 3 days before further experiments. For profilin1 over expression cells were already electroporated at DIV7 (together with mApple as well as control cells with mApple only). Fluorescence recovery after photobleaching experiments were performed using eGFP-actin. To visualize AMPA receptor clusters and insertion, SEP-GluR1 (addgene, (Kopec et al., 2006)) was electroporated, as well as truncated WGA (Yoshihara et al., 1999) for anterograde and retrograde tracing. The electroporation of DNA constructs was performed at 5 V, 1 mA and a 220 Hz train, the cultures were afterwards transferred back into culture medium and incubated at 37°C and 5 % CO_2. For analysis of TE morphology at distinct developmental time points, OHCs were electroporated with AlexaFlour594 (abcam) diluted in HBSS (end-concentration 1 mM) with the following settings: 10 V, 10 ms (single pulses) and afterwards quickly fixed in 4% PFA in 0.1 M phosphate buffer.

2.6.2.1 Biolistic transfection via Helios Gene Gun®

To study multiple cell types in single OHCs the gene gun method was used. The method is also known as biolistic particle delivery which describes the way of transfection. First, the implementation requires the preparation of so called bullets. The gene gun and the associated bullet preparation station are delivered by BioRad® and the bullets were prepared as described in the distributer's instructions. Briefly, gold microcarries (12.5

mg/tubing) were sonificated in 100 µL of 0.05 M spermidine, followed by adding 25 µg of DNA. 100 µL of 1 M $CaCl_2$ was added dropwise to the solution and incubated for 10 min at RT. 1 mL 96 % ice-cold ethanol was added to the bullet solution and centrifuged for 60 s at 100 x g. The supernatant was discarded and the washing steps repeated 3 times, for spermidine removal. Afterwards the DNA gold microcarries were dissolved in 3 mL PVP solution (0.05 mg/mL in ethanol) and added to the tubing which was dried in advance. The tubing was incubated for 3 min, so that the DNA gold microcarries can set down, afterwards the ethanol was removed. After the rotation of the tubing, to distribute the DNA gold carries, the tubing was dried for another 5 min and was then cut. The bullets fit in the revolver belonging to the gene gun. For the actual transfection, the gene gun revolver was loaded with bullets and a culture insert was placed under the gun, protected by a filter (3 µm, Millipore). The DNA gold microcarries were shot with helium at a pressure of 100 psi and the OHC placed back into culture medium and were at least incubated for another 24 h.

2.6.3 Preparation of fixed brain slices and diolistic labeling of single neurons

To analyze single hippocampal neurons in respect to their dendritic complexity and spine morphology in the preferably live near way (*in vivo*), mice at different developmental time points were sacrificed. Directly afterwards the mouse was fixed on a plate and the thorax was opened to have free access to the hearth. The right hearth atrium was opened by a cut and a fixation solution (4 % PFA, 4 % sucrose in 0.1 M PB) was delivered into the tip of the left ventricle by a butterfly cannula (0.5 x 13 mm G25). By the existing hearth activity the fixation solution is transported throughout the organism, until the liver gets completely pale by the exchanged of blood by fixation solution. Afterwards the mouse was decapitated, the skull opened and the brain completely removed. The olfactory bulb and the cerebellum were quickly removed, the hemispheres separated by a razor blade and the brain transferred into 3 mL fixation solution for another 30 min at 4°C. The hemispheres were transferred into PBS and cut into 400 µm transversal slices (if not mentioned otherwise in the results part). Therefore, the hemispheres were embedded into agar (2% agar in 0.1 M PB), cut by a vibratome (VT 1000 S, Leica Microsystems, Germany) and slices were collected and again incubated in fixation solution for 1h at 4°C.

For cell labeling with diolistics, bullets for the Helios gene gun had to be prepared at least 24 h in advance. Therefore, tungsten particles (50 mg, 1.7 µm diameter, BioRad) were

distributed on a glass slide and diluted with 100 µL dye solution (3 mg of DiI in 100 µL methylene-chloride). After the mixture was dried, it was removed from the slide, suspended in 3 mL water and homogenized by sonification. Finally, the dye solution was diluted to a 1:50 ratio which was transferred into a tubing. By using the BioRad tubing station the particles were set down, the liquid removed, the tubing dried and cut. To label the coronal sections described above, they were stick to a membrane and protected by a filter (3 µm, Millipore) which was placed between gene gun and slices. The dye particles were delivered by the helios gene gun ® via helium pressure (120 psi). The slices were incubated overnight in PBS and cell nuclei were marked by DAPI staining (1:1000 for 10 min), followed by mounting of the slices with fluoromount (Biomedia). Labeled cells were imaged within one week, to avoid the increase of background fluorescence and dye degradation.

2.6.4 Immunohistochemistry

In this thesis OHCs on the one hand and microtome slices of hippocampi (*in vivo*) on the other hand were treated with antibodies against proteins of interest. For hippocampal microtome slices mice were sacrificed by cervical dislocation and decapitated. Hippocampi were removed and fixed in 4% PFA in 0.1 M PB overnight. Hippocampi were transferred into 30% sucrose in 0.1 M PB until they were dehydrated. For coronal 30 µm hippocampal slices a microtome (Frigomobil, Jung) was used. Hippocampal microtome slices were incubated with a blocking solution (10% goat serum, 0.2 % TritonX-100 in PBS) for 1 h at RT. The tissue was incubated with the primary antibody (1:1000 synaptoporin, SySy, 1:500 synaptopodin, Sigma) in PBS, containing 1% goat serum, overnight at 4 °C. The secondary antibody (1:500 Cy2, Cy3 goat, Dianova) was diluted in PBS and incubated for 2 h at RT. In the last 10 min DAPI (1:1000 diluted in PBS) was added for labeling of the cell nucleus. OHCs were stained against synaptoporin, synaptopodin or if transfected with truncated WGA, against lectin. After a 2 h fixation in 4 % PFA in 0.1 mM PB and washing with PBS, OHCs were treated with 1% Triton-X in TBS (20 mM Tris/HCl, 0.14 M NaCl) over night at 4 °C to allow the penetration of the antibodies deep into the tissue. This was followed by a incubation in blocking solution (20 % goat serum in TBS) for 1 h at RT. Afterwards, OHCs were incubated in the primary antibody solution (1% goat serum in PBS, antibody dilution 1:500) overnight at 4 °C. The next day the slices were washed several times with TBS and the secondary antibody (anti-rabbit Cy3 1:500, 1 % goat serum

in TBS) was applied for 3 h at RT. OHCs transfected with SEP-GluR1 (Addgene) were fixed and blocked for 1 h at RT (20 % goat serum in PBS). To increase the signal, anti-GFP antibody was used as described above. To prevent permeabilization of the cell membranes all permeabilization steps were avoided, or appropriate reagents excluded from the staining solutions. Briefly, the slices were kept in the primary antibody solution (1% goat serum in PBS, 1:500 anti-GFP antibody in PBS) overnight at 4°C. The next day the slices were washed several times with PBS and secondary antibody was applied (anti-rabbit Cy2 1:500, 1 % goat serum in PBS) for 3 h at RT.
In both cases, the microtome slices and the OHCs, the tissue was washed with PBS and mounted with fluoromount (Biomed).

Table 8: Antibodies applied in this thesis

Antibodies	Description	manufacturer	Dilution
Anti-synaptopodin	Rabbit polyclonal IgG	Sigma – SE-19	1:500
Anti-synaptoporin	Rabbit polyclonal	SySy – 102002	1:1000
Anti-Lectin	Rabbit polyclonal	Sigma - T4144	1:500
Anti-GFP	Rabbit polyclonal IgG	Millipore – AB3ß8ß	1:500
Anti-STEP	Mouse monoclonal IgG1	Cell signaling – 4396	1:500
Anti-mouse Cy2	Goat polyclonal	Dianova – 115-225-062	1:500
Anti-rabbit Cy2	Goat polyclonal	Dianova – 111-225-144	1:500
Anti-rabbit Cy3	Goat polyclonal	Dianova – 111-165-144	1:500

2.7 Imaging techniques

2.7.1 Imaging and analysis of fixed tissue

For the analysis of dendritic complexity an Axioplan 2 microscope equipped with an Apotome module (Zeiss) was used with a z-stack size of 1 µm and a 20x objective (0.8 NA). The images acquired were 3D analyzed by the Neurolucida and Neuroexplorer software (Microbrightfield) to determine apical and basal dendritic morphology of pyramidal neurons. Images of the anti-synaptoporin staining for the analysis of mossy fiber projections were acquired with a 10x objective (0.3 NA) at the same setup. Unless

otherwise specified for all other imaging experiments a confocal laser-scanning microscope (Fluoview1000 setup, Olympus) was used, equipped with the following objectives: 20x (NA 0.5), 40x (NA 1.3), 60x (NA 1.0). All further analysis was performed by using the ImageJ software (US National Institutes of Health).

2.7.2 Live imaging

For time-lapse imaging, OHCs were incubated 20 min at 32°C in an imaging chamber (RC-22, Warner Instruments), perfused with carbogenated aCSF via a peristaltic pump at a flow rate of 1 mL/min. For detailed analysis of neuronal structure z-stack (0.35 µm step size) images were taken with a 60x objective (NA 1.0), followed by overview images through the 20x objective (NA 0.5). For structural mobility analysis of TEs and dendritic spines images were taken every 5 min over a total 20 min. The participation of dendritic spines in long-term potentiation was analyzed by morphological changes and displays therefore a useful tool to investigated the influence of single proteins in this process. The influence of FMRP on LTP was achieved by the induction of chemical LTP in *fmr1* KO and WT OHCs. Therefore, dendritic stretches were imaged as described above, followed by a 10 min application of glycine (10 mM glycine in aCSF). The recordings described above were repeated 60 min after glycine was removed from the system. Image analysis was performed via ImageJ. A spine in the *stratum lucidum* on the proximal apical dendrites of CA3 pyramidal neurons was classified as a TE when the area exceeded at least three times the size of the average spine area in the *stratum radiatum*. TE area was measured taking the outline of a TE in z level images at their maximum expansion. Spines in the *stratum radiatum* were analyzed by the measurement of the spine length, head diameter and neck width. Dendritic stretches imaged from living cells and fixed ones were analyzed in respect to spine density by counting of spines on a dendritic stretch which was measured in length.

2.7.3 Fluorescence recovery after photobleaching (FRAP).

Fluorescence recovery after photobleaching (FRAP) experiments on single TEs were performed as described in detail previously (Michaelsen-Preusse et al., 2014; Michaelsen-Preusse et al., 2016). In eGFP-actin or cytoplasmic GFP (for diffusion studies) expressing neurons a single TE or dendritic spine was bleached using a 405 nm laser line with a power

of 2.3-3 mW (~ 30%) for 30 ms. A SIM scanner allowed parallel imaging of GFP emission at 488 nm. A time-lapse series was acquired with an interval of 2 s for a total time of 120 s (0.2 s for total 11.2 s for diffusion studies). At this time point, a plateau in the fluorescence recovery was reached. The analysis was performed using ImageJ. The background corrected mean intensity values for each time point were calculated per spine and plotted against the time. The fluorescence intensity of each time point was normalized to the average value derived from five pre-bleaching images (relative fluorescence). Nonlinear curve fitting was performed in GraphPad Prism where the net recovery after photobleaching is provided by the following equation: Y=Y0 + (Plateau-Y0)*(1-exp(-K*x)) where Y0 is the Y value when time is zero directly after the bleaching impulse, Plateau is the Y value at infinite times, expressed as a fraction of the fluorescence before bleaching and was used to determine the dynamic actin pool (F-actin dynamic). The stable pool (F-actin stable) is the fraction of fluorescence which does not recover within the imaging period of 2 min (11.2 s) calculated as 1-(GFP dynamic), K is the rate constant, Tau is the time constant, expressed in seconds, it is computed as the reciprocal of K. From this equation, the actin turn-over rate was calculated as the time at 50% recovery of pre-bleaching fluorescence levels.

2.8 Electrophysiology – whole cell patch clamp recordings

AMPA receptor driven synaptic transmission can be studied by whole cell patch clamp recordings. Therefore, OHCs (DIV13-15) were incubated for 20 min at 32 °C in the recording chamber, perfused with aCSF (containing 0.0005 M TTX, 0.01 M bicuculline, 0.01 M APV) via a peristaltic pump at a flow rate of 1 mL/min. Whole-cell recordings at CA3 pyramidal neurons were performed using 5-7 MΩ glass pipettes filled with intracellular solution. To abolish the influence of mossy fiber activity, 4 µM DCG-IV was applied. Miniature EPSCs (mEPSCs) were recorded at -60 mV via voltage clamp. A Multiclamp 700B amplifier (Molecular Devices) and a Digidata 1332A digitizer (Molecular Devices) were used to obtain recordings. MEPSCs were recorded for 2 min duration in a 5 min interval over a period of 30 min (under control conditions and with DCG-IV application). Data were analyzed by using Mini Analysis (Synaposoft), with an amplitude threshold of 7 pA.

2.9 Behavior experiments

Different behavioral tests allow the analysis of the functionality of different brain regions. In this thesis the influence of FMRP on hippocampal circuits was investigated.

2.9.1 Morris water maze

The Morris water maze task was developed in the Richard Morris laboratories and could be shown to be specifically hippocampus dependent (Morris, 1981; Morris, 1984; Logue et al., 1997). To study the influence of a FMRP knockout on hippocampal function, both *fmr1* WT and KO mice were exposed to the procedure. The setup included a 160 cm diameter pool which was filled with water (20 ± 1 °C) colored in white (non-toxic, Titanoxid, Euro OTC Pharma). The pool was located in a small clean room, surrounded by three close walls. On every wall one cue (all with different structures) was placed approximately 50 cm to the pool wall and served as landmark for the mice. Every experimental procedure contained two or three phases: 1st pretraining, 2nd training and in specific cases 3rd reversal. The pretraining served as an experiment close situation were swimming and visual abilities were proven, as well as the mice were familiarize with the handling by the experimenter. The training was performed in the early phase of the light phase in a 12 h light/dark cycle, with access to water and food *ad libitum*. For the pretraining the mice passed through two trails a day, were they were placed in the maze, opposite to the platform position while the platform was visible (above water surface, cued with a Falcon). The platform position varied between every trial, while the mice had maximum 45 s to reach it. In case of success the mice were left on the platform for 10 s, otherwise the mouse was placed on the platform and as well left for 10 s. The pretraining was performed at 3 consecutive days; at the last day of pretraining the water in the maze was increased, so that the platform was under the water surface. For the actual training phase, the platform was not visible under the water surface and constantly placed in the middle of the North West quadrant of the maze. The mice passed through 4 trials in a 5 min interval per day for 8 consecutive days, starting from 4 distinct positions that were half-randomly changed day by day. Here, the maximum duration of a trial was 60 s, in case of success the mice were left on the platform for 10 s, otherwise they were placed on the platform and as well left for 10 s. In case of reversal experiments the platform was positioned opposite to the position of the training and the experiment accomplished as described above. For every training day the escape latency, distance swam and the displayed search strategies were analyzed. As memory

reference tests a probe trial without a platform was performed at day 3 and 9 of training if not mentioned otherwise. Here, the quadrant preference (as the % if time spent in a quadrant) and the platform crossings (crossings of the virtual platform) were analyzed.
To reveal whether the behavior of the mice was hippocampus-dependent, the trials were analyzed in respect to search strategies (Garthe et al., 2009; Garthe and Kempermann, 2013)). Here, the behavior of the mice can be classified as hippocampus-dependent and as hippocampus-independent. Therefore, the pool was virtually divided into an edge area (close to the pool wall), annulus zone and a goal corridor, the time spent in these areas served as tool to classify the search strategies. Random search (> 60 % surface coverage), scanning (10 % to 60 % surface coverage) and chaining (> 80 % in the annulus zone) were classified as hippocampus-independent search strategies. Hippocampus-dependent search strategies were directed search (> 80 % in 40° goal corridor) and direct swimming (> 90 % in 10° goal corridor).

2.9.2 Marble burying

Marble burying behavior experiments were performed to analyze species stereotypic behavior in an age- and hippocampus-dependent manner (Deacon and Rawlins, 2005). Therefore, standard mice cages were filled up to 5 cm with bedding. The bedding was flatted and compressed slightly. 12 marbles (with same color and size) were placed in a standardized scheme. The mice were left alone in the room, with no electricity on or plugged in to avoid ultrasound disturbance. After 60 min the number of marbles buried was counted.

2.10 Data presentation and statistical analysis

When not described differently, data are shown as mean ± SEM. An α level of $p < 0.05$ was chosen to reject the null hypothesis. Two different groups were compared by an unpaired Student´s T-test (Microsoft Excel), while the comparison of three or more experimental groups was performed via one-way ANOVA in GraphPad Prism.

3. Results

Patients with fragile X syndrome (FXS) can display a wide range of cognitive deficits as hyperactivity, hypersensitivity, autistic-like behavior and excessive adherence to patterns, while body function is mainly normal (Cohen et al., 1988; Merenstein et al., 1996; Tsiouris and Brown, 2004). These phenotypes point to disturbed brain functions but gross brain inspections of patients could not reveal any differences compared to healthy individuals. However, dendritic spines of patient brain tissue could be shown to display an immature spine structure (Irwin et al., 2001b; Grossman et al., 2006). An immature spine phenotype, meaning a long and thin structure could be studied in the mouse model of the FXS as well in the cortex, the amygdala, cerebellum and in the hippocampus (He and Portera-Cailliau, 2013).

At least some behavioral characteristics of patients point to a deficit in hippocampal function as adherence to patterns and problems in pattern recognition (Cohen et al., 1988). Indeed, in several regions of the hippocampus a higher proportion of spines displaying an immature structure could be found (He and Portera-Cailliau, 2013).

The effect of a FMRP deletion on spine structure was especially studied in the CA1 region in which a mainly immature spine structure could be revealed. Previous studies investigating spine morphology and the number of synapses formed by CA3 collaterals as well and the findings were inconclusive. While some reported an immature spine phenotype comparable to the one described for CA1 neurons (Huber et al., 2002; Bear et al., 2004; Volk et al., 2007; Bilousova et al., 2009; Cruz-Martin et al., 2010, 2012; Portera-Cailliau, 2012; He and Portera-Cailliau, 2013; Padmashri et al., 2013), others failed to detect differences between *fmr1* KO cells and WT neurons (Levenga et al., 2011).

This thesis is providing a detailed analysis of spine structures in the DG, CA3, CA2 and CA1 areas of the hippocampus in the absence of FMRP, especially focusing on the structure and function of the synapse formed between thorny excrescences at proximal apical dendrites of CA3 pyramidal neurons and large mossy fiber terminals along the axons of DG granule cells. This synapse was previously shown to be the detonator synapse directing the storage of information in the CA3 network (Urban et al., 2001).

3.1 Increased mossy fiber dependent input to CA3 pyramidal neurons accompanied by altered AMPA receptor insertion and spine apparatus formation in *fmr1* KO neurons

The main excitatory input to CA3 pyramidal neurons is comprised of LMTs of DG granule cells and is especially powerful (Henze et al., 2002). FXS patients and the mouse model display behavioral deficits that point towards an impairment of this synapse, characterized by excessive adherence to patterns and impairments in the recognition of facial expression (Cohen et al., 1988; Merenstein et al., 1996; Tsiouris and Brown, 2004; Garber et al., 2008). To investigate a potential effect on the synaptic transmission by the deletion of FMRP miniature excitatory postsynaptic currents (mEPSCs) were recorded from CA3 pyramidal neurons (whole-cell mode, V_m = -70 mV, 0.5 µM TTX). The recordings were performed in OHCs between DIV13-15 of *fmr1* WT and KO mice. As a first step, mEPSCs were recorded under baseline conditions in *fmr1* WT and KO cells over 30 min, with duration of 2 min in 5 min intervals. To prove that the effects found were due to the mossy fiber input only, DCG-IV was applied in a second set of experiments suppressing mossy fiber release function (Nicoll and Schmitz, 2005). The mEPSC frequency was found to be significantly increased by 66.6 % in *fmr1* KO CA3 pyramidal neurons in comparison to *fmr1* WT cells (figure 3 A-B, *fmr1* WT 2.44 ± 0.19 Hz, 4.08 ± 0.26 Hz; $p < 0.001$), while the amplitude was not altered (figure 3 C, *fmr1* WT 10.67 ± 0.34 pA, *fmr1* KO 10.18 ± 0.19 pA; $p = 0.31$). The application of 4 µM DCG-IV for at least 15 min reduced the frequency of both the *fmr1* WT and KO cells significantly to the same level (figure 3 A-B, *fmr1* WT 1.63 ± 0.22 Hz, *fmr1* KO 1.94 ± 0.16 Hz; $p = 0.28$; *fmr1* WT/ *fmr1* WT + DCG-IV $p < 0.001$; *fmr1* KO/ *fmr1* KO + DCG-IV $p < 0.001$), while the amplitude was not affected (figure 3 C, *fmr1* WT 10.30 ± 0.33 pA, *fmr1* KO 10.60 ± 0.39 pA; $p = 0.25$; *fmr1* WT/ *fmr1* WT + DCG-IV $p = 0.20$; *fmr1* KO/ *fmr1* KO + DCG-IV $p = 0.38$). Thus, the increased mEPSC frequency upon the deletion of FMRP appeared due to altered mossy fiber dependent input but not commissural inputs. As a next step, the molecular mechanisms that might lead to an altered synaptic function were investigated. For this purpose, CA3 hippocampal neurons in slice cultures were electroporated with mApple and SEP-GluR1. The expression of SEP-GluR1 is an established tool to study the insertion of GluR1 containing AMPA receptors at synapses (Nicoll and Schmitz, 2005; Kopec et al., 2006; Kopec et al., 2007; Makino and Malinow, 2009; Korte and Schmitz, 2016). Here, the AMPA receptor subunit GluR1 is fused to super-ecliptic pHluorin (SEP). Only receptor

components released from vesicles that are directly inserted into the membrane display green fluorescence which allows for an analysis specifically of surface receptors. 72 h after transfection, OHCs (DIV14) were either transferred into normal medium (baseline) or into medium with increased potassium levels (60 mM KCl, synaptic activation medium) for 20 min and afterwards transferred back to the former medium for 60 min. Interestingly, already under baseline conditions the SEP-GluR1 signal was stronger in *fmr1* KO TEs as compared to WT neurons, indicating an increased content of surface AMPA receptors

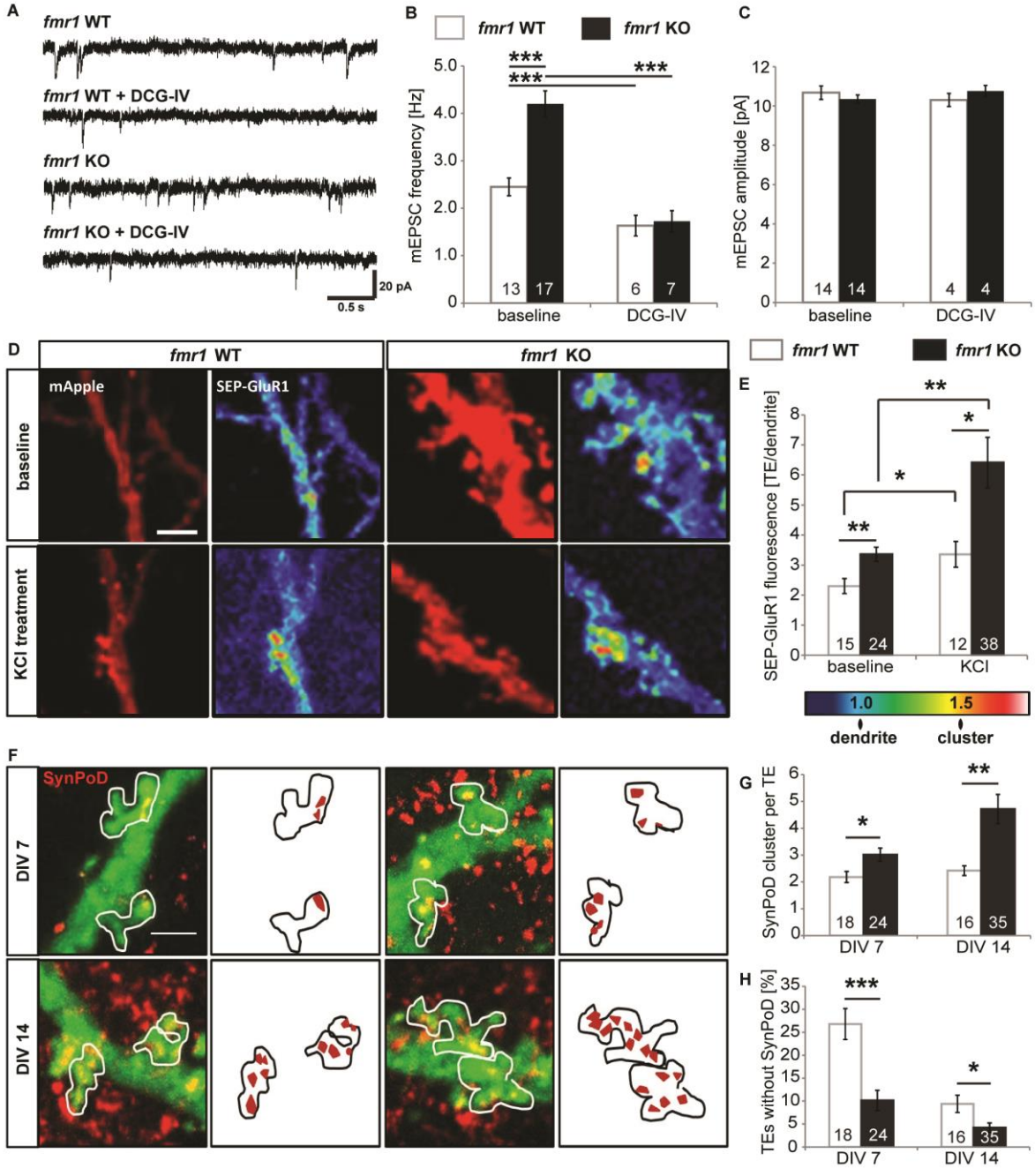

Figure 3: Altered mossy fiber dependent input to CA3 pyramidal neurons in slices from *fmr1* KO mice accompanied by an increased number of surface AMPA receptors and synaptopodin clusters. (**A**) Representative 3.5 s whole cell recordings of CA3 pyramidal neuron mEPSCs of *fmr1* WT and KO cultures under baseline conditions and treated with 4 µM DCG-IV. (**B**) Quantitative analysis of the mEPSC frequency with a threshold of 7 pA under baseline conditions (*fmr1* WT baseline n = 13 cells of 7 mice; *fmr1* KO baseline n = 17 cells of 13 mice) and treated at least 15 min with DCG-IV (*fmr1* WT n = 6 cells of 4 mice; *fmr1* KO n = 7 cells of 7 mice); (**C**) Quantitative analysis of CA3 pyramidal neuron mEPSC amplitude under baseline conditions (*fmr1* WT n = 13 cells of 7 mice; *fmr1* n = 17 cells of 13 mice) and upon at least 15 min DCG-IV treatment (*fmr1* WT n = 6 cells of 4 mice; *fmr1* KO n = 7 cells of 7 mice); (**D**) Representative images of DIV 14 CA3 neurons expressing mApple and SEP-GluR1 under baseline conditions and upon stimulation with 60 mM KCl (scale bar 5 µm); (**E**) quantification of fluorescence intensity at single TEs normalized to dendrite fluorescence intensity values of the SEP-GluR1 signal under baseline conditions (*fmr1* WT baseline n = 15 cells of 4 mice; *fmr1* KO n = 24 cells of 5 mice) and after KCl treatment (*fmr1* WT KCl treatment n = 12 cells of 4 mice; *fmr1* KO n = 38 cells of 6 mice; (**F**) representative images of CA3 pyramidal neurons at DIV7 and DIV14, respectively, electroporated with mApple (green) and stained with anti-synaptopodin (red, scale bar 5 µm); white boxes indicate the distribution of synaptopodin clusters in single TEs; (**G**) quantification of the number of synaptopodin clusters per TE (DIV7 *fmr1* WT n = 18 cells of 4 mice; *fmr1* KO n = 24 cells of 5 mice; DIV14 *fmr1* WT n = 16 cells of 4 mice; *fmr1* KO n = 35 cells of 8 mice); (**H**) quantification of the number of TEs without synaptopodin clusters; data are presented as mean ± SEM; Student´s T-test, significances are indicated by *** p-value < 0.001, ** p-value < 0.01 and * p-value < 0.05.

(figure 3 D-E, *fmr1* WT baseline 2.30 ± 0.25, *fmr1* KO 3.36 ± 0.24;p=0.006). Synaptic activation via KCl led to a significant increase in the SEP-GluR1 signal both in WT neurons (46%) and in *fmr1* KO cells (91%), however, this increase was more pronounced in the absence of FMRP (figure 3 D-E, *fmr1* WT KCl treatment 3.36 ± 0.43, n = 12 cells of 4 mice; *fmr1* KO 6.41 ± 0.84, n = 38 cells of 6 mice, p=0.049; *fmr1* WT baseline/KCl treatment p = 0.041; *fmr1* KO baseline/KCl treatment p = 0.006). The results thus indicate that TEs in *fmr1* KO cells were not only larger, but also had an increased number of surface AMPA receptors, pointing to an increase in synaptic strength. Furthermore, the insertion of AMPARs upon increased synaptic activity was enhanced.

These findings hint towards an increased state of maturity for TEs of *fmr1* KO neurons. Therefore, as a next step, an anti-synaptopodin staining was performed. Synaptopodin is an actin-binding protein localized to the spine apparatus, which was reported to be involved in synaptic plasticity and is mainly found in mature spines (Mundel et al., 1997; Deller et al., 2000; Vlachos et al., 2009; Zhang et al., 2013; Korkotian et al., 2014). CA3 pyramidal neurons of both genotypes expressing mApple were analyzed at DIV7 and DIV14 (figure 3 F-H). While TEs at DIV7 displayed no detectable morphological alterations, the anti-synaptopodin staining revealed already at this early time point a significantly increased number of clusters per TE (*fmr1* WT 2.18 ± 0.20, *fmr1* KO 3.01 ± 0.25; p=0.022). This phenotype was even more pronounced at DIV14 (figure 3 F-G, *fmr1* WT 2.42 ± 0.18, *fmr1* KO 4.71 ± 0.54; p=0.008). In line with these findings the proportion of TEs without synaptopodin clusters was significantly higher in WT cultures, both at DIV7 and DIV14 in

comparison to *fmr1* KO neurons (figure 3 H, DIV7 *fmr1* WT 26.77 ± 3.37, *fmr1* KO 10.16 ± 2.21; p<0.001; DIV14 *fmr1* WT 9.40 ± 1.89, *fmr1* KO 4.23 ± 1.01; p=0.011).
Taken together the deletion of FMRP strongly affected synaptic function due to altered TE maturation. Here, the question arose whether the strong functional alterations were in addition accompanied by alterations in the morphology of the respective synaptic compartments.

3.2 Thorny excrescence morphological development in *fmr1* KO mice

To investigate TE morphology *in vitro*, OHCs were obtained from P5 mice and cultured for 7 (DIV7), 10 (DIV10), 14 (DIV14) and 28 (DIV28) days. Several time points of TE development were chosen to study the effect of FMRP deletion during synapse development. Single CA3 pyramidal neurons were electroporated with dye (AlexaFlour594) and fixed afterwards. Previous publications could reveal functional and structural differences within the CA3 area, therefore the CA3 region was divided into two subregions CA3a/b distal to the DG and CA3c which is located proximal to the DG (Kesner, 2013). In this thesis the same classification was used and referred as distal (CA3a/b) and proximal (CA3c). No difference in TE morphology could be found between *fmr1* KO and WT slices at DIV7 (figure 4 A-E). Here, neither the deletion of FMRP nor the different subregions had an effect on TE morphology. At DIV10 only proximal CA3 pyramidal neurons displayed an increased total number of TEs along the apical dendritic tree in OHCs obtained from *fmr1*KO mice, comparted to WT littermates (figure 4 D, *fmr1* WT 6.80 ± 1.14; *fmr1* KO 18.17 ± 1.61; p < 0.001). No differences were found between *fmr1* WT and KO cells with respect to TE area, density and the TE maximum distance to the soma at DIV10 (figure 4 A-E). The most prominent effect could be found at DIV14 in distal CA3 neurons while there was no effect on proximal CA3 pyramidal neurons. Distal CA3 pyramidal neurons showed an increase in TE area at the apical dendritic tree in *fmr1* KO OHCs (figure 4 A-B, *fmr1* WT 3.44 ± 0.23; *fmr1* KO 4.54 ± 0.35; p = 0.030) while the density was not altered compared to WT OHCs (figure 4 A-C). A significant increase in the total TE number (figure 4 D, *fmr1* WT 15.57 ± 3.30; *fmr1* KO 25.29 ± 2.41; p = 0.048) accompanied by an elongation of the TE area, displayed by the distance of the furthest TE to the soma (figure 4 E, *fmr1* WT 44.41 ± 5.10; *fmr1* KO 67.51 ± 5.53; p = 0.015) could only be found in distal CA3 pyramidal neurons in cultures of *fmr1* KO mice, compared to cultures of WT littermates. Therefore, distal CA3 pyramidal neurons in

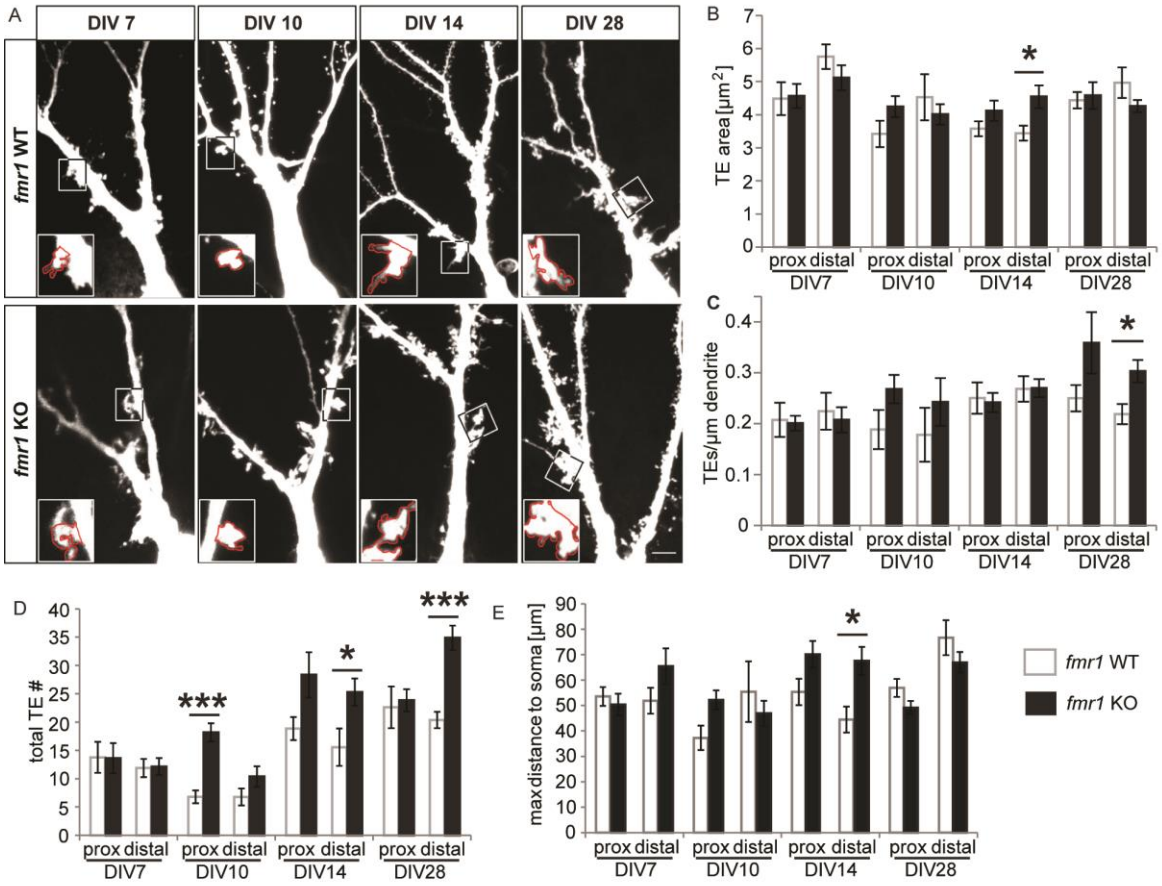

Figure 4: TE morphology is altered in a region- and age-dependent manner in *fmr1*KO mice *in vitro* (**A**) Representative examples of distal CA3 pyramidal neurons in organotypic hippocampal slice cultures of WT (upper row) and *fmr1* KO (lower row) mice filled with AlexaFluor 594 via single cell electroporation at different developmental time points (DIV7, DIV 10, DIV 14, DIV 28); scale bar 10 µm, inserts show high resolution images of representative TEs, red outlines display the analysis of the TE area (scale bar 2 µm); (**B-E**) quantification of TE area, TE density along the apical tree (TEs/µm dendrite), total number of TEs per cell and the maximum distance of the farthest TE to the soma, CA3 pyramidal neurons were divided into cells proximal (prox) and distal to the DG (DIV7 *fmr1* WT proximal n = 8 cells of 3 mice; *fmr1* WT distal n = 9 cells of 3 mice; DIV10 *fmr1* WT proximal n = 8 cells of 4 mice; *fmr1* WT distal n = 6 cells of 4 mice; DIV14 *fmr1* WT proximal n = 7 cells of 4 mice; *fmr1* WT distal n = 7 cells of 3 mice; DIV28 *fmr1* WT proximal n = 10 cells of 3 mice; *fmr1* WT distal n = 8 cells of 3 mice; DIV7 *fmr1* KO proximal n = 8cells of 3 mice; *fmr1* KO distal n = 6 cells of 3 mice; DIV10 *fmr1* KO proximal n = 10 cells of 5 mice; *fmr1* KO distal n = 7 cells of 4 mice; DIV14 *fmr1* KO proximal n = 9 cells of 5 mice; *fmr1* KO distal n = 7 cells of 4 mice; DIV28 *fmr1* KO proximal n = 6 cells of 3 mice; *fmr1* KO distal n = 8 cells of 3 mice); data are presented as mean ± SEM; Student´s T-test, significances are indicated by *** p-value < 0.001, ** p-value < 0.01 and p-value < 0.05.

DIV14 cultures displayed an increase in total TE number and maximum TE distance to cell body due to the deletion of FMRP (figure 4 C-D). At the latest time point chosen (DIV28) both the maximum distance to the soma and TE area were indistinguishable from WT cells (figure 4 B & E) whereas the total TE density was still increased compared to control cells (*fmr1* WT 0.22 ± 0.02; *fmr1* KO 0.30 ± 0.02; p 0.018) accompanied by an increase in TE number in distal CA3 neurons only (figure 4 C-D; *fmr1* WT 20.38 ± 1.44; *fmr1* KO 34.86 ± 2.17; p < 0.001). Taken together, the deletion of FMRP had the most

pronounced effect during development at DIV14 in distal CA3 pyramidal neurons only. To verify whether the effects found in cultures can be found in brain slices directly obtained from mice. Brain slices of both *fmr1* WT and KO mice were diolistically stained with DiI.

3.3 TE density is altered in a region- and age-dependent manner in *fmr1* KO mice *in vivo*

The TE morphological analysis in OHCs revealed a strong effect of the FMRP deletion especially at DIV14 and in distal neurons only. To prove a potential developmental effect *in vivo* as well TE morphology was investigated early in development at P19 and later in young adulthood between P30-40. Additionally, the CA3 pyramidal neurons analyzed were classified as proximal cells and distal cells in relation to the DG corresponding to the classification found in the literature CA3c (proximal cells) and CA3a/b (distal cells). Earlier publications could show that the CA3 area consists of these two functional und morphological distinguishable subregions (Lorente de Nó, 1934; Li et al., 1994; Kesner, 2013). To study TE morphology mice were perfused with PFA and 400 µm thick brain slices were diolistically labeled with DiI to allowed for a detailed analysis of neuronal

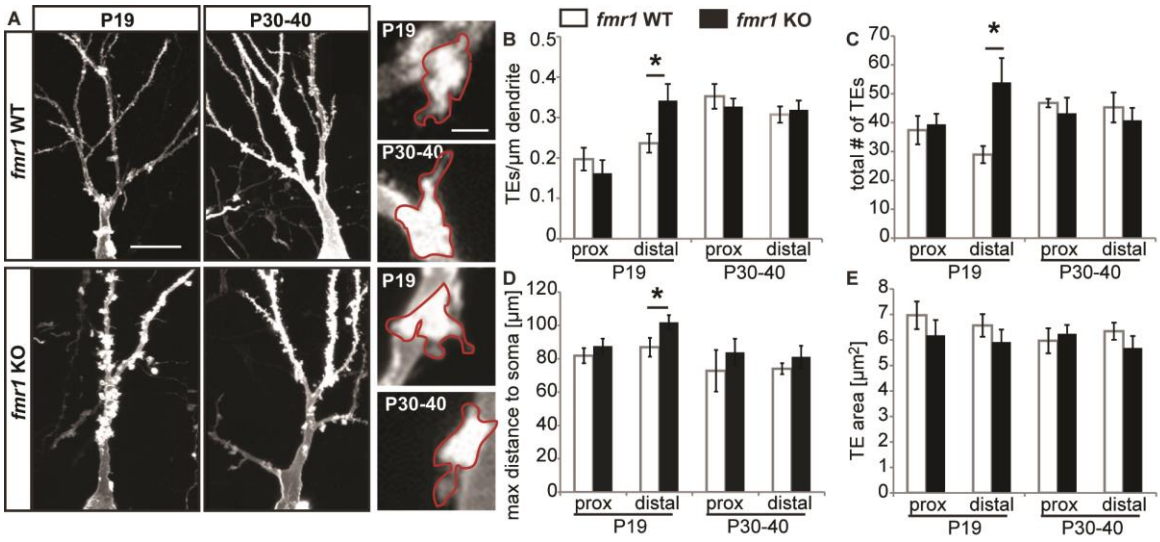

Figure 5: TE density is altered in a region- and age-dependent manner in *fmr1*KO mice *in vivo* (**A**) Apical dendritic trees of DiI labeled distal CA3 pyramidal neurons in hippocampal slices of 19 days and 30-40 days old *fmr1* KO and WT mice (scale bar 20 µm), inserts show high resolution images of representative TEs, red outlines display the measurement of TEs (scale bar 2 µm); (**B-E**) quantification of TE density along the apical tree (TEs/µm dendrite), total number of TEs per cell, the maximum distance of the farthest TE to the soma and average TE area at P19 and P30-40, CA3 pyramidal neurons were divided into cells proximal (prox) and distal to the DG (P19 *fmr1* WT proximal n = 15 cells of 5 mice; *fmr1* WT distal n = 18 cells of 6 mice; P30-40 *fmr1* WT proximal n = 8 cells of 4 mice; *fmr1* WT distal n = 6 cells of 4 mice; P19 *fmr1* KO proximal n = 16 cells of 8 mice; *fmr1* KO distal n = 9 cells of 8 mice; P30-40 *fmr1* KO proximal n = 10 cells of 5 mice; *fmr1* KO distal n = 7 cells of 4 mice; data are presented as mean ± SEM; Student´s T-test, significances are indicated by * p-value < 0.05.

structures. CA3 pyramidal neurons were analyzed with respect to their TE density along the apical dendritic tree, the total number of TEs, the distance between the cell soma and the furthest TE; and the average area of TEs. The TE density was found to be significantly increased in hippocampi of P19 *fmr1* KO mice in distal CA3 pyramidal neurons only (*fmr1* WT 0.24 ± 0.02 TEs/µm dendrite; *fmr1* KO 0.34 ± 0.04 TEs/µm dendrite; p = 0.044), while proximal cells were unaltered in comparison to WT littermates (figure 5 A-B). The increased TE density was accompanied by a significantly increased number of TEs (figure 5 A & C, *fmr1* WT 28.94 ± 2.96; *fmr1* KO 53.89 ± 8.46; p = 0.019). Interestingly, the distance between the furthest TE and the soma was increased as well only distally in *fmr1* KO CA3 pyramidal neurons compared to *fmr1* WT cells (figure 5 A & D; *fmr1* WT 86.91 ± 5.59; *fmr1* KO 101.84 ± 4.25; p = 0.044). While distal neurons of P19 mice were affected by the deletion of FMRP, P30-40 neurons were unaltered in comparison to WT littermates in all parameters (figure 5 A-E). The TE area was not altered in both P19 and P30-40 *fmr1* KO mice compared to WT littermates (figure 5 A-E). Taken together, the deletion of FMRP had an age- and CA3 subregion dependent effect on TEs. In order to study the mechanism of underlying structure formation TEs were investigated in greater detail in OHCs.

3.4 The deletion of FMRP causes a decrease in TE motility accompanied by altered actin dynamics

Neuronal structures like dendritic spines, LMTs and TEs underlie continuous morphological changes mediated by a highly dynamic actin network. The actin network is tightly regulated to allow for fast modulations of neuronal morphology most likely correlated to synaptic transmission. It has been shown previously that spatial learning and environmental enrichment increased the number and size of LMTs (Schöpke et al., 1991; Pleskacheva et al., 2000; Ramírez-Amaya et al., 2001; Galimberti et al., 2006; Holahan et al., 2006; Rekart et al., 2007; Gogolla et al., 2009; Ruediger et al., 2011) and that activity regulates morphological plasticity of the presynaptic compartment (Chierzi et al., 2012). Moreover, also TEs display structural plasticity (Frotscher et al., 1977; Zhao et al., 2012). Therefore, as a next step short-term changes in TE morphology were investigated.

TEs show a great range of structural variations (Wilke et al., 2013). Previous publications revealed TEs as structures with multiple synapses (Amaral and Dent, 1981; Chierzi et al., 2012) hence, structural plasticity of the postsynaptic compartment might play an important

functional role for the output of CA3 neurons. To analyze TE dynamics, CA3 pyramidal neurons were transfected at DIV11 in OHCs with fGFP. TE motility was studied under baseline conditions; therefore stretches of proximal apical dendrites were imaged at 5 min intervals for 20 min in DIV14 cultures. Remarkably, the deletion of FMRP caused a significant decrease in the average change in TE area per 5 min interval (figure 6 A-B, *fmr1* WT 5.7 ± 0.5 %, *fmr1* KO 3.8 ± 0.3%; p=0.002). Changes in spine shape were correlated to the dynamic actin cytoskeleton which is highly enriched in dendritic spines (Fischer et al., 1998; Fukazawa et al., 2003; Honkura et al., 2008; Hotulainen et al., 2009; Bosch et al., 2014; Michaelsen-Preusse et al., 2016). Therefore, the question arose whether the decrease in structural plasticity could be directly linked to alterations in actin polymerization rates. Fluorescence recovery after photobleaching (FRAP) experiments were used to monitor actin dynamics in single TEs of *fmr1* KO neurons and WT cells, an approach that was previously applied to monitor actin dynamics at spines in the CA1 region (Michaelsen-Preusse et al., 2014; Michaelsen-Preusse et al., 2016). As TE size differed significantly between *fmr1* KO and WT cells, potential differences in diffusion rates were analyzed which would interfere with the read-out of actin dynamics using GFP-actin FRAP. Cytoplasmic eGFP was expressed in single CA3 neurons and FRAP experiments showed neither an alteration in the recovery rate after the bleaching impulse (Fig. 6 E; *fmr1* WT 0.55 ± 0.18, *fmr1* KO 0.60 ± 0.08; p=0.785) nor in the stable actin pool (*fmr1* WT 0.08 ± 0.02, *fmr1* KO 0.08 ± 0.02; p=0.977). This indicates that there are no significant changes in the diffusion rate.

FMRP was shown to be an important mRNA binding protein. Besides its binding abilities, it also regulates the translation of mRNAs which reveals FMRP as an important modulator of synaptic activity (Ashley et al., 1993; Bagni and Greenough, 2005). Since the regulation of actin dynamics is crucial to fulfill synaptic function, by e.g. increasing the spine surface enabling an increased area for receptor insertion, the tight regulation of actin polymerization is of high importance (Matsuzaki et al., 2001; Holtmaat and Svoboda, 2009). Actin dynamics are under control of several actin-binding proteins and whole protein complexes. It was shown that especially profilins and cofilin1 maintain actin remodeling (Blanchoin et al., 2000). Therefore, RNA immunoprecipitation was used to reveal a potential role of FMRP in the regulation of actin binding proteins, especially profilin1 (PFN1), profilin2a (PFN2a) and cofilin1 (CFL1). For a brain region specific analysis, cell lysates obtained from hippocampal tissue were used and mRNAs bound to

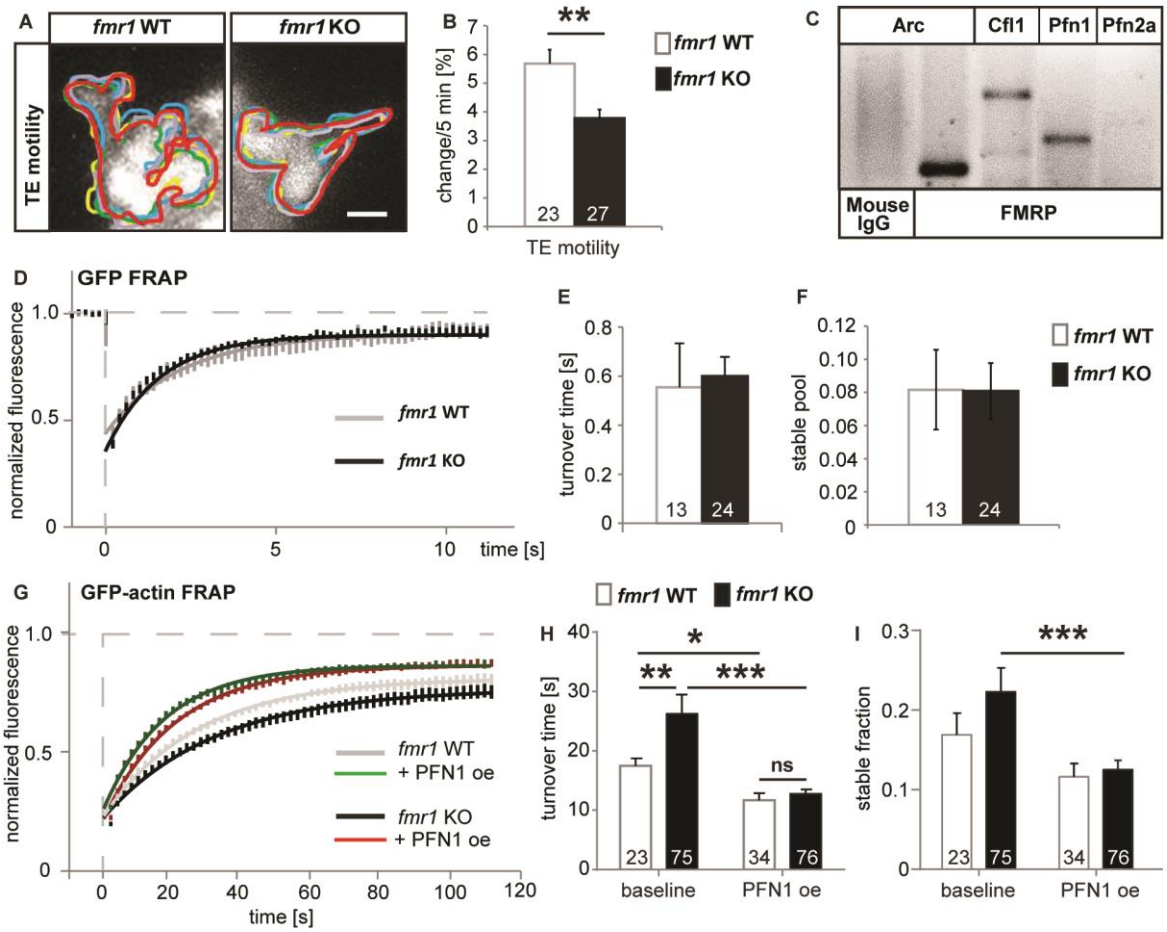

Figure 6: TE motility and actin dynamics are altered in *fmr1* KO neurons and can be rescued by profilin1 over expression.
(A) Representative images of TEs in *fmr1* KO and WT hippocampal slice cultures (DIV14, colored outlines indicate TE area at different time points during the time-lapse imaging; scale bar 2 µm); **(B)** quantification of TE motility at DIV14; percent changes per 5 min; over a total imaging period of 20 min (*fmr1* WT n = 23 TEs of 8 mice; *fmr1* KO n = 27 TEs of 9 mice); **(C)** RNA immunoprecipitation of FMRP tested for Arc (positive control), cofilin1 (Cfl1), profilin1 (Pfn1) and profilin2a (Pfn2a), the precipitation of mouse IgG tested for Arc served as negative control (all performed with mouse hippocampus); (**D**) recovery curve of TEs expressing cytosolic eGFP at DIV14; **(E)** turnover time in s and (**F**) quantification of the stable fraction of actin filaments which do not recover within the imaged time window (*fmr1* WT n = 13 TEs of 8 mice; *fmr1* KO n = 24 TEs of 6 mice); (**G**) recovery curve of TEs expressing eGFP-actin or eGFP-actin and profilin1 at DIV 14; (**H**) turnover time in s under baseline conditions (*fmr1* WT n = 23 TEs of 5 mice; *fmr1* KO n = 34 TEs of 9 mice) and with over expressing PFN1 (*fmr1* WT n = 75 TEs of 13 mice; *fmr1* KO n = 76 TEs of 17 mice; p = 0.5); (**I**) quantification of the stable fraction of actin filaments which do not recover within the imaged time window under baseline conditions and upon PFN1 over expression; data are presented as mean ± SEM; Student´s T-test, for FRAP experiments are displayed via non-linear regression and tested with a two-way ANOVA combined with a Bonferroni post-hoc test significances are indicated by *** p-value < 0.001, ** p-value < 0.01 and * p-value < 0.05.

FMRP were investigated. Indeed, the analysis revealed that FMRP bound the mRNAs of PFN1 and CFL1 but not PFN2a (figure 6 C). It could be previously shown that FMRP binds the mRNA of ARC (Park et al., 2008) which could be reproduced here, therefore Arc served as a positive control. Previous studies showed that PFN1 is an important modulator of actin dynamics in neurons (Michaelsen et al., 2010a; Michaelsen-Preusse et al., 2016), and that PFN1 levels are decreased in the hippocampus of *fmr1* KO mice. To find a

potential role of PFN1 downstream of FMRP, eGFP-actin FRAP experiments were performed. Therefore, single CA3 neurons were electroporated with eGFP-actin and actin dynamics were analyzed by live cell imaging in aCSF. The experiments revealed a significant decrease in actin polymerization rates in TEs of *fmr1* KO mice (Fig. 6 G-H), notably the same phenotype has been described for spines of PFN1 deficient neurons (Michaelsen-Preusse et al., 2016). While actin polymerization was slower in TEs as indicated by an increase in the turnover time (figure.6 H; *fmr1* WT 17.47 ± 1.27 s, *fmr1* KO 26.25 ± 3.23 s, p=0.002), the stable pool of actin filaments that did not recover during the 2 min time window was not significantly altered in FMRP depleted cells (Fig. 6 I, *fmr1* WT 0.17 ± 0.03, *fmr1* KO 0.22 ± 0.03; p=0.141). Further in line with a proposed role of PFN1 downstream of FMRP (Michaelsen-Preusse et al., 2016), the significant alteration in actin turnover between *fmr1* KO and WT cells was abolished in cells overexpressing PFN1 (figure 6 G-H, *fmr1* WT 11.67 ± 1.11 s, *fmr1* KO 12.78 ± 0.71 s; p = 0.5). The data additionally support the function of PFN1 which is known to contribute to the elongation of actin filaments by adding actin monomers (Perelroizen et al., 1996; Witke, 2004). In line with this, the general turnover time was decreased in *fmr1* WT and KO cells due to the PFN1 overexpression (figure 6 H) accompanied by a decreased stable pool (figure 6 I).

So far it could be shown that in the absence of FMRP, TEs are larger and more numerous, and that their spread along the apical dendrite was increased. Additionally, TEs displayed a decreased motility together with decreased actin dynamics which was at least partially dependent on the misregulation of PFN1 in *fmr1* KO cells.

In order to obtain a complete analysis about the effect on CA3 pyramidal neurons due to the knockout of the *fmr1* gene, dendritic spines in the *stratum radiatum* were as well investigated in detail.

3.5 Morphology and motility of dendritic spines in *stratum radiatum* are affected by the loss of FMRP

The apical dendritic tree of CA3 pyramidal neurons displays a high complexity and offers therefore the possibility of a high synapse density in a compact way. Thus, the dendritic complexity of the apical dendritic tree can provide a first hint of the computational power of these cells (Jan and Jan, 2010). Here, CA3 pyramidal neurons were filled with dye (AlexaFlour594) by taking advantage of single cell electroporation in organotypic hippocampal slice cultures (OHCs). At DIV14 the cells were filled and directly afterwards

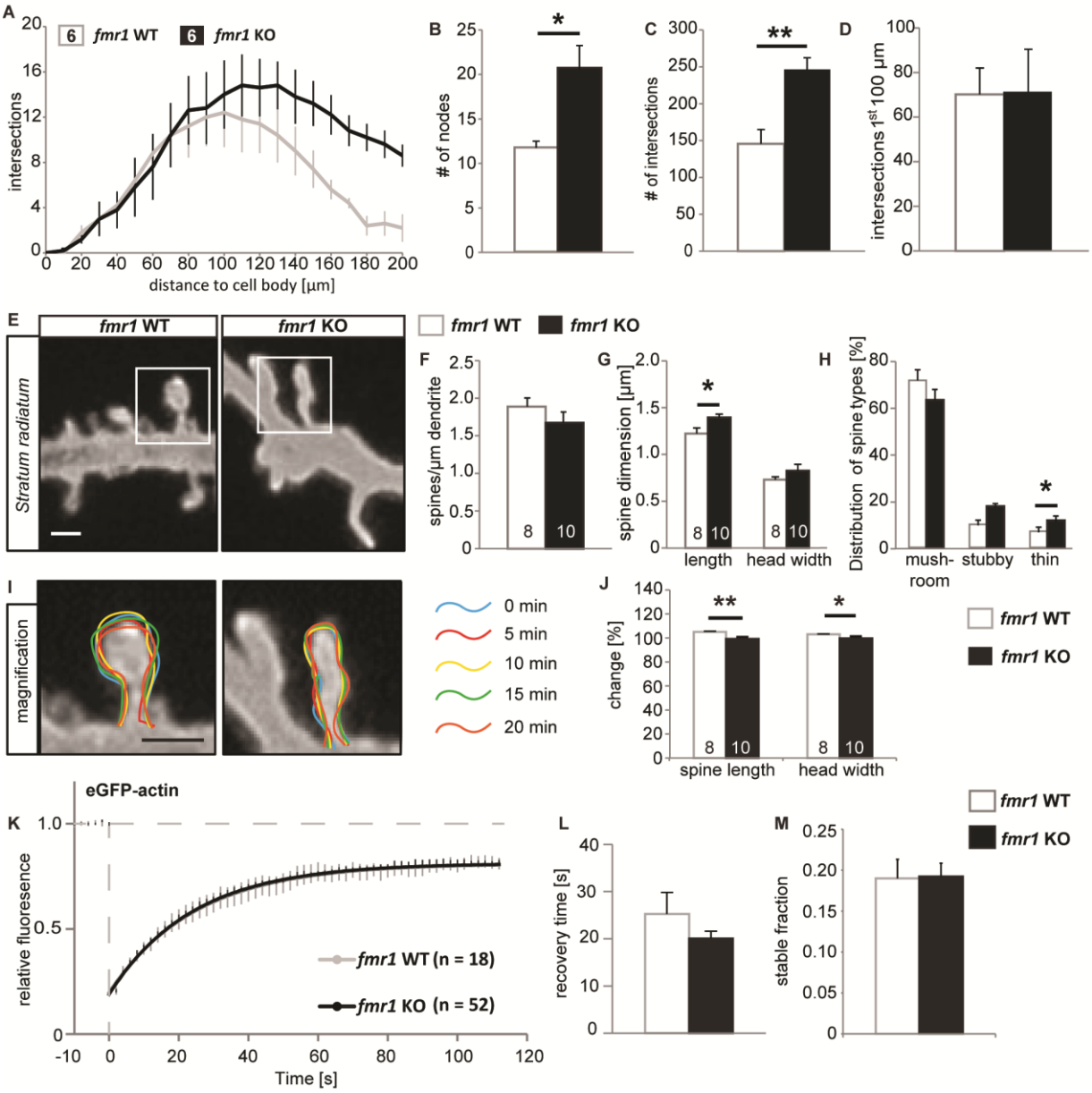

Figure 7: The dendritic complexity, spine structure and motility are altered in CA3 pyramidal neurons in OHCs obtained from *fmr1* KO mice

(A) Sholl analysis of *fmr1* KO and WT CA3 pyramidal neurons at DIV14; (**B-C**) quantification of the number of nodes, Sholl intersections at DIV 14 of both genotypes (*fmr1* WT n = 6 cells of 3 mice; *fmr1* KO n = 6 cells of 3 mice); (**D**) number of Sholl intersections on the first 100 µm of dendrite at DIV 14 in *fmr1* KO and WT CA3 neurons; (E) example images of stretches of apical dendrites of CA3 pyramidal neurons of both genotypes; (F-H) quantification of spine density, morphology and spine subtype composition in both genotypes at DIV 14 (*fmr1* WT n = 8 cells of 4 mice; *fmr1* KO n = 10 cells of 4 mice); (I) magnification of dendritic spines (indicated by white boxes in E) of *fmr1* WT and KO cells (colored outlines indicate different recordings in the time laps imaging, color matching time points showing at the right); (J) Quantification of spine length and head width motility of both genotypes (*fmr1* WT n = 8 cells of 6 mice; *fmr1* KO n = 11 cells of 10 mice); (K) recovery curve of TEs expressing eGFP-actin at DIV14; **(L)** turnover time in s and (**M**) quantification of the stable fraction of actin filaments which do not recover within the imaged time window (*fmr1* WT n = 11 spines of 4 mice; *fmr1* KO n = 22 spines of 10 mice); data are presented as mean ± SEM; Student´s T-test, for FRAP experiments are displayed via non-linear regression and tested with a two-way ANOVA combined with a Bonferroni post-hoc test significances are indicated by *** p-value < 0.001, ** p-value < 0.01 and * p-value < 0.05.

fixed. Sholl analysis was performed which counted the intersections of dendritic stretches with spheres of increasing radius starting from the cell soma at an increment of 10 µm. The analysis uncovered a significant increase of the dendritic complexity starting at a distance of 160 µm to the soma in *fmr1* KO cells compared to *fmr1* WT cells (figure 7 A). This effect was accompanied by a significant increase in the number of dendritic nodes (*fmr1* WT 11.75 ± 0.75, *fmr1* KO 20.60 ± 2.66; p=0.024) and over all intersections (figure 7 B-C, *fmr1* WT 145.40 ± 19.67, *fmr1* KO 246.60 ± 15.66, p=0.004). An increased dendritic complexity can increase the storage capability of the cell. This study displayed earlier that the deletion of FMRP caused an increased amount of TEs *in vivo* and *in vitro* (figure 4 C & 5 D), so the question arose whether this effect would in parts result from an increase in the dendritic complexity in the same area. Additionally, TEs mainly appeared at dendritic nodes. The detailed analysis of intersections in the first 100 µm from the soma where TEs are located (figure 4 D & 5 E) was not revealing differences between *fmr1* KO and WT cells (figure 7 D, *fmr1* WT 70.20 ± 11.79, *fmr1* KO 71.40 ± 18.99, p=0.959). The pronounced effect found for TEs in *fmr1* KO mice is therefore not accompanied by an increased dendritic complexity in this area. Nevertheless, an increased dendritic complexity in the *stratum radiatum* was found. Therefore, dendritic spines in the *stratum radiatum* were investigated as a next step. The number of spines showed no differences between *fmr1* KO and WT cells (figure 7 E-F, *fmr1* WT 1.89 ± 0.12 spines/µm dendrite, *fmr1* KO 1.67 ± 0.14 spines/µm dendrite, p = 0.283). However, analysis of the spine morphology displayed a significantly increased spine length (*fmr1* WT 1.22 ± 0.06 µm, *fmr1* KO 1.39 ± 0.04 µm; p=0.021). Spines can be classified due to the dimensions of their length and head to neck ratio (Zagrebelsky et al., 2005). Here, one can distinguish mushroom (spine head/spine neck > 1.5), thin (spine head/spine neck < 1.5, spine length > 1 µm) and stubby (spine head/spine neck < 1.5, spine length < 1 µm) like spines. The classification of spines revealed a significantly increased proportion of thin spines (*fmr1* WT 0.10 ± 0.02 %, *fmr1* KO 0.17 ± 0.02; p = 0.015) caused by the deletion of FMRP. Thus, the results shown here support the hypothesis of an immature spine phenotype described above. Additionally, dendritic spines were less motile with respect to changes in spine length and head width, monitored by time-lapse imaging with a 5 min interval for 20 min.

Here, the deletion of FMRP caused a significant reduction in spine length motility (*fmr1* WT 105.05 ± 0.66 %, *fmr1* KO 99.07 ± 0.23 %; p = 0.004) as well as spine head width motility (figure 7 I-J, *fmr1* WT 103.03 ± 0.33 %, *fmr1* KO 99.50 ± 0.36 %; p = 0.041).

Changes in spine shape are correlated to the dynamic actin cytoskeleton which is highly enriched in dendritic spines (Fischer et al., 1998; Fukazawa et al., 2003; Honkura et al., 2008; Hotulainen et al., 2009; Bosch et al., 2014; Michaelsen-Preusse et al., 2016). Thus, potential alterations in the actin polymerization rates were investigated by FRAP experiments. FRAP was used to monitor actin dynamics in single spines of *fmr1* KO neurons and WT cells.

Previously an interaction of FMRP with the mRNA of profilin1 (PFN1) was shown, an important modulator of actin dynamics in neurons. In addition, PFN1 levels were decreased in the hippocampus of *fmr1* KO mice (Michaelsen-Preusse et al., 2016). Indeed, FRAP experiments using single CA3 neurons expressing GFP-actin revealed a significant decrease in actin polymerization rates in TEs of *fmr1* KO mice (figure 7 G-I). However, spines at dendritic stretches in the *stratum radiatum* displayed no differences in actin polymerization between *fmr1* KO and WT cells (figure 7 K-L). At this point, it is interesting to note that the data provided a first example that different subtypes of spines on CA3 neurons were affected differentially by the loss of FMRP, a fact that might have a strong impact on information processing in these cells. While dendritic spines in the *stratum radiatum* receive associational/commissural input, TEs in the *stratum lucidum* are contacted by mossy fiber projections of DG granule cells. As described earlier the input by large mossy fiber terminals is crucial for CA3 function, therefore these presynaptic compartments were studied further in *fmr1* KO organotypic hippocampal slices at DIV14.

3.6 The deletion of FMRP causes an elongation and widening of the mossy fiber projection *in vitro* and *in vivo*

As a first step, the mossy fiber projection was investigated in OHCs. Therefore, OHCs were immunohistochemically stained with an anti-Synaptoporin antibody. Synaptoporin is a vesicle associated protein which is highly enriched in LMTs and is crucial for the formation of the mossy fiber synapse (Grabs et al., 1994; Grosse et al., 1998). The staining allows to analyze the projecting axon bundle as a whole from the DG throughout the CA3 into the CA2 area. In OHCs cultured for 14 days (days of *in vitro* 14, DIV14) a widening of the projection could be found in the *fmr1* KO, compared to slices obtained from WT littermates (figure 8 A-B). Interestingly, the distance to the soma of the furthest TE was increased in *fmr1* KO cells compared to WT as well (figure 4 E). Additionally, cultures of *fmr1* KO mice displayed an elongation of the mossy fiber projection (*fmr1* WT

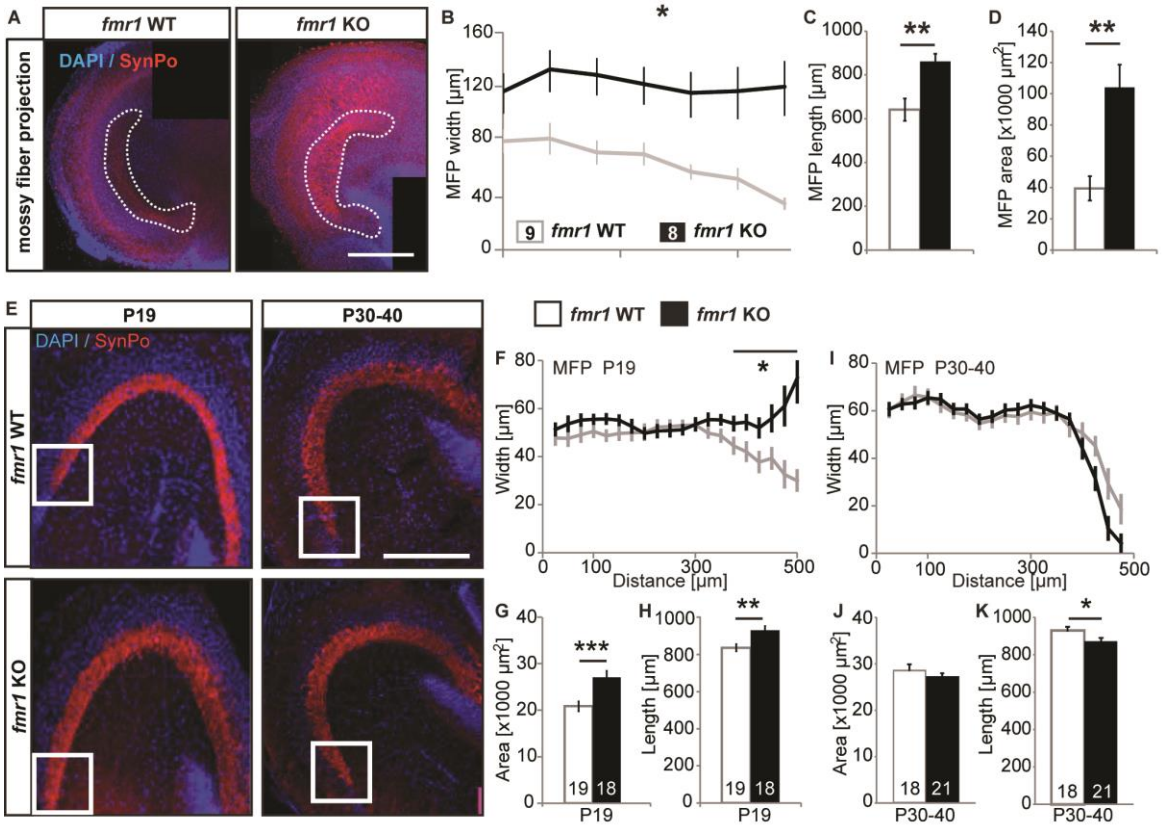

Figure 8: The deletion of FMRP strongly affects width and length of the mossy fiber projection *in vitro* and *in vivo* (**A**) hippocampal slice cultures of WT and *fmr1* KO mice at 14 DIV labeled with DAPI (blue) and anti-synaptoporin (red), scale bar 200 µm; (**B-D**) quantification of width, length and area of the suprapyramidal mossy fiber projection at DIV14 (*fmr1* WT n = 9 hippocampal slices of 5 mice; *fmr1* KO n = 8 hippocampal slices of 4 mice). (**E**) hippocampal slices of WT and *fmr1* KO mice P19 and P30-40 labeled with DAPI (blue) and anti-synaptoporin (red), (scale bar 200 µm, white boxes indicate the most distal part of the mossy fiber projection); (**F-H**) quantification of width, area and length of the suprapyramidal mossy fiber projection at P19 (*fmr1* WT n = 19 hippocampal slices of 4 mice; *fmr1* KO n = 18 hippocampal slices of 4 mice; (**I-K**) quantification of width, area and length of the suprapyramidal mossy fiber projection at P30-40 (*fmr1* WT n = 18 hippocampal slices of 4 mice; *fmr1* KO n = 21 hippocampal slices of 4 mice; data are presented as mean ± SEM; Student´s T-test, significances are indicated by *** p-value < 0.001, ** p-value < 0.01 and * p-value < 0.05.

861.86 ± 35.08 µm, *fmr1* KO 641.04 ± 51.06 µm; p = 0.004) accompanied by an overall increased area (*fmr1* WT 39,416.94 ± 7,766.37 µm^2, *fmr1* KO 104,025.76 ± 14,583.22 µm^2; p = 0.003), compared to cultures of WT littermates. To uncover the effect of a FMRP deletion *in vivo*, 30 µm slices were prepared derived from freshly removed hippocampi that were fixed and dehydrated. The tissue was prepared from 19 days old mice (postnatal day 19, P19) to match the developmental stage of the cultures. Since it was shown that the association of the mossy fiber synapse appears in the second postnatal week (Wilke et al., 2013), an additional analysis of the mossy fiber projection later in development (P30-40) was performed. Comparable to the phenotype found in cultures a widening of the mossy fiber projection appeared in *fmr1* KO hippocampal slices as well. Interestingly, the

widened projection only appeared in the very distal region (figure 8 E-F) which was previously described as an own subarea by itself. The widening of the mossy fiber projection distal to the DG can be correlated to the widen TE distribution along the apical dendritic tree at distal CA3 pyramidal neurons in *fmr1* KO cells compared to WT cells shown before (figure 5 A & D). The deletion of FMRP caused an elongation of the mossy fiber projection as well (figure 6 H, *fmr1* WT 844.94 ± 19.29 µm, n = 19; *fmr1* KO 940.09 ± 22.61 µm; p=0.003), leading to an overall increase of the mossy fiber projection area (figure 6 G, *fmr1* WT 21341.5 ± 828.83 µm^2, *fmr1* KO 940.09 ± 22.61 µm; p=0.003). An exaggerated phenotype was found at P19 where the synapse is still in the developing process. At P30-40 two things were found, 1st hippocampal slices of *fmr1* WT mice displayed a different expansion of the mossy fiber projection throughout the *cornu ammonis* generally. The width of the very distal part of the projection was decreased in comparison to control mice at P19 (figure 8 F & I). 2nd an alteration of the mossy fiber width and area was no longer detected under the influence of a FMRP KO (figure 8 I-J). Interestingly, the length of the mossy fiber projection was even altered controversy in comparison to the mossy fiber projection in P19 mice. Here, hippocampal slices of *fmr1* KO mice displayed a significantly reduced length of the projection (*fmr1* WT 928.81 ± 20.25 µm; *fmr1* KO 872.41 ± 14.77 µm, p=0.032). These results mainly match with an earlier publication; where the authors could show no alterations in the suprapyramidal mossy fiber projection obtained from Timm-stained hippocampal slices of adult mice (Mineur et al., 2002). This synapse is formed between LMTs and spines of the CA3 pyramidal neurons, the TEs in the *stratum lucidum*. As this synapse has been shown to be highly involved in pattern separation (Bakker et al., 2008), it is of special interest for an understanding of behavioral deficits in FXS patients. Since the mossy fiber projection is altered due to the deletion of FMRP the output synaptic compartments were investigated at the most pronounced time point at DIV14 as well.

3.7 Mossy fiber boutons are decreased in size in *fmr1* KO dentate gyrus granule cells *in vitro*

The synaptic outputs of DG granule cells are termed large mossy fiber terminals which form a projection from the DG throughout the CA3 into the CA2 area. They consist of mossy fiber boutons which build the excitatory contacts to thorny excrescences of CA3 pyramidal neurons and filopodial extensions that contact inhibitory interneurons

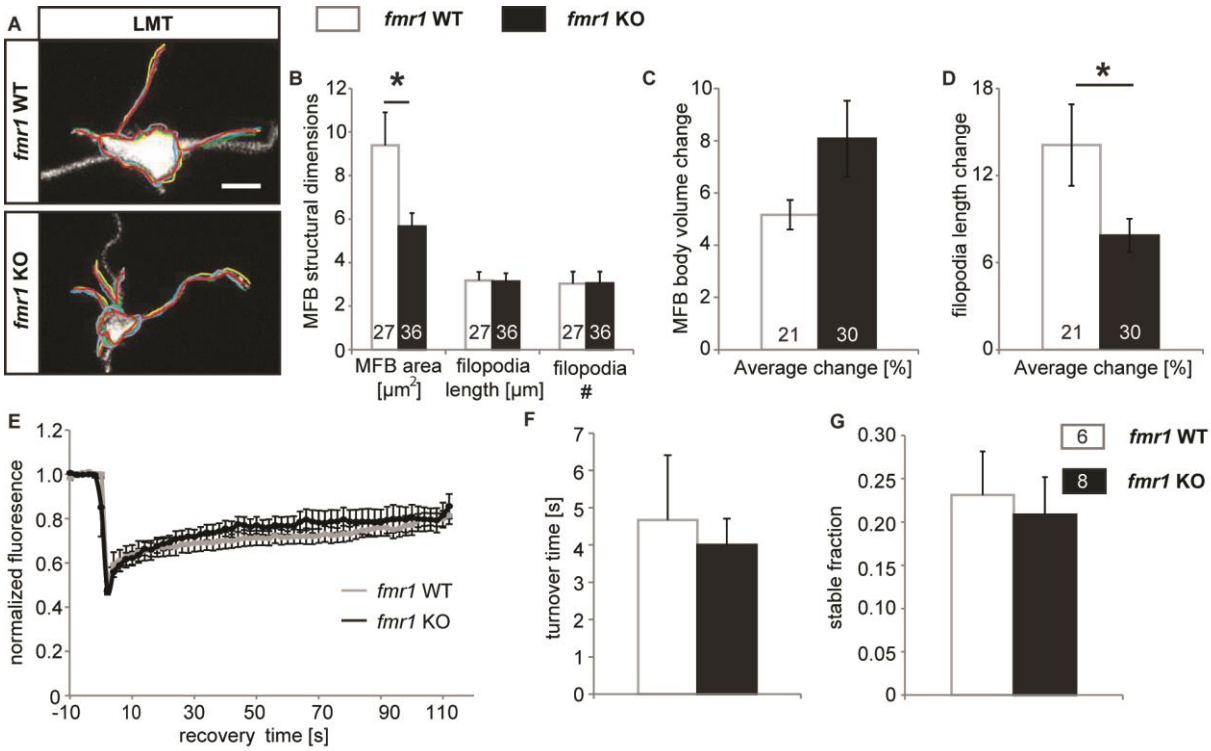

Figure 9: Large mossy fiber terminal morphology and actin dynamics in *fmr1* KO mice (**A**) Representative images of single LMTs in *fmr1* KO and WT DIV14 hippocampal slice cultures (colored lines indicate LMT body area/ filopodia length at different time points during time-lapse imaging; scale bar 2 µm); (**B**) quantification of LMT morphology at DIV14 (*fmr1* WT n = 27 LMTs of 7 mice; *fmr1* KO n = 35 LMTs of 10 mice); (**C**) analysis of mossy fiber bouton structural motility; DIV14, 5 min intervals, over a time period of 20 min (*fmr1* WT n = 21 LMTs of 6 mice; *fmr1* KO, n = 30 LMTs of 10 mice); (**D**) analysis of filopodia structural motility at DIV14 (*fmr1* WT n = 21 LMTs of 6 mice; *fmr1* KO n = 30 LMTs of 10 mice); (E) Course of the fluorescence recovery curves recorded after bleaching of eGFP-actin in LMT bodies (FRAP), (F) recovery time needed to reach 50 % of the basal fluorescence and (G) quantification of the stable fraction of actin filaments which do not recover within the imaged time window (*fmr1* WT n = 6 cells of 4 mice; *fmr1* KO n = 8 cells of 6 mice); data are presented as mean ± SEM; Student´s T-test, significances are indicated by *** p-value < 0.001, ** p-value < 0.01 and * p-value < 0.05.

(Blackstad and Kjaerheim, 1961; Hamlyn, 1962; Frotscher, 1985; Acsády et al., 1998). Therefore, the LMT morphology allows a feedforward excitation and inhibition of CA3 pyramidal neurons (Ruediger et al., 2011). Additionally, LMTs display an especially high amount of FXS granules where FMRP is concentrated (Akins et al., 2012). Thus, the morphology of LMTs is most likely tightly linked to their function. To reveal the influence of a FMRP KO on LMT morphology, DG granule cells were transfected with fGFP via the gene gun method.

While the bouton area was significantly decreased in *fmr1* KO cells (*fmr1* WT 9.38 ± 1.51 µm^2, *fmr1* KO 5.66 ± 0.61 µm^2; p = 0.02), the length and number of filopodia per LMT was not altered at DIV14 (figure 9 A-B). The analysis of the bouton motility did not reveal a significant change (figure 9 C) and only a tendency towards an increased motility could be found (*fmr1* WT 5.16 ± 0.56 %; *fmr1* KO 8.07 ± 1.45 %; p = 0.12). In contrast to this,

LMT filopodia did not display morphological changes per se but a significant decrease in motility (*fmr1* WT 14.09 ± 2.81 %, *fmr1* KO 7.87 ± 1.14 %; p = 0.049). As described above, actin dynamics are crucial for structural plasticity, therefore as a next step they were analyzed in the boutons of LMTs. DG granule cells were transfected with eGFP-actin to study the influence of a FMRP KO on LMT actin dynamics. The fluorescence recovery in LMT boutons did not reveal differences in actin dynamics between *fmr1* KO and WT cells, neither in the turnover time nor in the stable fraction (figure 7 E-G). These changes at single LMTs due to a deletion of FMRP can point to a broad defect of the mossy fiber projection as well. As the area of TEs was increased and LMT area was in contrast to this decreased, next it was analyzed whether this would be also reflected in the connectivity pattern between dentate gyrus and the CA3 region. Additionally, further hippocampus-dependent behavior and in detail dependent on the DG-CA3 pathway with the absence of FMRP was studied.

3.8 Increased connectivity between CA3 and DG is accompanied by altered behavior in *fmr1* KO mice

In this thesis was shown that the deletion of FMRP caused an increase in the number and size of TEs *in vivo* and *in vitro*, accompanied by a decrease of LMT area. Since in addition the AMPA receptor driven synaptic transmission was also increased, the question arose whether this effect is caused by an altered connectivity. Therefore, single CA3 pyramidal neurons in OHCs were electroporated with the DNA of a truncated form of wheat germ agglutinin (WGA) at DIV7. At DIV14 the cultures were fixed and afterwards immunohistochemically stained by taken advantage of an anti-Lectin antibody (Yoshihara et al., 1999). WGA is a plant lectin and is transported retrogradly and anterogradly to synaptic partners of the expressing cell. Therefore, it provides the opportunity to investigate the number of DG granule cells that are connected to the CA3 pyramidal neuron which was transfected. Supporting the hypothesis raised from the data obtained before, the connectivity was found to be significantly increased between CA3 pyramidal neurons and DG granule cells in *fmr1* KO OHCs, compared to WT OHCs (*fmr1* WT 5.30 ± 0.63, *fmr1* KO 8.33 ± 0.65; p=0.008). The increased amount of WGA positive DG granule cells point to a hyperconnectivity in the mossy fiber pathway in the absence of FMRP. Next, *fmr1* KO mice and WT littermates were tested in a modified Morris water maze paradigm.

In this thesis the focus lay on the hippocampal network and the alterations described here were located in an important pathway necessary for pattern separation and completion as well as spatial memory formation. The Morris water maze allows to study the capability of mice to form a spatial map. Since, the most prominent phenotype was found at an age of P19 the training started at this age as well. 19 days old mice are especially sensitive and the water temperature had to be set higher than room temperature (25 ± 1 °C) to avoid hypothermia. Additionally, a small maze was chosen with a diameter of 106 cm and a big platform with a diameter of 14 cm. Mice at this age, irrespective of the genotype, displayed a nervous behavior. A pretraining of 3 days was performed so that the mice could get

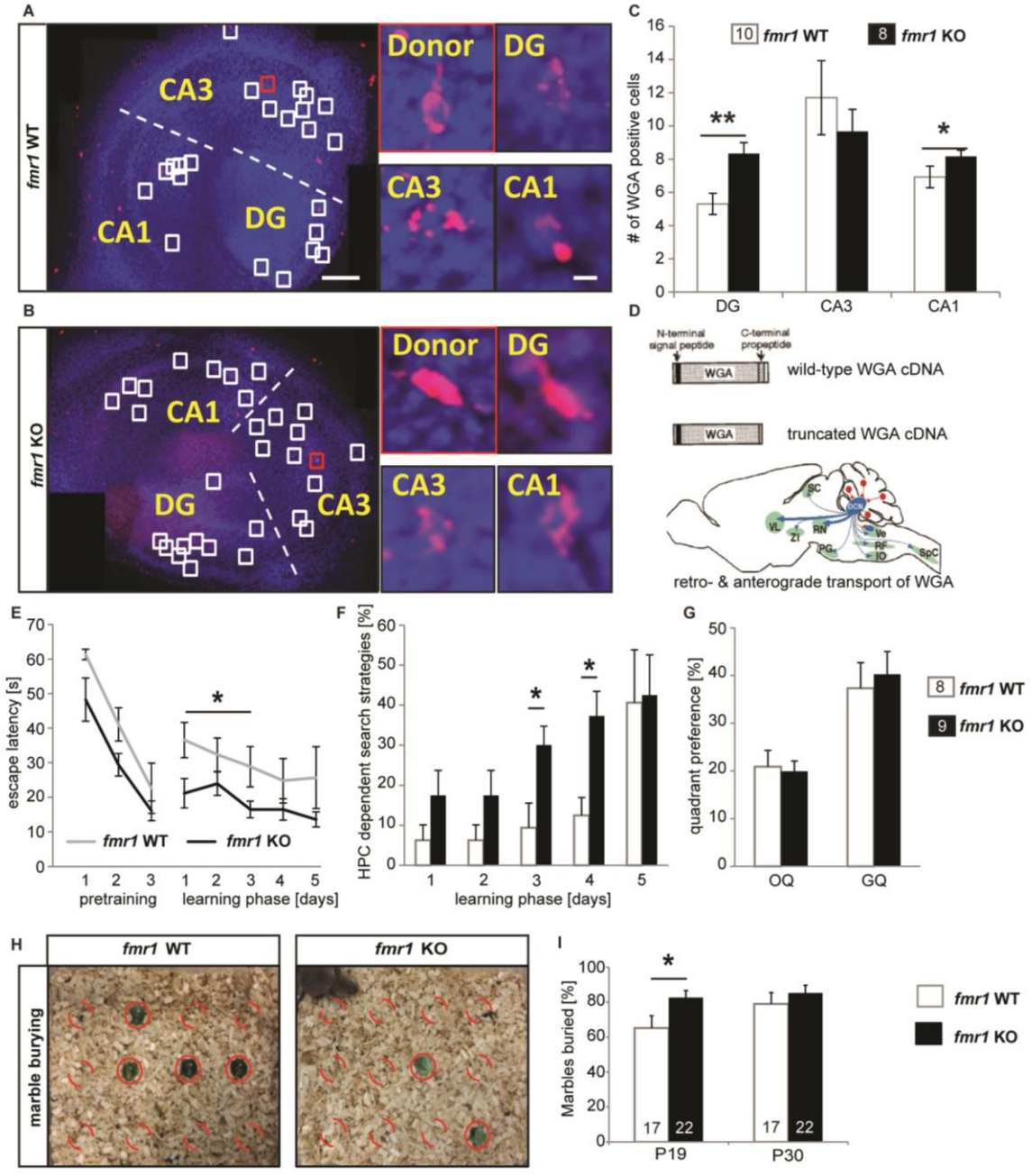

Figure 10: The connectivity of CA3 pyramidal neurons to DG granule cells is altered in *fmr1* KO mice accompanied with changes in hippocampus-dependent behavior.
(**A**-B) Single CA3 neurons in organotypic hippocampal slice cultures electroporated with a truncated WGA that was visualized using an anti-lectin antibody (red), nuclei labeled with DAPI (blue), (WGA positive cells are indicated in white boxes, scale bar 50 µm), high resolution images show the donor cell (WGA transfected CA3 pyramidal neuron) and examples of WGA-positive neurons in DG, CA3 and CA1 (scale bar 5 µm); (**C**) quantification of the number of WGA positive neurons of the distinct hippocampal subregions for both genotypes at DIV14 (*fmr1* WT n = 10 hippocampal slices of 4 mice; *fmr1* KO n = 8 hippocampal slices of 5 mice, p=0.008); (**D**) Structure of wildtype and truncated WGA, and its distribution upon the application to granule cells of the cerebellum (adapted from Yoshihiro et al., 1999); (**E**) course of the escape latency during 3 days of pretraining and 5 days of learning of both genotypes starting with an age of P19 in the Morris water maze; quantitative analysis of the hippocampus-dependent search strategies displayed by the mice; (**F**) quadrant preferences analyzed in the learn reverence test (probe trial) at day 6 (*fmr1* WT n = 8 mice; *fmr1* KO n = 9 mice); (**H**) representative examples of marbles buried at P19 for both genotypes; (**I**) quantification of the number of marbles buried by *fmr1* KO and WT mice at different ages (P19 *fmr1* WT n = 17 mice; *fmr1* KO n = 22 mice; P30 *fmr1* WT n = 17 mice; *fmr1* KO n = 22 mice); data are presented as mean ± SEM; Student´s T-test, significances are indicated by *** p-value < 0.001, ** p-value < 0.01 and * p-value < 0.05.

accustomed to the task and the handling by the experimenter. The mice had a maximum exploration time of 60 s. This task additionally allowed to rule out deficits in vision or exploratory behavior of the animals. The pretraining revealed no differences in exploratory behavior between *fmr1* KO and WT mice. In the learning phase, with a hidden platform, the FXS mouse model displayed a significant decrease in the escape latency at the first 3 days of training while there were no significant differences at the last 2 days (figure 10 D). The search strategies during the trials were analyzed, to obtain a detailed analysis of hippocampal function of the mice. The swimming patterns were categorized into different search strategies. While some search strategies are not hippocampus-dependent (random search, scanning and chaining), others depend on a correctly formed spatial map which includes directed search and direct swimming (Garthe et al., 2009). Mice that memorized the platform position display an increased proportion of hippocampus-dependent search strategies over time. Interestingly, the deletion of FMRP led to an increased proportion of hippocampus-dependent search strategies, already at day 1 which became significant at day 3 and 4 of training. The results supported the hypothesis of a premature hippocampal network in a critical time window in *fmr1* KO mice compared to WT littermates. At the last day in the learning phase neither the escape latency nor the proportion of hippocampus-dependent search strategies differed between *fmr1* KO and WT mice. Consistent with these results the memory reference test which was performed after the training period could not reveal any alterations in the quadrant preference due to a FMRP deletion (figure 10 F).

The Morris water maze task is a reliable method to study hippocampus-dependent learning. The disadvantage of the Morris water maze is the relatively long training time which renders the analysis of a specific age more difficult. Second the task was shown to be rather dependent on the Schaffer collateral pathway than the mossy fiber pathway (Aou et al., 2003).

To allow a more age specific hippocampus-dependent analysis the marble burying task (Poling et al., 1981; Broekkamp et al., 1986; Handley, 1991; Deacon, 2006) was used to assess stereotypic behavior in both *fmr1* WT and KO mice (figure 10 G-H). Additionally, the task is of special interest since symptoms of FXS patients include stereotypic behavior and excessive adherence to patterns (Cohen et al., 1988; Hernandez et al., 2009) which can also be observed in the FXS mouse model (The-Dutch-Belgian-Fragile-X-Consortium, 1994). In this respect, it is noteworthy that especially the mossy fiber pathway is known to be important for pattern completion (Leutgeb et al., 2007). Therefore, the mice were exposed to 12 marbles in a cage with high bedding and allowed to bury. The TE and mossy fiber projection phenotype could be detected at P19 only while it was absent at the later time point investigated (P30-P40). Therefore, mice of both ages were studied. Here, the deletion of FMRP led to a significantly increased number of marbles that were buried by *fmr1* KO animals compared to WT littermates (*fmr1* WT 65.20 ± 7.01, *fmr1* KO 82.58 ± 4.01, $p=0.033$). This effect was only found in young mice (P19) whereas both genotypes were indistinguishable at P30 (figure 10 H). A significant functional and structural effect was revealed on the synaptic output of DG granule cells in *fmr1* KO mice. To investigate a potential effect of the deletion of FMRP on the synaptic input as well, DG granule cell dendritic complexity and spine morphology were analyzed.

3.9 Dentate gyrus granule cells display an immature spine phenotype in *fmr1* KO mice

The dentate gyrus (DG) is the informational gateway into the hippocampus and has therefore been shown to be crucial for hippocampal function as for instance spatial and episodic memory formation (Doetsch and Hen, 2005; Ming and Song, 2005; Aimone et al., 2006). Research just recently started to reveal more and more the role of the dentate gyrus. In this respect, it was found that pattern separation relies on the DG (Kesner et al., 2000; Leutgeb et al., 2007). FXS patients as well as the mouse model displayed excessive adherence to patterns (Cohen et al., 1988; Garber et al., 2008; Hernandez et al., 2009),

pointing to an impairment of the DG.

Therefore, the morphology of dentate granule cells in *fmr*1 KO animals was analyzed first. For this purpose organotypic hippocampal slice cultures (OHCs) were transfected with fGFP via the gene gun method at least 24 h before imaging. Neuronal structures as well as structural plasticity were investigated at 14 days *in vitro* (DIV14).

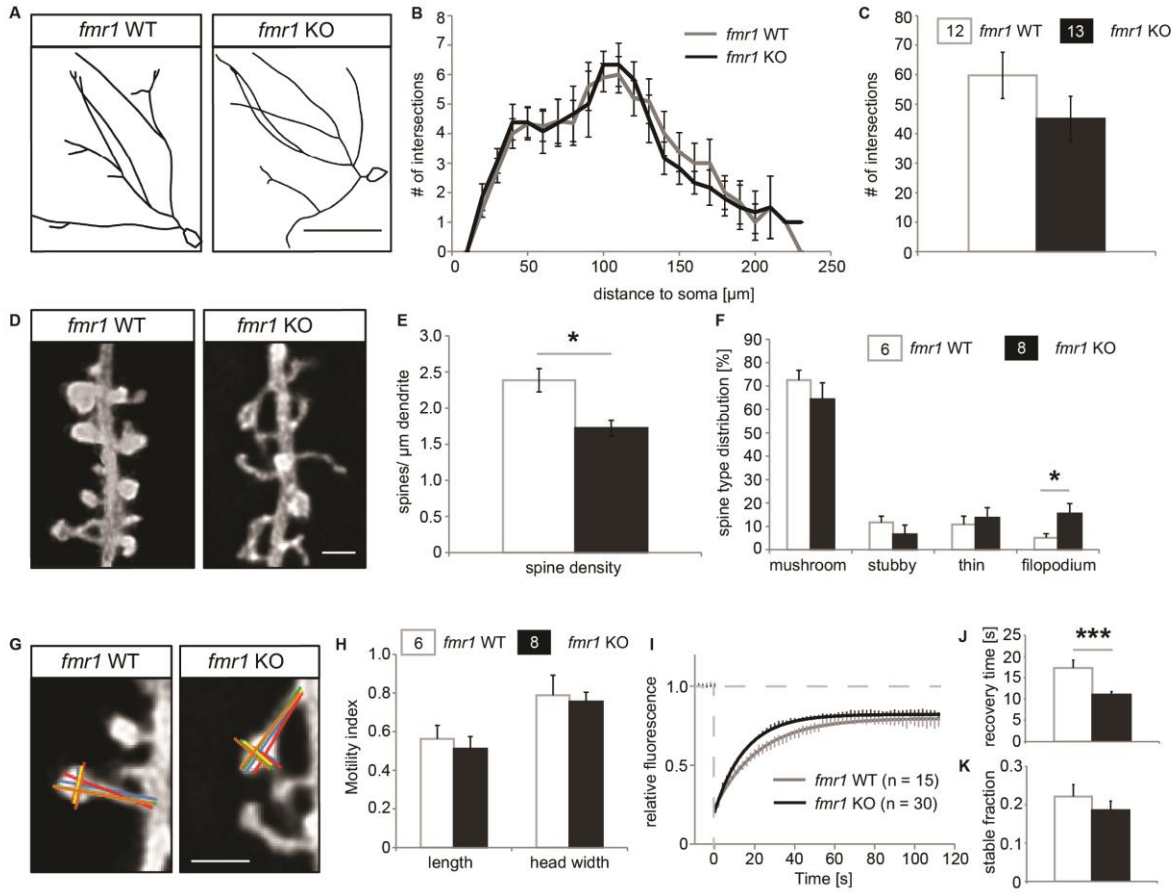

Figure 11: Granule cells of the DG show no defects in dendritic complexity but an increased proportion of immature spines and altered actin dynamics upon the deletion of FMRP. (A) Representative tracings of DG granule cells transfected with eGFP in DIV14 OHCs obtained from *fmr1* WT and KO mice, visualized by Neurolucida and Neuroexplorer (Microbrigthfield, scale bar 100 µm). (B) Quantitative analysis of dendritic complexity of DG granule cells, performed via Sholl analysis, in *fmr1* WT and KO OHCs. (C) Overall number of Sholl intersections of both genotypes (*fmr1* WT n = 12 cells of 8 mice; *fmr1* KO n = 13 cells of 8 mice). (D) Representative stretches of dendrites of DG granules cells transfected with eGFP at DIV14 in OHCs, obtained from *fmr1* WT and KO mice (scale bar 1 µm). (E) Quantitative analysis of the number of spines per µm dendrite of DG granule cells from *fmr1* WT and KO mice and (F) distribution of spine types of DG granule cells, classified as mushroom, stubby, thin and filopodium (*fmr1* WT n = 6 cells of 5 mice; *fmr1* KO n = 8 cells of 4 mice). (G) Representative spines and their length and head width motility, displayed by different colors for different time points (scale bar 1 µm). (H) Motility index (Bagni and Greenough, 2005; Sullivan et al., 2006; Chierzi et al., 2012) of spine length and spine head width changes, recorded every 5 min over a total of 20 min (*fmr1* WT n = 6 cells of 5 mice; *fmr1* KO n = 8 cells of 4 mice). (I) fluorescence recovery curves recorded after bleaching of eGFP-actin in dendritic spines (FRAP), (J) recovery time needed to reach 50 % of the basal fluorescence and (K) quantification of the stable fraction of actin filaments which did not recover within the imaged time window (*fmr1* WT n = 15 cells of 4 mice; *fmr1* KO n = 30 cells of 6 mice); data are presented as mean ± SEM; Student´s T-test, significances are indicated by *** p-value < 0.001, ** p-value < 0.01 and * p-value < 0.05.

The dendritic complexity, studied by Sholl analysis, showed no differences between *fmr1* WT and KO littermates (figure 11 A-C). Interestingly, a significant decrease in spine density was elucidated (figure 11 D-E; *fmr1* WT 2.38 ± 0.16 spines/µm dendrite, *fmr1* KO 1.72 ± 0.10 spines/µm dendrite; p = 0.02). The decreased number of spines per µm dendrite was accompanied by altered spine morphology (figure 11 F). *Fmr1* KO cells displayed an increased proportion of filopodia like spines in comparison to *fmr1* WT DG granule cells (*fmr1* WT 5.03 ± 1.82 %, *fmr1* KO 15.44 ± 4.28 %; p = 0.05). The question arose where the structural changes originate. Therefore, their motility with respect to spine length and head width was analyzed. The motility reflected the change in 5 min over a total of 20 min. The deletion of FMRP had no effect on structural plasticity neither of the length nor the head width (figure 11 G-H). While motility was not altered, actin dynamics in dendritic spines of *fmr1* KO were changed (figure 11 I). The dynamic actin cytoskeleton was studied by taking advantage of eGFP-actin which was expressed in single DG granule cells via single cell electroporation in OHCs. The GFP signal was bleached by a 405 nm laser and the recovery of the GFP fluorescence was determined as a read out of dynamic actin filaments due to actin polymerization. Here, the recovery time could be found to be significantly reduced in *fmr1* KO spines (*fmr1* WT 17.33 ± 1.86 s, *fmr1*KO 11.06 ± 0.71 s; p < 0.001) in comparison to *fmr1* WT cells in OHCs. Interestingly, the stable pool was not altered. While the recovery was initially slower in FMRP KO spines, the plateau level was the same. Here, a strong effect of the deletion of FMRP on the synaptic input, the dendritic spines, could be revealed.

DG granule cells and CA3 pyramidal neurons are extensively characterized (Lisman, 1999; Leutgeb et al., 2004), while the role of the directly adjacent CA2 pyramidal neurons remains so far largely elusive. They share several features with CA3 neurons but are still different in many aspects (Shinohara et al., 2012; Kohara et al., 2014) and less is known about their involvement into neurological diseases. Thus, the impact of a FMRP KO on the morphology of CA2 pyramidal neurons was documented as well.

3.10 TE-like spines along CA2 pyramidal neurons in *fmr1* KO mice exhibit an exaggerated phenotype

Classically, hippocampal function is described by the trisynaptic circuit. Here, the information is described to be transmitted from the entorhinal cortex to the dentate gyrus and further through CA3 and CA1 (Fujita, 1962; Andersen and Lømo, 1967; Herreras et

al., 1987; Remondes and Schuman, 2004). However, the hippocampus consists of another region the CA2 area which is functionally and morphologically distinguishable from its neighbors. The CA2 area is located between CA3 and CA1. Research started just recently to uncover the characteristics of the large pyramidal neurons in this area by taking advantage of newly developed antibodies. Still, findings are controversial with respect to neuron morphology and their role in the hippocampal pathways. In studies defining CA2 pyramidal neurons via cellular and anatomical criteria, CA2 neurons were described to receive strong afferents from the supramammillary nucleus (SUM) or from both ECII and ECIII innervating CA1 pyramidal cells. Additionally, they receive direct input from CA3

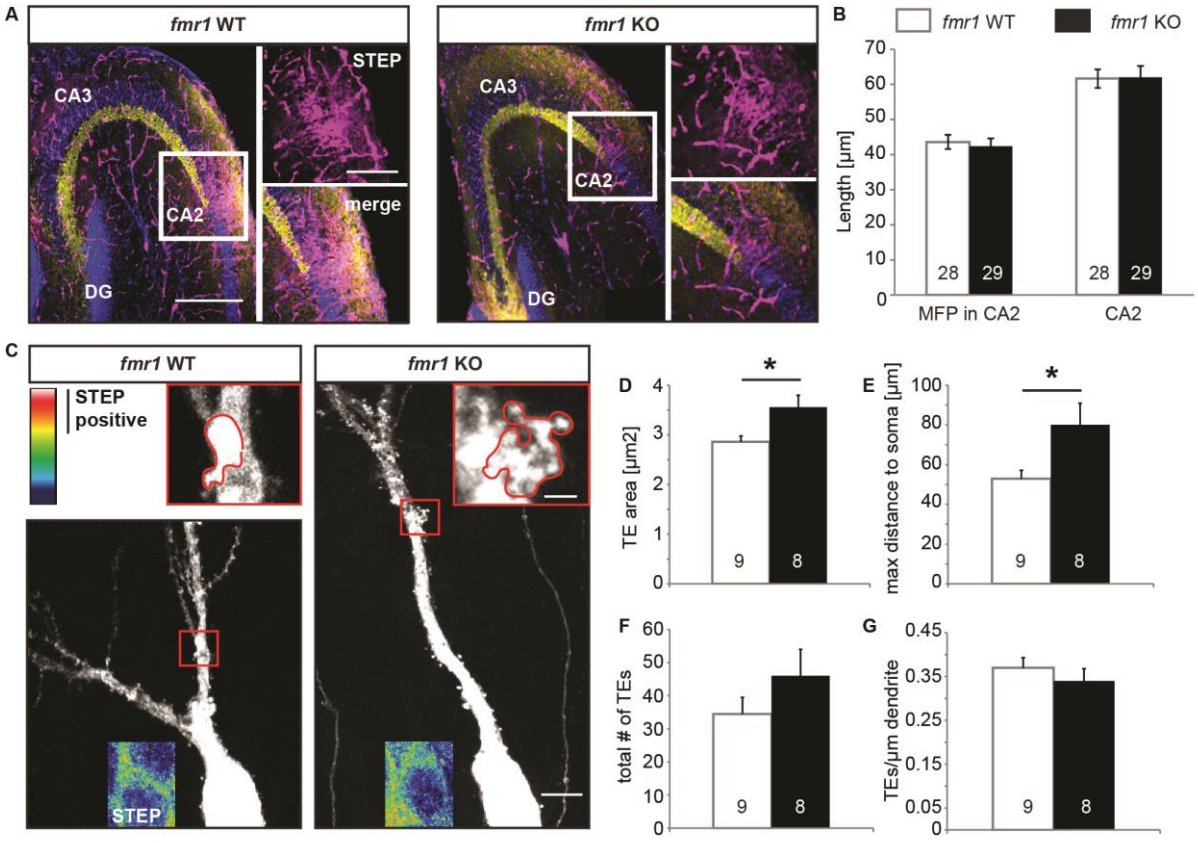

Figure 12: The deletion of FMRP has no effect on the CA2 area size but on the morphology of TE-like spines of its pyramidal neurons

(A) representative images of 30 µm hippocampal slices immunohistochemically stained against Synaptoporin (yellow), DAPI (blue) and STEP (red), white boxes show the merge zone of CA2 (STEP) and the mossy fiber projection (yellow) of both genotypes (scale bar 200 µm), white boxes are magnified at the right (scale bar 50 µm); (**B**) quantification of the length of the mossy fiber projection (MFP) entering the CA2 area and the length of the CA2 area (*fmr1* WT n = 28 slices of 5 mice; *fmr1* KO n = 29 slices of 8 mice); (**C**) representative images of the proximal apical part of CA2 pyramidal neurons (scale bar 20 µm), 16 color images of an anti-STEP staining revealing the cell as a CA2 pyramidal neuron, magnifications of red boxes are shown in the right upper corner (scale bar 2 µm); (**D-G**) quantification of TE area, the maximum distance of the farthest TE to the soma, total number of TEs per cell and TE density along the apical tree (*fmr1* WT n = 9 cells of 4 mice; *fmr1* KO n = 8 cells of 4 mice); data are presented as mean ± SEM; Student´s T-test, significances are indicated by *** p-value < 0.001, ** p-value < 0.01 and * p-value < 0.05.

pyramidal neurons which is dominated by feedforward inhibition (Haglund et al., 1984; Maglóczky et al., 1994; Bartesaghi and Gessi, 2004; Chevaleyre and Siegelbaum, 2010). Another recent study using specific molecular markers for CA2 pyramidal neurons found that granule cells of the DG project into CA2, while ECIII cells did not project directly to CA2. Here, CA2 pyramidal neuron efferents innervate both deep and superficial sublayers of CA1 pyramidal neurons (Kohara et al., 2014). The usage of molecular markers could additionally reveal that CA2 pyramidal neurons indeed display TE-like spines which is contrary to earlier studies as well (Lorente de Nó, 1934). In this thesis an anti-STEP antibody was used as a specific marker for CA2 pyramidal neurons (Kohara et al., 2014). The aim was to analyze whether the mossy fibers project into CA2 and whether CA2 pyramidal neurons would be affected by the deletion of FMRP. Above, it was indeed shown that the mossy fiber projection is drastically altered in a mouse model of the FXS (figure 8). The analysis of the projection width revealed a widening especially in the last 200 µm accompanied by an overall elongation of the projection. Additionally, the TE area along distal CA3 pyramidal neurons could be found to significantly widened as well *in vitro* and *in vivo* (figure 4 D & 5 E). As described earlier the mossy fiber projection was reaching into the CA2 area as well, thus the expansion of the CA2 area and the mossy fiber projection in the CA2 area were investigated. Therefore, hippocampal slices were prepared of P19 mice, the critical time point of an FMRP deletion found earlier, and immunohistochemically stained against Synaptoporin and STEP (figure 12 A). Also here, the results supported the finding that indeed DG granule cells project into the CA2 area (figure12 A). Here, the question arose whether the elongated mossy fiber projection found in *fmr1* KO mice was accompanied by an elongated CA2 area. Surprisingly, no effect on the CA2 region was found, neither the CA2 area nor the mossy fiber projection in CA2 were altered in *fmr1* KO mice compared to WT littermates (figure 12 B). Taken together, the results obtained by DAPI, anti-synaptoporin and anti-STEP staining uncovered an elongated mossy fiber projection accompanied by an elongated CA3 area in a mouse model of the FXS.

As a next step, STEP-positive pyramidal neurons were analyzed in greater detail. Therefore, single CA2 pyramidal neurons were filled with dye (AlexaFlour594) via single cell electroporation and directly afterwards fixed. The fixed OHCs were immunohistochemically stained against STEP to allow a correct identification of CA2 pyramidal neurons (figure 12 C). Only STEP-positive neurons were included into the analysis of TE-like spines along the proximal apical dendritic tree. The deletion of FMRP

caused a significant increase of the TE-like area (figure 12 D; *fmr1* WT 2.86 ± 0.12 µm^2, *fmr1* KO 3.55 ± 0.24 µm; p = 0.030), as well as an increase in the maximum distance to the cell body (figure 12 E; *fmr1* WT 52.94 ± 4.18 µm, *fmr1* KO 80.09 ± 10.82 µm; p = 0.044), compared to *fmr1* WT CA2 neurons. Interestingly, as shown before both TE area and maximum distance to the soma of the furthest TE were increased in CA3 pyramidal neurons of *fmr1* KO cultures as well, compared to *fmr1* WT cultures (figure 4 B & E). The total number of TE-like spines along CA2 pyramidal neurons and the number of TEs per µm dendrite displayed no differences between *fmr1* KO and WT cells.

Generally, in *fmr1* WT cultures the area of TE-like spines in CA2 was decreased in comparison to the TE area along CA3 pyramidal neurons (figure 12 D; 5 B). Contrary, the maximum distance to the soma, number of TE-like spines and TE-like spine density was higher at CA2 pyramidal neurons, compared to CA3 cells in *fmr1* WT cultures (figure 12 E - G; 4 C –E).

Taken together, CA2 pyramidal neurons identified by an anti-STEP staining, displayed TE-like spines that were altered by a deletion of FMRP comparable to TEs of CA3 pyramidal neurons. Additionally, the widen mossy fiber area (figure 8 B) in this area went together with an increase of the maximum distance of the furthest TE-like spine to the soma, caused by the absence of FMRP. Until this point this study provided new insights into the hippocampal circuits and the misregulation that arose from the deletion of FMRP. As described earlier all the excitatory cells investigated interact with pyramidal neurons of the CA1 area which plays an important role for spatial memory formation. Thus, CA1 pyramidal neuron dendritic and spine morphology were investigated in *fmr1* KO and WT mice.

3.11 Basal dendritic complexity is increased at CA1 pyramidal neurons of *fmr1* KO compared to WT mice *in vivo*

Throughout the hippocampus and even throughout the entire central nervous system the CA1 area is the most investigated brain area which is also reflected in of the number of publications found on google scholar (google). While the number of publications found for CA1 is 360,000 those about the CA3 region or cortical layers count less than half. Multiple methods were developed using and investigating the CA1 area throughout the last decades by taking advantage of its functional and morphological characteristics. Additionally, the CA1 area was found to be highly essential for learning and memory

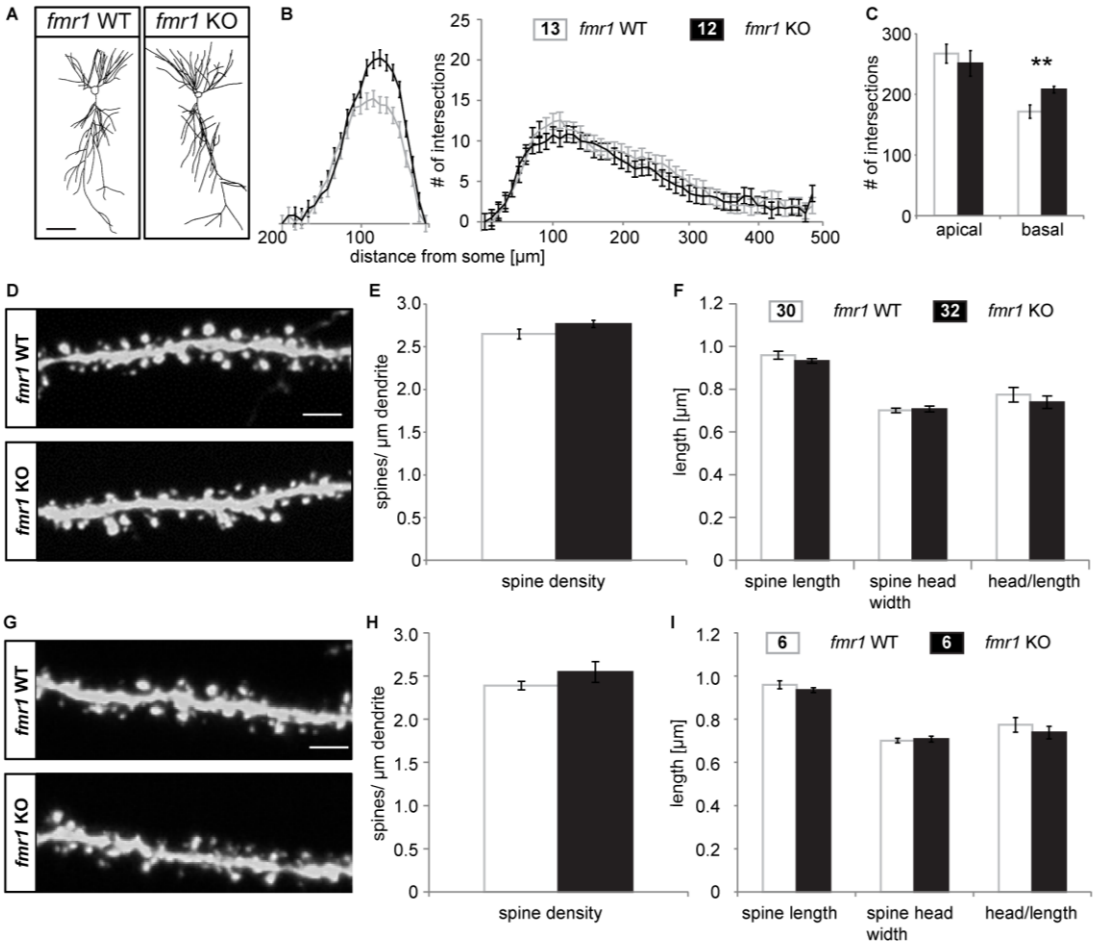

Figure 13: CA1 pyramidal neurons display a defect in the complexity of the basal dendrites upon the deletion of FMRP, while spine morphology is not altered *in vivo*
(A) Representative tracings of CA1 pyramidal neurons expressing eGFP obtained from brain slices of *fmr1* WT and KO mice both heterozygous for eGFP, visualized by Neurolucida and Neuroexplorer (scale bar 100 µm). (**B**) Quantitative analysis of the basal and apical dendritic complexity, performed via Sholl analysis, in *fmr1* WT and KO OHCs. (**C**) Overall number of Sholl intersections of both genotypes (*fmr1* WT n = 13 cells of 4 mice; *fmr1* KO n = 12 cells of 4 mice); (**D**) Representative stretches of apical dendrites of CA1 pyramidal neurons expressing eGFP, obtained from *fmr1* WT and KO mice (scale bar 1 µm). (**E**) Quantitative analysis of the number of spines per 1 µm dendrite apical of CA1 pyramidal neurons in brain slices of *fmr1* WT and KO mice and (**F**) spine morphology determined by spine length, head width and the ratio of spine head to spine length (*fmr1* WT n = 30 cells of 4 mice; *fmr1* KO n = 32 cells of 4 mice); (**G**) Representative stretches of basal dendrites of CA1 pyramidal neurons expressing eGFP, obtained from *fmr1* WT and KO mice (scale bar 1 µm). (**H**) Quantitative analysis of the number of spines per 1 µm dendrite basal of CA1 pyramidal neurons in brain slices of *fmr1* WT and KO mice and (**I**) spine morphology determined by spine length, head width and the ratio of spine head to spine length (*fmr1* WT n = 6 cells of 3 mice; *fmr1* KO n = 6 cells of 3 mice); data are presented as mean ± SEM; Student´s T-test, significances are indicated by *** p-value < 0.001, ** p-value < 0.01 and * p-value < 0.05.

formation, reflected by its indispensability for the formation of a spatial map in mice performing the Morris water maze (Aou et al., 2003). Since CA1 pyramidal neurons are computationally wired downstream of all other hippocampal areas, the phenotypes described here for the DG and CA3 might have affected the CA1 area as well. To complete the detailed analysis of dendritic complexity and spine morphology in the mouse

hippocampus caused by the absence of FMRP the CA1 area was investigated as well. Previous studies already faced the question how function and morphology are altered in CA1 pyramidal neurons in the fragile X syndrome. Interestingly, results on dendritic spine number and morphology are controversial. While some cases revealed an immature spine phenotype correlated with behavioral and cognitive deficits, others could not found differences compared to healthy tissue (Rudelli et al., 1985; Wisniewski et al., 1985; Hinton et al., 1991; Wisniewski et al., 1991; Comery et al., 1997; Irwin et al., 2000; Greenough et al., 2001; Irwin et al., 2001a; Nimchinsky et al., 2001; McKinney et al., 2005; Cruz-Martin et al., 2010; Bhakar et al., 2012; Portera-Cailliau, 2012; He and Portera-Cailliau, 2013). Different types of tissue were investigated ranging from primary dissociated cultures of the FXS mouse model to *in vivo* and analysis of human brain slices.

In this study both hippocampal slices and organotypic hippocampal slice cultures of *fmr1* KO mice (The-Dutch-Belgian-Fragile-X-Consortium, 1994) were used. As a first step, brain slices were obtained from *fmr1* WT and KO mice expressing GFP under the Thy1 promotor, allowing the analysis of dendritic spines at CA1 pyramidal neurons (figure 13 A). First, CA1 pyramidal neurons were analyzed with respect to dendritic complexity using the Sholl analysis (figure 13 A-B). While the deletion of FMRP had no effect on the dendritic complexity of apical dendrites basal dendrites displayed a significantly increased complexity in the first 100 µm from the soma (figure 13 B-C; *fmr1* WT 171.77 ± 11.09, *fmr1* KO 207.80 ± 5.59 µm; $p = 0.019$).
As described in previous studies (Grossman et al., 2006; Levenga et al., 2011; He and Portera-Cailliau, 2013), the spine density at apical and basal dendrites were investigated as well as the dimensions of single spines. Neither the number of spines per µm dendrite nor spine morphology differed between *fmr1* WT and KO mice at apical and basal dendrites of CA1 pyramidal neurons (figure 13 D-I). As a next step, an *in vitro* approach was used to uncover deficits in synaptic function of CA1 pyramidal neurons in *fmr1* KO mice.

3.12 Activity-dependent structural plasticity is impaired in a mouse model of the FXS

The *in vivo* study revealed no differences in the morphology or number of dendritic spines along the apical and basal dendritic tree, while the complexity of basal dendrites but not apical dendrites was increased. Therefore, the *in vitro* studies were performed at spines at

basal dendrites. Here, organotypic hippocampal slice cultures (OHCs) provide a suitable model to investigate neuronal morphology. As the spine morphology was not altered at apical and basal dendrites of *fmr1* KO cells under baseline conditions, the reaction to activity-dependent structural plasticity was analyzed. Since only basal dendrites of CA1 pyramidal neurons displayed an altered dendritic complexity upon the deletion of FMRP, spines along basal dendrites were investigated further. It was previously shown that the induction of LTP induces spine head growth accompanied with receptor insertion (Matsuzaki et al., 2004; Holtmaat and Svoboda, 2009). As discussed earlier FMRP is an important mRNA binding protein, interacting with several mRNAs of proteins that could be crucial for structural plasticity upon LTP. Therefore, CA1 pyramidal neurons in OHCs were transfected with fGFP via single cell electroporation at DIV11. At DIV14 OHCs were transferred into a recording chamber perfused with carbonated aCSF at 35°C. After 20 min of preincubation a stretch of dendrite was imaged. For spine motility, time-lapse imaging was performed every 5 min over a total 20 min. To induce chemical LTP, 10 mM glycine in aCSF was perfused into the recording chamber for 10 min. After additional 60 min in aCSF the same stretch of dendrite was imaged again (figure 14 A). The deletion of FMRP had no effect on the spine density at basal dendrites under baseline conditions as well as after the induction of cLTP (figures 14 B). The morphology of single spines was analyzed as well, they were classified as described before into mushroom, stubby and thin spines (Zagrebelsky et al., 2005). Under baseline conditions no differences between *fmr1* WT and KO cells were found in spine phenotypes. The induction of cLTP led to an increase of mushroom spines in OHCs obtained from *fmr1* WT mice (*fmr1* WT baseline 69.91 ± 3.92, *fmr1* WT cLTP 80.85 ± 2.84 µm; $p = 0.039$), accompanied by a reduction in the proportion of thin and stubby spines which was not significant. Spines displaying a filopodia-like structure were not changed in *fmr1* WT cells upon the induction of cLTP. In contrast, cells in OHCs from *fmr1* KO mice displayed an impairment in activity-dependent structural plasticity as the increase in mushroom spines found in the *fmr1* WT could not be detected (figure 14 C). Therefore, following LTP induction a significant difference in the proportion of mushroom spines between WT and *fmr1* KO neurons was found (*fmr1* WT cLTP 80.85 ± 2.84 µm, *fmr1* KO cLTP 65.44 ± 5.59 µm; $p = 0.028$). Hence, the proportions of stubby and thin spines were significantly increased in *fmr1* KO cells that were exposed to glycine, compared to WT neurons (*fmr1* WT cLTP stubby 4.29 ± 1.50 µm, *fmr1* KO cLTP 12.12 ± 2.90 µm; $p = 0.030$; *fmr1* WT cLTP thin 5.47 ± 1.38 µm, *fmr1* KO cLTP 15.53 ± 4.36 µm; $p = 0.048$). The significantly reduced proportion

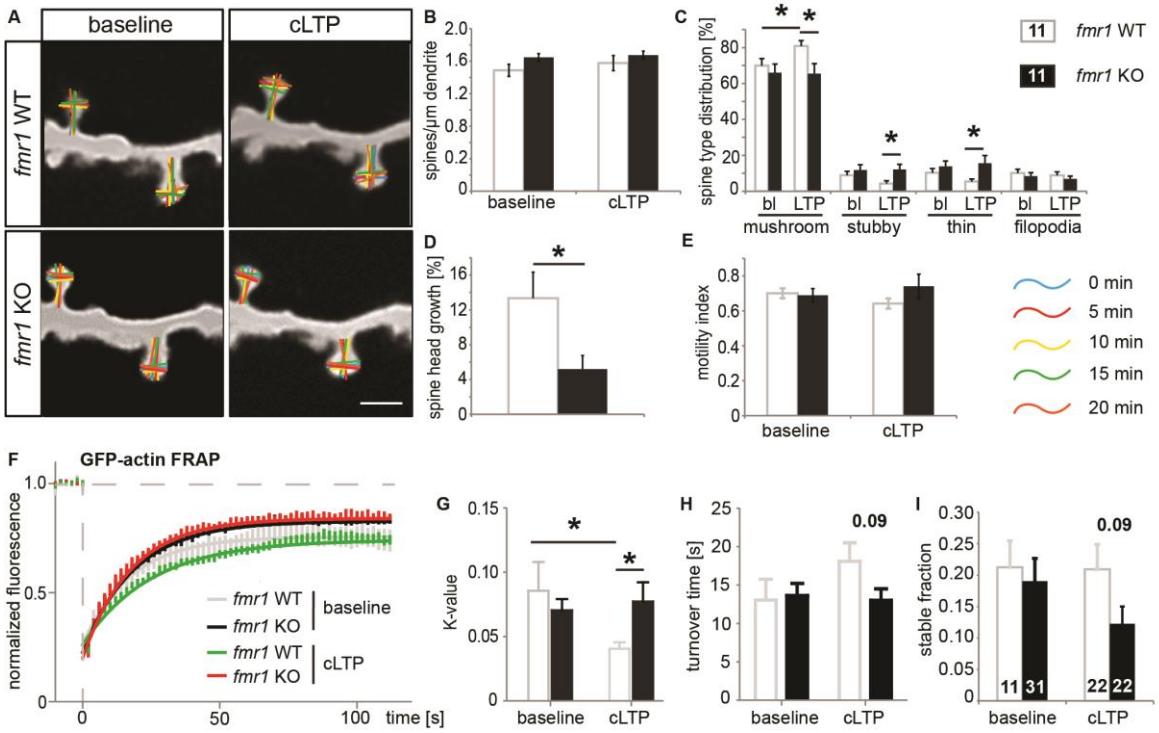

Figure 14: Dendritic spines of CA1 pyramidal neurons show a more immature phenotype, accompanied by altered actin dynamics upon the induction of LTP in *fmr1* KO cells

(A) Representative stretches of basal dendrites of CA1 pyramidal neurons in OHCs (DIV14) transfected with eGFP obtained from *fmr1* WT and KO mice, colored lines display the motility of the spine length and head width (scale bar 1 µm). (**B**) Quantitative analysis of the spine density in *fmr1* WT and KO OHCs under baseline conditions and upon induction of cLTP via glycine. (**C**) distribution of spine types categorized in mature and immature morphology under baseline conditions and upon the induction of cLTP via glycine application; (**D**) Quantitative analysis of the % spine head growth after induction of cLTP in both (**E**) motility index of spines at basal dendrites of CA1 pyramidal neurons in OHCs of *fmr1* WT and KO mice under baseline conditions and upon the induction of cLTP (*fmr1* WT n = 11 cells of 6 mice; *fmr1* KO n = 11 cells of 6 mice); (**F**) recovery curve of spines at basal dendrites expressing eGFP-actin under baseline conditions and upon induction of cLTP at DIV 14 (**G**) K-value displaying the curve course of the fluorescence recovery under baseline conditions and upon induction of cLTP via glycine application; (**H**) turnover time in s under baseline conditions and upon induction of cLTP (**I**) quantification of the stable fraction of actin filaments which do not recover within the imaged time window under baseline conditions (*fmr1* WT n = 11 spines of 3 mice; *fmr1* KO n = 28 spines 5 mice) and upon induction of cLTP via application of glycine (*fmr1* WT n = 22 spines of 3 mice; *fmr1* KO n = 22 spines of 4 mice); data are presented as mean ± SEM; Student´s T-test, for FRAP experiments are displayed via non-linear regression and tested with a two-way ANOVA combined with a Bonferroni post-hoc test; significances are indicated by *** p-value < 0.001, ** p-value < 0.01 and * p-value < 0.05.

of mushroom spines in *fmr1* KO cells was as well reflected in the spine head growth upon cLTP. Here, single dendritic spines were analyzed with respect to the percentage of spine head growth following cLTP induction. While cells of *fmr1* WT mice displayed a spine head increase of 13.33 ± 3.00 %, FMRP depleted cells only showed a spine head growth of 5.19 ± 1.57 % (figure 14 D, p = 0.026). Taken together, the deletion of FMRP had no effect on spine morphology under baseline conditions; however structural plasticity was impaired in these cells. Interestingly, spine head motility was not altered; neither under

baseline conditions nor upon cLTP induction (figure 14 E). As a next step, actin dynamics of spines along basal dendrites of CA1 pyramidal neurons were investigated. Therefore, single neurons were transfected with eGFP-actin. The induction of cLTP caused a significantly altered K-value meaning different courses of the fluorescence recovery (K-value *fmr1* WT baseline 0.09 ± 0.02, *fmr1* WT cLTP 0.04 ± 0.01; p = 0.015), accompanied by an increase of the turn-over time in WT cells (figure 14 F-H; *fmr1* WT baseline 15.02 ± 3.46 s, *fmr1* WT cLTP 26.86 ± 6.572 s; p = 0.230). The amount of stable actin was not affected by cLTP induction in WT cells (figure 14 I), therefore a deceleration of actin dynamics appeared which supports earlier findings (Fukazawa et al., 2003; Bramham, 2008). While in the early phase of LTP the actin network is more plastic possibly to allow spine head expansion at a later time point, analyzed here, actin polymerization rates are reduced. The actin dynamics in *fmr1* KO cells were unaltered compared to WT cells under baseline conditions. Interestingly, *fmr1* KO cells did not show the activity-dependent significant changes in actin dynamics observed in WT neurons (figure 14 F-I).

Taken together a detailed analysis about mainly structural consequences on excitatory neurons of the hippocampus were investigated in *fmr1* KO mice. After the effect of a FMRP deletion on hippocampus-dependent behavior was already studied in young mice (P19) using the Morris water maze paradigm, the same was analyzed in adult mice as well.

3.13 The deletion of FMRP facilitates relearning in the Morris water maze task

To study the effect of a FMRP deletion on hippocampus-dependent behavior in adult mice, 3 months old *fmr1* WT and KO mice were exposed to the Morris water maze task accomplished as described earlier (figure 15 A). The data found, provide the information of both the capability to form long- and short-term memory. Therefore, the first trials per day were compared for memory progress from day to day only (figure 15 D), the average of 4 trials a day reflects the memory progress during the training (figure 15 E). In both cases no differences were found between *fmr1* KO and WT mice regarding the escape latency needed to find the platform (figure 15 D-E). Still, both genotypes were able to learn the platform position, displayed by a significant decrease of the escape latency from learning day 1 to 8 (*fmr1* WT $p < 0.001$, $F = 9.116$; *fmr1* KO $p < 0.001$, $F = 8.650$, one-

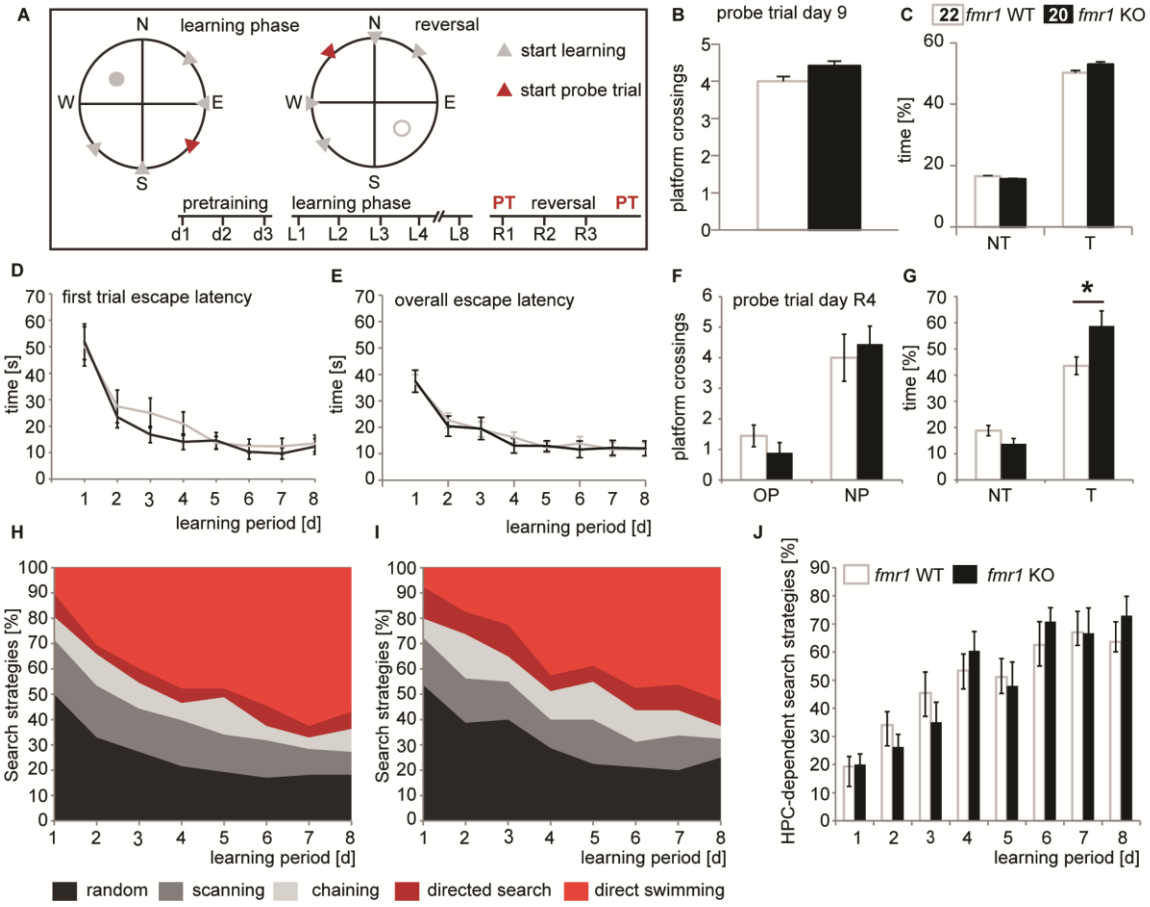

Figure 15: The deletion of FMRP has no effect on the formation hippocampus-dependent memory but on the relearning in the Morris water maze task
(A) Schematic drawing of the experimental procedure and construction of the Morris water maze (circles divided in quadrants of the learning phase and the reversal experiments), starting positions are marked with grey arrow heads, starting positions of probe trials after the learning phase and reversal experiments are marked with red arrow heads, the platform position of the learning phase is shown by a grey filled circle, the platform position of the reversal experiment is displayed by an empty grey circle; (**B**) quantitative analysis of the platform crossings in the probe trial at day 9 of both genotypes and (**C**) the proportion of time spent in the target quadrant (T) and in the other quadrants (NT) by *fmr1* WT and KO mice; (**D-E**) escape latency in s of the first trial per day only and the average of 4 trials per day during 8 days of training of both genotypes; (**F-G**) quantitative analysis of the platform crossings with the old platform position (of the learning phase) and the new platform position in the reversal experiment; and the proportion of time spent in the target quadrant (T) and the other quadrants (NT); (**H)** Proportion of search strategies displayed by the *fmr1* WT and (**I**) KO mice during 8 days of training; (**J**) Quantitative analysis of the proportion of hippocampus-dependent search strategies during 8 days of training displayed by both genotypes (*fmr1* WT n = 22 mice; *fmr1* KO n = 20 mice); data are presented as mean ± SEM; Student´s T-test; significances are indicated by *** p-value < 0.001, ** p-value < 0.01 and * p-value < 0.05.

way ANOVA repeated measures). The memory reverence test performed at day 9 uncovered no effect of a FMRP deletion on the learning capability. Here, the platform was removed and the number of potential platform crossings (figure 15 D) and the time spent in the target quadrant (figure 15 C) analyzed. To investigate the relearning capability of the mice a reversal task was performed. After the memory reverence test, the platform was placed opposite to the previous position. The mice went through 4 trials per day on 3

consecutive days, starting from 4 semi-random chosen starting positions (figure 15 A, reversal). At the 4th day of the reversal training the platform was again removed to perform a memory reverence test. Here, both the crossings of the old platform position and the crossings of the new platform position did not reveal any differences between *fmr1* KO and WT mice (figure 15 F). Investigating the time spent in the distinct quadrants of the maze showed that *fmr1* KO mice spent significantly more time in the quadrant of the new platform, compared to WT littermates (figure 15 G, *fmr1* WT 43.54 ± 3.36 %, *fmr1* KO 58.66 ± 5.81 %; $p = 0.049$). To uncover effects on hippocampus-dependent learning in greater detail the swimming tracks of the mice were studied and categorized into search strategies. Both genotypes showed first a high proportion of hippocampus-independent search strategies, decreasing with learning days accompanied by a continuous increase in hippocampus-dependent search strategies (figure 15 H-J; *fmr1* WT $p < 0.001$, $F = 8.369$; *fmr1* KO $p < 0.001$, $F = 5.464$ one-way ANOVA repeated measures; interaction $p = 0.9871$ two-way ANOVA). Here, the deletion of FMRP had no significant effect on the learning behavior of the mice. Until now very young mice (P19-30) and young adult mice (3 months old) were analyzed with respect to their learning capability in the Morris water mate task. While the young *fmr1* KO mice learned the platform position faster compared to WT littermates; in adult animals (3 months old mice) no differences could be found between both genotypes (figure 10 E-F, 15 H-J). *Fmr1* KO mice during development and in adulthood were studied before, however, information about aging in these animals is still missing. Here, as a first step the capability of hippocampus-dependent learning of mice lacking the *fmr1* gene was investigated.

3.14 Aged mice lacking the *fmr1* gene display normal learning capabilities in the Morris water maze task

FXS is a disorder which emerges first during development in patients. Therefore, the developmental time period is also the most studied, leaving patients and their families with no expertise what to expect during the aging process in this disorder, including life expectancy or cognitive abilities. Some studies showed that males with an *fmr1* premutation (Strehl et al. 2014) starting already in their 40s to develop progressively more severe problems in performing tasks for working memory, but not visual-spatial memory (Cornish et al., 2009). Additionally, some studies revealed an increased

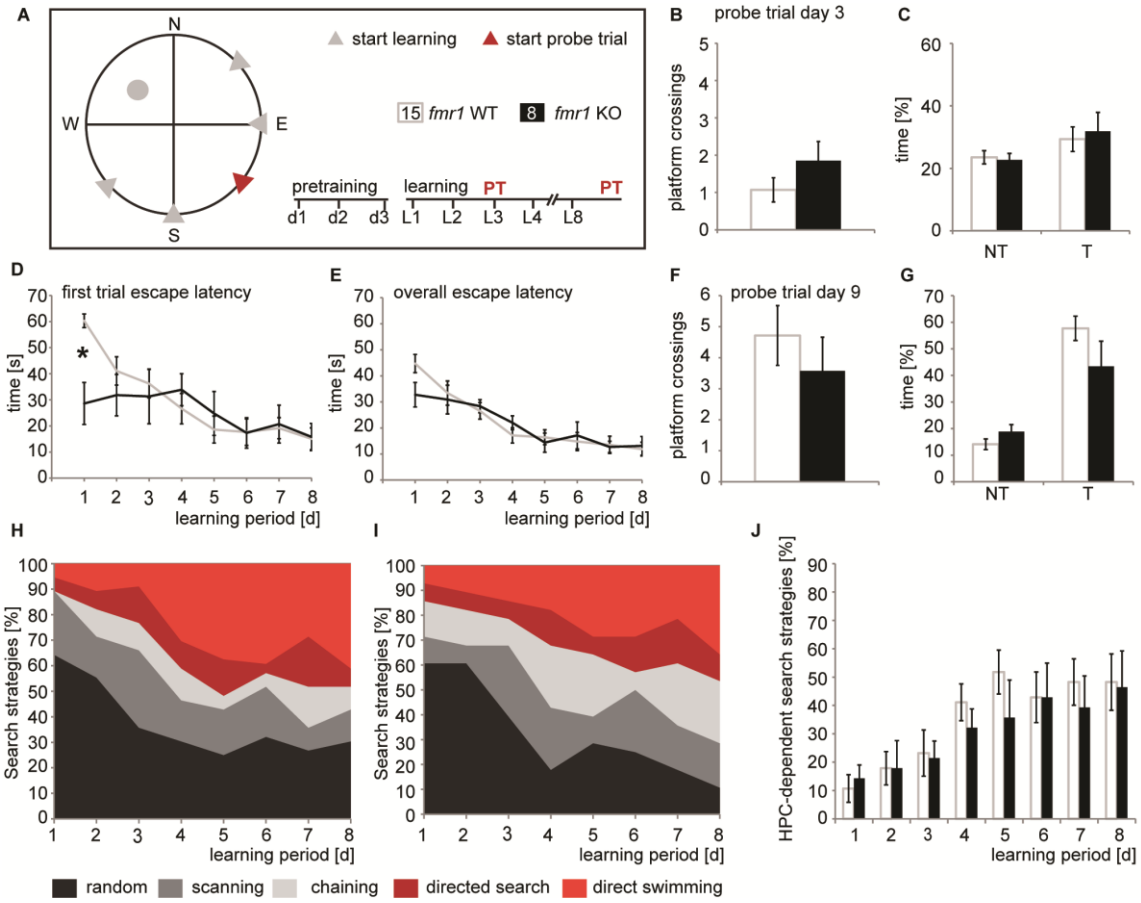

Figure 16: The deletion of FMRP has no effect on the formation hippocampus-dependent memory in the Morris water maze task in 19 months old mice
(A) Schematic drawing of the experimental procedure and construction of the Morris water maze (circles divided in quadrants of the learning phase), starting positions are marked with grey arrow heads, starting positions of probe trials at day 3 and 9 are marked with red arrow heads, the platform position of the learning phase is shown by a grey filled circle; (**B**) quantitative analysis of the platform crossings in the probe trial at day 3 of both genotypes and (**C**) the proportion of time spent in the target quadrant (T) and in the other quadrants (NT) by *fmr1* WT and KO mice; (**D-E**) escape latency in s of the first trial per day only and the average of 4 trials per day during 8 days of training of both genotypes; (**F-G**) quantitative analysis of the platform crossings at day 9; and the proportion of time spent in the target quadrant (T) and the other quadrants (NT); (**H**) Proportion of search strategies displayed by the *fmr1* WT and (**I**) KO mice during 8 days of training; (**J**) Quantitative analysis of the proportion of hippocampus-dependent search strategies during 8 days of training displayed by both genotypes (*fmr1* WT n = 15 mice; *fmr1* KO n = 8 mice); data are presented as mean ± SEM; Student´s T-test; significances are indicated by *** p-value < 0.001, ** p-value < 0.01 and * p-value < 0.05.

risk for progressive cerebellar ataxia, tremor and dementia (Hagerman et al., 2001; Brunberg et al., 2002; Cornish et al., 2009). Taken all these together the mouse model of the FXS can deliver important information about brain function during aging. To obtain a first look into hippocampal function, the Morris water maze task was performed with 19 months old mice, with both *fmr1* KO and WT genotypes. The first trial on every day was compared between *fmr1* KO mice and WT littermates, to analyze the learning process day per day. Here, a significant decrease of the escape latency was found in *fmr1* KO mice

compared to WT mice (Figure 16 D). While the first day revealed differences between both genotypes the course of the learning process was not altered with respect to the escape latency in the first trial (*fmr1* WT $p < 0.001$, $F = 8.775$, *fmr1* KO $p = 0.003$, $F = 4.026$ one-way ANOVA repeated measures; interaction $p = 0.5496$ two-way ANOVA). The average learning progress during the training were displayed by the average escape latency of trials a day, showed not differences between *fmr1* KO and WT mice (figure 16 E). The analysis of the search strategies displayed by the mice showed no significant differences between the genotypes (figure 16 H-J). Mice of both genotypes significantly increased the proportion of hippocampus-dependent search strategies from learning day 1 to 8, accompanied by a decrease in hippocampus-independent search strategies. Interestingly, at day 8 aged mice (19 months old) displayed only 46-48 % of hippocampus-dependent search strategies while the young adult mice (3 months old) showing 63-73% hippocampus-dependent search strategies (figure 16 H-J, figure 15 H-J). Two memory reverence tests were applied. After 3 days no significant preference for the target quadrant was found in mice of both genotypes accompanied by a low number of platform crossings (figure 16 B-C). At day 9 of the learning phase both *fmr1* KO mice and WT littermates displayed a high number of platform crossings showing no significant difference between the genotypes (figure 16 F). The analysis of the quadrant preference revealed no effect of a FMRP deletion as well (figure 16 G). Taken together, the deletion of FMRP had no effect on 19 months old mice with respect to hippocampus-dependent memory formation in the Morris water maze task. A strong behavioral phenotype was elucidated only in very young mice (P19-30).

4. Discussion

The fragile X syndrome (FXS) is the most common monogenetic cause of autism (Hagerman and Hagerman, 2002) and reflects the tight regulation of synaptic function. The lack of only one protein, here FMRP, interferes with normal brain development and cellular function leading to hyperactivity, stereotypic behavior and excessive adherence to patterns in patients (Cohen et al., 1988; Hernandez et al., 2009). To investigate the detailed cellular mechanisms causing these phenotypes and in order to develop possible treatments a mouse model was designed already in the early 90s of the 20th century carrying a knockout of the *fmr1* gene (The-Dutch-Belgian-Fragile-X-Consortium, 1994). Several characteristics of FXS were found in the mouse model as well. Both patients and the mouse model do not display any gross neuroanatomical alterations, therefore, research focused early synaptic structures, and indeed an apparent defect in dendritic spine morphology was revealed in several brain regions (Portera-Cailliau, 2012; He and Portera-Cailliau, 2013). Since then several studies tried to correlate the behavioral phenotypes found in FXS to altered synaptogenesis which is characterized by changes in spine number, spine morphology and stability (Comery et al., 1997; Irwin et al., 2000; Huber et al., 2002; Cruz-Martin et al., 2010; Thomas et al., 2011; Portera-Cailliau, 2012; He and Portera-Cailliau, 2013). Neurons of several brain regions were investigated but still findings are controversial while numerous studies found increased spine density, an immature spine morphology (He and Portera-Cailliau, 2013) and altered synaptic plasticity displayed by decreased field EPSCs (Zhang et al., 2009), others reported no differences in these parameters upon the deletion of FMRP (Godfraind et al., 1996; Pan et al., 2010). The dominating phenotype of spines found is their immaturity (Bakker et al., 1994; Nimchinsky et al., 2001; Irwin et al., 2002; Galvez and Greenough, 2005; McKinney et al., 2005; Grossman et al., 2006). The hippocampus is one of the brain regions affected in FXS which could be a reason for phenotypes like excessive adherence to patterns. Indeed, dendritic spines of CA1 pyramidal neurons were found to display an overabundance of long and thin spines (Antar et al., 2006; Grossman et al., 2006; de Vrij et al., 2008; Bilousova et al., 2009; Grossman et al., 2010; Swanger et al., 2011).

Besides neurons of the DG, CA3 and CA1 area insights into CA2 pyramidal neurons affected by a *fmr1* KO were provided. The focus of this work lay on the mechanistic and functional phenotypes of several synapses in the hippocampus accompanied by a

behavioral analysis of the mouse model. Interestingly, the deletion of FMRP had very different consequences on the dendritic spines of the hippocampal subregions - even within one type of neuron. In line with the fact that FXS is a neurodevelopmental disorder a developmental component could be as well found in a subregion-dependent manner for spinogensis.

4.1 The deletion of FMRP causes altered connectivity and synapse maturation of the hippocampal mossy fiber pathway

Patients with FXS can display several behavioral abnormalities as hyperactivity, stereotypic behavior and excessive adherence to patterns (Cohen et al., 1988; Hernandez et al., 2009), phenotypes that can be found as well in a mouse model lacking the *fmr1* gene (The-Dutch-Belgian-Fragile-X-Consortium, 1994). Since the disorder is the most common source for inherited monogenetic cognitive impairment and autism (Hagerman et al., 2001) several studies tried to reveal cellular mechanism responsible. A defect in synaptogenesis displayed by alterations in spine density, morphology and stability could be found which was correlated to the behavioral phenotypes (Comery et al., 1997; Irwin et al., 2000; Huber et al., 2002; Cruz-Martin et al., 2010; Thomas et al., 2011; Portera-Cailliau, 2012; He and Portera-Cailliau, 2013). The excessive adherence to patterns indicates impairments especially in hippocampal network formation. Therefore, neurons of DG, CA3 and CA1 were intensively investigated with respect to spine morphology and the majority of studies reported an overabundance of long and thin spines, pointing to an immature spine phenotype (Antar et al., 2006; Grossman et al., 2006; de Vrij et al., 2008; Bilousova et al., 2009; Grossman et al., 2010; Levenga et al., 2011; Swanger et al., 2011). So far, a detailed morphological analysis was restricted to the prototypical mushroom spines forming the post-synapse of the Schaffer collaterals or recurrent collaterals of CA3 neurons and to the perforant path fibers. However, the hippocampal synapses highly involved in processing pattern separation and completion have not been studied in the FXS mouse model before. In fact, the DG is highly involved in pattern separation whereas pattern completion is mediated throughout the mossy fiber connection to the CA3 region (Leutgeb et al., 2007; Bakker et al., 2008). Both processes are impaired in FXS which is reflected by the excessive adherence to patterns observed in patients (Cohen et al., 1988; Hernandez et al., 2009).

Therefore, the main part of this thesis focused on one of the most powerful and

morphological complex synapse type in the hippocampus, the synapse formed by the large mossy fiber terminals (LMTs) of DG granule cells and TEs of CA3 pyramidal neurons. It was extremely interesting to note that in contrast to other synaptic alterations described in this thesis and in earlier studies in *fmr1* KO animals, TEs were found to be premature in *fmr1* KO mice. The TE morphology was strongly altered which was especially pronounced in a specific time window in vivo and in vitro (P19, DIV14). An increased area and an extended distribution of TEs along the apical dendritic tree were accompanied by a widening of the mossy fiber projection in *fmr1* KO animals compared to WT littermates. Interestingly, at earlier (DIV7) and later time points (P30-40, DIV28) these phenotypes were abolished or even reversed. Besides the widened and elongated mossy fiber projection confocal laser scanning microscopy revealed that the LMT boutons were strongly decreased in size which led to an increased TE to LMT ratio upon the deletion of FMRP. Given this imbalance of pre- and postsynaptic structures it was not surprising that synaptic transmission was affected as well in *fmr1* KO mice in comparison to WT mice. Here, the mossy fiber dependent miniature EPSCs were found to be increased in frequency but not amplitude. Interestingly, the number of inserted AMPA receptors was drastically increased in TEs under baseline conditions in *fmr1* KO cells compared to WT cells. Upon an elevation of activity via KCl application the TEs of both WT and *fmr1* KO neurons displayed an increase of inserted AMPA receptor which was significantly stronger in *fmr1* KO TEs. This points to a dysregulation of synaptic plasticity at TE synapses upon the depletion of FMRP. The increased TE area described earlier is therefore in line with an increased AMPA receptor content. This is furthermore supported by an increase in synaptopodin clusters per TE at DIV14, which points to an elevated number of synaptic sites in single TEs upon the deletion of FMRP. Notably, the number of synaptopodin-clusters was already increased at DIV7 underlining the premature phenotype described earlier. Additionally, the decrease in motility and the accompanying slower actin dynamics in TEs in *fmr1* KO mice provide further evidence for morphological stability which goes together with the increased synapse area via receptor insertion.

In the literature an increased mEPSC amplitude is correlated with an increased presynaptic release probability whereas an increased mEPSC frequency points to an increased amount of AMPA receptors (El-Husseini et al., 2000; Tyler and Pozzo-Miller, 2001). In this thesis an increased mEPSC frequency could be found. The results point towards hyperexcitability of CA3 pyramidal neurons since they are contacted by more DG granule cells revealed by the retrograde tracer. Thus one enlarged TE with an increased number of synapses and

therefore increased amount of inserted AMPA receptors is contacted by an increased number of smaller LMTs of individual DG granule cells in *fmr1* KO mice (figure 17). Thus, this hyperconnectivity is reflected by an increased frequency of mEPSCs but not the amplitude in *fmr1* KO cells.

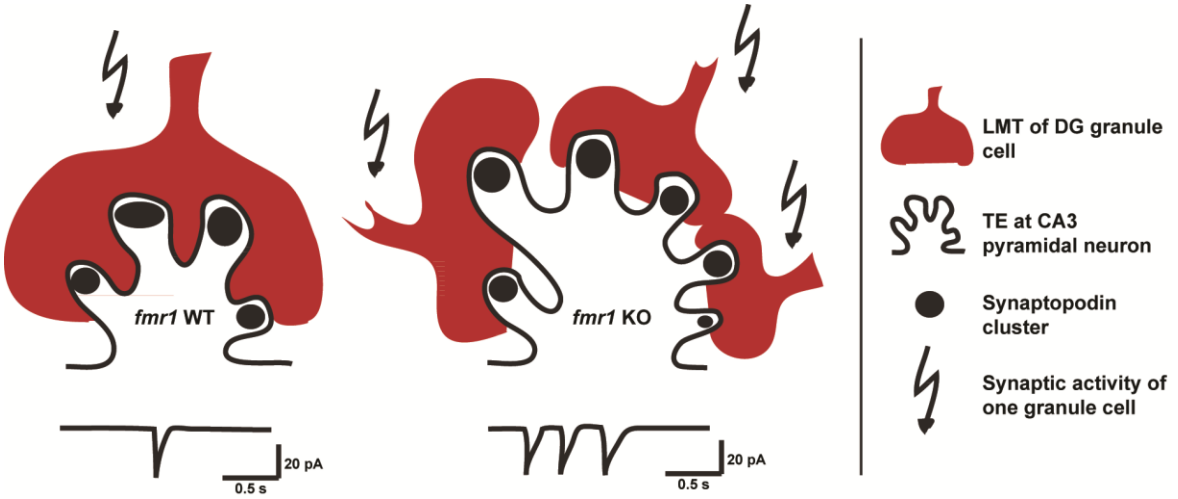

Figure 17: Schematic drawing of LMT-TE synaptic transmission in *fmr1* KO cells. A single thorny excrescence (TE) displays an increased area and number of synapses in *fmr1* KO mice in comparison to WT littermates (left). TEs of mice lacking FMRP are contacted by an increased number of large mossy fiber terminals (LMTs) that are projected from different DG granule cells causing an increased frequency in mEPSC recordings (lower sector).

Taken together, it can be concluded that TE synapses are premature. This is supported by the fact that they show an increased TE area, by the number of synapses and by the amount of inserted AMPA receptors early in postnatal development. These findings are in contrast to the well-known and in this thesis as well shown spine immaturity at regular dendritic spines in the CA3 and CA1 area of the hippocampus which was shown to be accompanied by a decreased AMPA receptor content and impaired LTP (Bilousova et al., 2009; Zhang et al., 2009; Cruz-Martin et al., 2010; Levenga et al., 2011; Cruz-Martin et al., 2012; Portera-Cailliau, 2012; He and Portera-Cailliau, 2013).

Since previous studies could show that TEs are premature when LMT input is removed (Frotscher et al., 1977; Gaiarsa et al., 1992), it points to a role of FMRP in correct TE formation. Future experiments aimed to unravel synaptic dysfunction in FXS should include the analysis of presynaptic partners which is mostly missing in the current literature to further elucidate the outcome for synaptic network development.

As a first step to correlate altered synaptic transmission and morphology at the LMT-TE synapse to behavior, the marble burying paradigm was used. It is commonly used to detect repetitive and obsessive compulsive behavior which is highly dependent on hippocampal networks (Webster et al., 1981; Handley, 1991; Deacon and Rawlins, 2005; Deacon,

2006). Here, *fmr1* KO mice of the same age that displayed the strong TE phenotype (P19), showed increased levels of repetitive behavior compared to WT littermates. At a later time point, corresponding to the time point where no differences could be found in TEs of both genotypes (P30-40), the changes between *fmr1* KO and WT littermates in marble burying were no longer detectable. Thus, the premature TE phenotype at CA3 pyramidal neurons accompanied by a hyperconnectivity from the DG might indeed have a significant effect on CA3 pyramidal neuron output which could even be potentiated by the fact that dendritic spines in *stratum radiatum* were in this thesis found to be immature. In parts this could be supported by altered learning behavior in the Morris water maze paradigm whose accuracy was shown to be mostly dependent on the Schaffer collaterals (Aou et al., 2003).

The behavioral tests performed here are only the starting point to understand the involvement of the LMT-TE synapse in autism spectrum disorders (ASD). They might reflect some of the behaviors found in autistic patients which include excessive adherence to patterns (repetitive behavior) and impairments in the detection of socially important patterns as recognition of facial expressions (Cohen et al., 1988; Merenstein et al., 1996; Tsiouris and Brown, 2004; Garber et al., 2008). These symptoms point to a prominent role of the DG and its projection and synapse formation with CA3 pyramidal neurons in the hippocampus, as they are encoding for new episodic memories (Squire, 1992; Lisman, 1999; Lisman et al., 2005; Leutgeb et al., 2007; Bakker et al., 2008). Here, pattern separation and completion play crucial roles to recognize the differences between new representations and already existing ones. Indeed, previous studies could report a reduced LTP in the DG of *fmr1* KO mice accompanied by an impaired adult neurogenesis (Eadie et al., 2009; Yun and Trommer, 2011; Guo et al., 2012; Lazarov et al., 2012). The data provided in this thesis could support and even expand the view of an altered synaptic transmission from DG granule cells to CA3 pyramidal neurons in the FXS which is most likely contributing to the pathogenesis of the FXS and other autism spectrum disorders (ASDs).

4.2 Synaptic structure in the mouse hippocampus is affected in a subregion dependent manner in a mouse model of the fragile X syndrome

The hippocampus is crucial for learning and memory processes; moreover, as well as pattern separation and completion. Some of these functions were found to be altered in fragile X syndrome (FXS) patients, leading to phenotypes like excessive adherence to

patterns (Cohen et al., 1988; Hernandez et al., 2009) and cognitive impairment. This renders the hippocampus an important structure affected in FXS. As described earlier the majority of studies showed that in patients as well as in the mouse model of the fragile X syndrome, dendritic spines of pyramidal neurons displayed an immature structure (Comery et al., 1997; Galvez and Greenough, 2005; Grossman et al., 2006; He and Portera-Cailliau, 2013). In these studies an immature structure is characterized by a reduction in mushroom-like spines and an increase in filopodia-like spines with a smaller head containing fewer AMPA receptors (Matsuzaki et al., 2001). However, reports about this spine phenotype are controversial showing sometimes an immature phenotype and sometimes no alteration by the deletion of FMRP. The high variation of methods and material used might make it difficult to compare reports of dendritic spine morphology in the mouse model of the FXS, e.g. while some studies exclusively obtained the data from primary hippocampal cultures others used fresh brain slices.

To provide a consistent view all excitatory neuron types of the hippocampal subregions were studied in this thesis. The findings were mostly achieved by use of slice cultures supported in parts by analysis of comparable developmental time points *in vivo*. In all cases the classical mouse model of the FXS was used. Here, the *fmr1* gene is knocked out which is located on the X chromosome (The-Dutch-Belgian-Fragile-X-Consortium, 1994).

Interestingly, spine morphology was altered differently dependent on the synaptic pathway investigated. In organotypic hippocampal slice cultures the overall morphology of DG granule cells was studied. Along the dendrites of DG granules cells a significantly decreased spine density accompanied by an increased proportion of filopodia could be found. This means a potentiated effect on the loss of computational power of the cell, displaying a reduced number of potential postsynaptic inputs which are even more immature as compared to WT littermates. These findings are constant with earlier reports showing an immature spine phenotype as well. However, an increased spine density at DG granule cells was described in a previous study (Grossman et al., 2010). This discrepancy might reside in the fact that the study was performed *in vivo* and the cells were labeled via Golgi staining. Both results underline the fact that FMRP is important for synapse maturation of spines at DG granule cells. Another structural feature that is important for the computational power of a neuron is the dendritic complexity. Granule cells and especially pyramidal neurons of the hippocampus display a relatively high dendritic complexity, a feature that might increase the area for information processing. However,

while spine density and morphology are strongly altered in *fmr1* KO cultures, the dendritic complexity was not affected.

Besides the postsynaptic input by dendritic spines, the presynaptic site, or output of the DG granule cells was found to be altered in the *fmr1* KO as well. It could be shown earlier that the mossy fiber projection is affected in adult *fmr1* KO mice, analyzed by Timm-staining (Ivanco and Greenough, 2002; Mineur et al., 2002). The Timm-staining reveals the zinc-rich terminals of the DG granule cells, but as well all other zinc-including structures. In this thesis an antibody was used to investigate the mossy fiber projection and the results were mostly consistent with the literature. In adult *fmr1* KO mice the mossy fiber projection was found to be mainly unaltered, except for the very distal area to the DG which was slightly narrowed. Contrary to the results obtained from adult mice (P30-40), very young mice (P19) displayed a drastic widening of the projection, especially very distal to the DG *in vitro* and *in vivo*. It is known that around this age the LMTs start to form functional synapses with the thorny excrescences of CA3 pyramidal neurons. Thus, an exaggerated phenotype at P19 might be compensated later leading to an opposite phenotype in adulthood.

While in literature only the mossy fiber projection was investigated until now, in this thesis also the large mossy fiber terminals (LMTs) were studied in detail in *fmr1* KO mice. Interestingly, they displayed a drastically decreased area of the LMT bouton while the filopodia were not altered in number or length. It could be shown earlier that the boutons of LMTs contact excitatory neurons while the filopodia interact with inhibitory neurons (Blackstad and Kjaerheim, 1961; Hamlyn, 1962; Frotscher, 1985; Acsády et al., 1998). Therefore, LMT morphology allows a feedforward excitation and inhibition (Ruediger et al., 2011). Thus, the discrepancy between alterations in core versus filopodia found here might have a negative impact on information processing in the hippocampus. Interestingly, the postsynaptic site of the LMTs, the thorny excrescences (TEs), displayed an opposite exaggerated phenotype as discussed earlier. So far a detailed morphological analysis was restricted only to the prototypical mushroom spines of the Schaffer collaterals or recurrent collaterals of the CA3 neurons and to the perforant path fibers. Yet the morphological details of the TEs that contribute to pattern completion by its synapse formation with LMTs have not been studied in the fragile X syndrome. Generally, knowledge about one of the most powerful and morphologically complex synapses is still sparse compared to other synapse types in the hippocampus. In contrast to other synaptic structures (Antar et al., 2006; Bilousova et al., 2009; Levenga et al., 2011; He and Portera-Cailliau, 2013), TEs

displayed a premature phenotype in *fmr1* KO mice. TEs are increased in size, accompanied by an increased distance of the furthest TE to the soma, especially during a critical time window at *fmr1* KO cells (P19, DIV14 in organotypic slice cultures) and only along CA3 pyramidal neurons that were located distal to the DG. The phenotype is accompanied by a widening of the mossy fiber projection at P19, as described above. At a later time point (P30-40; DIV28) this phenotype was abolished. Even earlier time points (DIV7, DIV10) could not reveal morphological differences between *fmr1* KO mice and WT littermates. This again points to a crucial function of FMRP in the formation of LMTs and TEs which associate to form synapses in the second postnatal week (Wilke et al., 2013), which is in line with the time window found in this thesis.

Despite the large TEs located in the *stratum lucidum*, regular spines contacting recurrent collaterals of CA3 pyramidal neurons were altered in a mouse model of the FXS. In line with a previous study (Bilousova et al., 2009) this thesis could reveal an immature phenotype of the dendritic spines as well. However, another study showed no differences upon the deletion of FMRP in dendritic spines of CA3 pyramidal neurons (Levenga et al., 2011). Discrepancies could result from differences in the developmental stages of the tissue investigated. While this thesis (DIV14) and the publication of Bilousova et al., 2009 (P7) delivered data of developing neurons, Levenga et al., 2011 investigated neurons from mature mice (27 weeks old). This is supporting the developmental role of FMRP which could be compensated in adult mice and could therefore lead to only a mild or no phenotype of dendritic spines in *fmr1* KO mice. Remarkably, data obtained in this thesis show that two different kinds of synapses are affected differentially at a single cell type. While TEs in the *stratum lucidum* appeared to be premature, dendritic spines in the *stratum radiatum* displayed a higher proportion of immature spines. At this time point, it is interesting to note that the data provide a first example that different subtypes of spines on CA3 neurons were affected differently by the loss of FMRP, a fact that might have an especially disturbing effect on the information processing in CA3 neurons.

CA3 pyramidal neurons were thought to be unique displaying TEs for a long time. Just recently a report could show that CA2 pyramidal neurons display spines with similar structural features (Kohara et al., 2014). CA2 pyramidal neurons were identified by a specific marker (Kohara et al., 2014). Before, CA2 pyramidal neurons were only identified by their location in the hippocampus and their dendritic structure, reporting that CA2 pyramidal neurons do not have TE-like spines (Lorente de Nó, 1934). Two different methods used to identify CA2 neurons led to different conclusions about the integration of

these neurons in the hippocampal network. The classical identification via morphology is showing that CA2 neurons receive afferents from the supramammillary nucleus (SUM) or from both ECII and ECIII innervating CA1 pyramidal neurons, additionally receiving direct input from CA3 pyramidal neurons dominated by feedforward inhibition (Haglund et al., 1984; Maglóczky et al., 1994; Bartesaghi and Gessi, 2004; Chevaleyre and Siegelbaum, 2010). However, the very recent study using CA2 specific markers showed that granule cells of the DG project directly into CA2, while ECII cells did not project directly to CA2. The innervation of the CA1 pyramidal neurons by CA2 cells takes place through both deep and superficial sublayers in CA1 (Kohara et al., 2014). In this thesis the CA2 area was found to be entered by the mossy fiber projection of DG granule cells as well. Interestingly, the expansion of the CA2 area was not altered in a mouse model of the FXS syndrome, while the mossy fiber projection in CA2 was widened but not changed in length, as described above. The fact that the cell body layer along the mossy fiber projection and the projection itself were elongated in CA3 in *fmr1* KO mice accompanied by no alterations in the CA2 area might point to an overall increase of the CA3 area in *fmr1* KO cultures.

While the CA2 area was not affected, the TE-like spines displayed a comparable phenotype as found in TEs of CA3 pyramidal neurons, an increase in TE area and maximum distance to the soma of the furthest TE-like spine which is in line with the investigated widening of the mossy fiber projection in a mouse model of the FXS.

The synapses of the excitatory neurons in the hippocampus described so far were all altered in *fmr1* KO mice which could be explained by high FMRP concentrations in the hippocampus, especially in fragile X granules (FXG) located in synapses, as the large mossy fiber terminals, in the healthy brain (Akins et al., 2012). As the CA1 area is downstream of these regions, it could be affected as well. Interestingly, no effects on spine density or spine morphology could be found *in vivo* and *in vitro.* This is in line with a number of previous studies who also found no alterations at the spines of CA1 neurons (Braun and Segal, 2000; Grossman et al., 2006; Levenga et al., 2011). However, the majority of earlier studies revealed a higher proportion of immature spines and an altered spine density in FXS patients and *fmr1* KO mice (Huber et al., 2002; Bear et al., 2004; Volk et al., 2007; Bilousova et al., 2009; Cruz-Martin et al., 2012; Portera-Cailliau, 2012). Interestingly, the DG and CA3 area show a high amount of both FMRP and FXG while CA1 neurons do not display FXG (Christie et al., 2009). Thus, the effect of an FMRP deletion on CA1 pyramidal neurons might be indeed different compared to the DG or CA3

neurons. Additionally, as discussed earlier *in vivo* versus *in vitro* studies as well as cell labeling techniques might have a great influence on the analysis. It might be interesting to note in this respect that different types of CA1 pyramidal neurons have been reported earlier (Graves et al., 2012) which display distinct expression patterns of metabotropic glutamate receptors (mGluRs) that directly interact with FMRP (Antar et al., 2004; Bear et al., 2004; Cruz-Martin et al., 2012). This fact becomes even more important, since methods like Golgi staining and GFP labeling under the Thy1 promotor label only a sparse number of cells and the selection process is not known.

4.3 Spine actin dynamics in *fmr1* KO neurons

The actin cytoskeleton mediates numerous essential cellular functions providing both highly plastic and stable networks (Hall, 1998). Plastic remodeling processes are strongly dependent on the actin network and its tight regulation which is especially important in dendritic spines. Spines are actin rich structures and are highly motile (Fischer et al., 1998). Structural plasticity is of high importance for the function of spines. The responses to external stimuli of the synapse are accompanied by an increase or decrease of the spine size, a process termed as activity-dependent structural plasticity which is especially reported for LTP or LTD (Matsuzaki et al., 2004; Holtmaat and Svoboda, 2009). Actin dynamics have to be tightly controlled to guarantee correct synaptic function, a task performed by actin-binding proteins (ABPs). It is supposed that for a fast remodeling of the spine as a reaction to changes in synaptic activity, it is important that both ABPs and β-actin mRNAs are translocated in an activity-dependent manner into dendritic spines. Here, FMRP could play a crucial role since it is an mRNA binding protein and was found to be involved in transport and translational control of mRNAs, including actin mRNA and the cytoskeleton associated Arc (Zalfa et al., 2003; Dictenberg et al., 2008). In this thesis mRNAs of two additional ABPs were found to be bound by FMRP, profilin1 and cofilin1. Interestingly, profilin2a mRNA was not associated with FMRP in the hippocampus which is especially interesting since *profilin1* and *profilin2a* display 65% amino acid sequence identity and high biochemical similarity (Gieselmann et al., 1995). Recently it was shown that the two profilin isoforms present in the brain have distinct functions in spines. While profilin1 is crucial for synaptogenesis, profilin2a is mandatory for adult spine plasticity. In line with this profilin1 protein levels were found to be decreased in *fmr1* KO mice

(Michaelsen-Preusse et al., 2016). Since profilin1 is involved in synaptogenesis its misregulation in *fmr1* KO mice can be at least in parts causing the documented development-dependent spine structure alterations. Additionally, the FXS itself is found to be a developmental disorder further in line with the developmental role of profilin1.

Spine Motility as well as spine actin polymerization was investigated at synapses of neurons located in distinct hippocampal subregions. Besides the immature spine structure, spines of CA3 pyramidal neurons displayed a reduction in motility in both TEs and dendritic spines in *stratum radiatum*, while DG granule cells and CA1 pyramidal neurons showed no alterations in spine motility in *fmr1* KO mice. Although spine structure was altered differentially at CA3 pyramidal neurons, both TEs and spines in the *stratum radiatum* showed reduced short-term structural plasticity. Surprisingly, actin polymerization rates were only reduced in TEs but not in regular spines in *fmr1* KO mice which could be due to a differently regulated actin cytoskeleton. Since profilin1 protein levels were reduced in *fmr1* KO hippocampi (Michaelsen-Preusse et al., 2016) and FMRP interacts with profilin1 mRNA, the hypothesis was tested whether the exaggerated phenotype found in TEs could be at least in parts due to misregulated profilin1 levels. An over expression of profilin1 in CA3 pyramidal neurons supported this hypothesis. In WT neurons a profilin1 overexpression led to a faster recovery of the GFP-actin fluorescence after photobleaching in line with a role of PFN1 in promoting actin polymerization. The over expression of profilin1 in CA3 neurons of *fmr1* KO mice rescued the defect in actin polymerization in a way that it reached comparable actin polymerization rates to WT cells overexpressing profilin1. Thus, the enlarged TEs and the reduced actin polymerization rate found in *fmr1* KO mice is at least partially dependent on the misregulation of profilin1.
Interestingly, the presynaptic sites, the LMTs, did not display defects in motility or actin polymerization although they showed the highest rates of FMRP and FXG (Christie et al., 2009). Whether this might be due to compensational mechanisms still has to be investigated. Dendritic spines of DG granule cells showed increased actin polymerization but no altered motility. It becomes apparent that alterations in motility and actin polymerization rates do not always correlate and that therefore the connection between the two parameters might be more complex. Still, the altered actin dynamics could deliver an explanation for the immature spine phenotype found in spines of DG neurons. While DG granule cells and CA3 pyramidal neurons displayed at least in parts strong phenotypes due to the deletion of FMRP, CA1 pyramidal neurons were not affected with respect to motility

and actin dynamics under basal conditions.

However, the induction of cLTP in *fmr1* WT cells results in a significant increase of the spine head width which could be previously reported as well (reviewed in Yuste and Bonhoeffer, 2001). It was shown that the spine head increase is accompanied with insertion of AMPA receptors resulting in synapse strengthening (Matsuzaki et al., 2001; Matsuzaki et al., 2004; Zito et al., 2004; Holtmaat and Svoboda, 2009). The increase of spine head growth upon LTP induction in WT cells is accompanied by an increased proportion of mushroom-like spines and therefore decreased proportion of stubby and thin spines. Spines of CA1 pyramidal neurons in *fmr1* KO cultures showed a significantly reduced spine head growth upon LTP compared to *fmr1* WT cells and a lack of activity-dependent changes in spine type distribution. Interestingly, the induction of LTP via glycine application resulted in a stabilization of actin dynamics in dendritic spines of *fmr1* WT CA1 neurons displayed by an increased turnover time, supporting previous findings (Fukazawa et al., 2003; Michaelsen-Preusse et al., 2016). Earlier studies revealed that the turn-over time was increased shortly after induction of LTP to provide the necessary plasticity increasing spine size and inserting receptors (Fukazawa et al., 2003; Bramham, 2008; Michaelsen-Preusse et al., 2016). While under baseline conditions the absence of FMRP has no effect on actin dynamics in dendritic spines compared to WT CA1 neuron, the induction of cLTP revealed altered actin dynamics in *fmr1* KO cells in comparison to WT cells. This is due to the fact that the actin stabilization found in spines of WT cells was absent in *fmr1* KO cells lacking changes in the turnover rate upon glycine application. Since the actin stabilization is mandatory for alterations in synaptic strength during LTP (Star et al., 2002; Honkura et al., 2008), the immature spine morphology found in the FXS (He and Portera-Cailliau, 2013) could be partially due to the incapability to stabilize the actin cytoskeleton.

Taken together, this thesis provides a first hint that defects in spine development and spine plasticity in the FXS mouse model results from impairments in the modulation of actin dynamics in the absence of FMRP. First insights were delivered that actin dynamics are regulated differently throughout the neurons of the hippocampal subtypes in *fmr1* KO mice, supported by differentially affected actin polymerization rates in spines. The alterations in actin dynamics described seem to be at least partially result from dysregulated profilin1 levels whose mRNA is bound by FMRP in the healthy nervous system.

4.4 Developmental influences on compulsive behavior and spatial learning in a mouse model of the fragile X syndrome

The hippocampus was shown to be crucial for learning and memory processes already early in the history of brain research (Scoville and Milner, 1957; Morris, 1981; Morris, 1984). Due to its vital functions and its anatomy the hippocampus became fast one of the most investigated brain regions. Over time the hippocampus was found to be highly involved in processes like pattern separation and completion as well which are impaired in FXS patients (Cohen et al., 1988; Hernandez et al., 2009).

Some behavioral phenotypes of FXS patients point to an impairment of hippocampal function as repetitive behavior, impairments in visual-spatial memory and facial expression recognition (Cohen et al., 1988; Merenstein et al., 1996; Tsiouris and Brown, 2004; Garber et al., 2008). Additionally, this thesis and several reports before found altered hippocampi of patients as well as of *fmr1* KO mice displayed by changes in the overall hippocampus volume, immature spine morphology along dendrites of hippocampal pyramidal neurons and defects in synaptic transmission (The-Dutch-Belgian-Fragile-X-Consortium, 1994; Bagni et al., 2012; He and Portera-Cailliau, 2013). Still, as mentioned before the reports about spine phenotypes are controversial as they are for synaptic function. There exist both reports about altered LTP capabilities like decreased field EPSCs in hippocampal slices (Zhang et al., 2012) and on the other hand studies which could not detect differences to WT littermates (Godfraind et al., 1996). It is no surprise that the behavioral studies including the hippocampus are as well numerous and controversial in *fmr1* KO mice (Bakker et al., 1994; Kooy et al., 1996; D'Hooge et al., 1997; Paradee et al., 1999; Dobkin et al., 2000; Van Dam et al., 2000; Mineur et al., 2002; Baker et al., 2010; Thomas et al., 2011; Bagni and Oostra, 2013; Amiri et al., 2014; Oddi et al., 2015). The studies differ with respect to the tests used but also the age of the mice and the mouse strains. Therefore, hippocampus-dependent behavior was examined using different approaches in this thesis.

To study hippocampal function several methods were developed. The marble burying task is one method not only uncovering potential hippocampal deficits but repetitive compulsive behavior as well (Deacon and Rawlins, 2005; Deacon, 2006). One of the most used tests is the Morris water maze revealing spatial memory formation (Morris, 1984). Here, both were performed in order to gain a more detailed analysis of disrupted hippocampal pathways. While repetitive compulsive behavior is mainly dependent on the DG and its connection to the CA3 (Bakker et al., 2008), the Morris water maze task was

shown to be mainly dependent on the Schaffer collaterals formed between CA3 and CA1 pyramidal neurons (Aou et al., 2003). The most prominent effect of TE morphology and the mossy fiber projection appeared early in development (P19) which correlated well with the most pronounced phenotype found in the Morris water maze task and marble burying of *fmr1* KO mice in this thesis. Since FXS is a developmental neurological disorder it is interesting that so far there were no reports about juvenile *fmr1* KO mice with respect to hippocampus-dependent behavior. Here, P19 *fmr1* KO mice displayed an increased amount of marbles buried after 60 min compared to WT littermates. This indicates increased repetitive behavior which could be observed in patients as well (Cohen et al., 1988; Hernandez et al., 2009). At a later developmental time point (P30-40) no differences between both genotypes could be found which is consistent with unaltered TE morphology and mossy fiber projection in *fmr1* KO mice compared to WT littermates of the underlying DG-CA3 network. Again, the reports about alterations in repetitive behavior in adult *fmr1* KO mice differ. While some earlier reports support the increased obsessive compulsive behavior found in this thesis (Mineur et al., 2002; Thomas et al., 2011), others found no effect of the FMRP deletion on repetitive behavior, tested by marble burying or observing grooming behavior in adult mice (Pietropaolo et al., 2011; Spencer et al., 2011). However, *fmr1* KO mice at P19 displayed the same levels of marbles buried as WT and KO mice at the age of P30 which is pointing to a premature phenotype as it was studied at the synapse that is thought to be involved in adherence to patterns, shown by an increased synaptic transmission, enlarged TE area and increased amount of synapses in TEs.

The deletion of FMRP led to an altered behavior in the Morris water maze task of P19 mice as well. Here, the mice (P19) displayed only at the beginning of the training a decreased escape latency and an increased proportion of hippocampus-dependent search strategies. Further along during the training escape latency and search strategy distribution were unaltered which might be due to the progressive age of the mice. At the last training day the mice already reached an age of 30 days, a time point that was not showing differences in the marble burying task or in the mossy fiber pathway anymore which renders the Morris water maze task not suitable to investigate a specific age of the animals. The results of the Morris water maze task revealed that *fmr1* WT at P19 do not display a progress in learning during the training. This effect could be explained by infantile amnesia which was shown to be present until P21 preventing the young mice from learning the platform position (Travaglia et al., 2016). Therefore, faster escape latency and increased hippocampus-dependent search strategies in *fmr1* KO mice (P19) point again to a

premature hippocampal function as with the increased marble burying behavior and at TEs with increased area and number of synapses compared to WT littermates.

At a later time point, adult mice of both genotypes showed no differences in the escape latency or in the proportion of search strategies. The reverence memory test was also not revealing an effect of a FMRP deletion on the spatial memory formation in the mice. A reversal test, where the platform was moved to another position, uncovered alterations in the relearning of the mice. Here, *fmr1* KO mice displayed an increased preference to the goal quadrant compared to WT littermates. The majority of studies could not find differences between both genotypes in the normal learning phase as well (The-Dutch-Belgian-Fragile-X-Consortium, 1994; D'Hooge et al., 1997; Paradee et al., 1999). Contrary to the findings of this thesis, several studies showed a less precise behavior reaching the platform in the reversal test of the *fmr1* KO mice (The-Dutch-Belgian-Fragile-X-Consortium, 1994; Kooy et al., 1996; D'Hooge et al., 1997; Baker et al., 2010). Most notably no pretraining was performed prior to the learning phase which is essential to avoid anxious behavior. The mouse model of the fragile X syndrome is more anxious, especially in its response to stressful stimuli (The-Dutch-Belgian-Fragile-X-Consortium, 1994; Chen and Toth, 2001; Frankland et al., 2004). Therefore, it is mandatory to habituate the mice to the experimental paradigm, including changing platform positions. In contrast to the studies listed above, a pretraining was performed prior to the learning phase in this thesis. The genetic background of the strains carrying the knockout of the *fmr1* gene and the sex can have great influences which were shown in earlier studies (Perrot-Sinal et al., 1996; Owen et al., 1997; Paradee et al., 1999). While in this study exclusively *fmr1* WT and KO mice in the FVB background were used for behavioral experiments the studies listed above obtained the data from C57BL/6J mice. However, in this thesis and previous studies only male mice were exposed to the Morris water maze (The-Dutch-Belgian-Fragile-X-Consortium, 1994; Kooy et al., 1996; D'Hooge et al., 1997; Baker et al., 2010).

The findings of the Morris water maze experiments were accompanied by a defect in actin stabilization and structural plasticity found in dendritic spines of the CA1 pyramidal neurons upon cLTP induction. This region is highly linked to the processes necessary for spatial memory formation (Aou et al., 2003). The impairment in the activity-induced structural plasticity might facilitate the relearning of the new platform position. While no differences between both genotypes were found under baseline conditions concerning actin dynamics and morphology of dendritic spines, cells of *fmr1* KO mice displayed an

increased amount of immature spines that were not displaying the actin stabilization found in WT littermates upon induction of LTP. Since LTP is considered to be a key molecular mechanism for learning and memory formation, the misregulated actin dynamics found upon LTP induction in CA1 pyramidal neurons, might indeed provide an explanation for the enhanced ability of *fmr1* KO animals to learn the new platform position and to forget the old position. The less stable actin network might allow the *fmr1* KO mice to relearn the new platform position easier than the WT littermates. This is in line with the proposed role of the stabilization of spines for memory formation and maintenance (Ackermann and Matus, 2003; Roberts et al., 2010). In the future memory maintenance should be further tested in *fmr1* KO mice to reveal increased memory extinction due to an impairment in spine stabilization which could be realized by repeating the reference memory test weakly after the actual training phase, as it was performed previously (Zagrebelsky et al., 2016).

The literature lacks detailed analysis about both aged patients and aged *fmr1* KO mice. Only 25 years ago the molecular origin of FXS was uncovered (Verkerk et al., 1991), while the disorder itself was described much earlier (Martin and Bell, 1943). The characterization of older FXS patients is therefore rare until now. It was previously shown that males with a *fmr1* premutation beginning in their 40s are developing progressively more severe problems in performing tasks for working memory, but not visual-spatial memory (Cornish et al., 2009). Furthermore, they displayed an increased risk for progressive cerebellar ataxia, tremor and dementia (Hagerman et al., 2001; Brunberg et al., 2002; Cornish et al., 2009). Until now only one patient was studied with respect to altered cellular mechanism. The patient died at the age of 62 and an immature spine phenotype was revealed in the cortex (Rudelli et al., 1985; Hinton et al., 1991). Besides that, nothing is known about the life-span and cognitive abilities in aged FXS individuals. To provide a fast first overview about an age effect on hippocampal function the FXS mouse model was tested in the Morris water maze paradigm. Here, no differences between *fmr1* KO and WT mice with an age of 19 months were studied. The mice were able to learn the platform position, displayed by a significant decrease in the escape latency from learning day 1 to 8. While mice of both genotypes showed no quadrant preference after 3 days of training, the time spend in the goal quadrant was significantly increased compared to the other quadrants after 9 days. Additionally, no effect of a FMRP deletion appeared in the investigated search strategies. Here, *fmr1* WT and KO mice showed an increase of the hippocampus-dependent search strategies, accompanied by a decrease in the proportion of

hippocampus-independent search strategies. Interestingly, the escape latency of the aged mice was not different to young adult mice at the 8th training day. Aged mice displayed less percentage of hippocampus-dependent search strategies (approx. 48 %) compared to young adult mice (approx. 75 %) at the last day of training. While the deletion of FMRP had no consequence on the learning behavior of the mice, it seemed to have on the life expectancy. While only 6 *fmr1* WT mice died before they could be used for the water maze at the respective age, 15 *fmr1* KO mice died. Therefore, an earlier time point should be chosen for future experiments to determine the effect of the FXS on hippocampus-dependent memory formation. It might indeed be the case that only animals with a less pronounced phenotype reached the age investigated here.

4.5 Conclusion and outlook

In this thesis it could be shown that FMRP has a crucial function in the development of hippocampal pre- and postsynaptic structures which is at least in parts due to its mRNA binding capabilities. Interestingly, dendritic spines of neurons in the hippocampus were altered differently upon the deletion of FMRP which is in line with previous publications (Levenga et al., 2011). This thesis delivered first insights in the DG-CA3 pathway which is involved in pattern separation and completion (Bakker et al., 2008). Here, the deletion of FMRP caused a phenotype which is described rarely in the literature, while the presynaptic site, the large mossy fiber terminals (LMTs) were decreased in size, the postsynaptic compartment, the thorny excrescences (TEs), were increased in size. Together with an increased connectivity between DG granule cells and CA3 pyramidal neurons this resulted in increased synaptic transmission. Still the information is lacking how single TEs are connected to LMTs. To investigate the connectivity at single synapses 3D structural analysis using electron microscopy could be used. This could additionally provide detailed information about the synapse localization within one TE to support the fact that an increased number of synaptopodin clusters could be found upon the deletion of FMRP. Besides that an increased number of AMPA receptors were found in *fmr1* KO mice. Here, an over expression of SEP-GluR1 was used, this can lead to a several folds amount of AMPA receptor subunits and can alter the composition of AMPA receptors due to altered GluR1/GluR2 ratios. Therefore, a knock-down of GluR1 together with an expression of SEP-GluR1 in single cells could deliver a more realistic analysis of AMPA receptor levels in TEs in *fmr1* WT and KO cells. It has to be highlighted that these phenotypes were exclusively found in the distal area of CA3 which is described in literature as CA3a/b and is suggested to be especially important for pattern completion (Kesner, 2013). Besides a subregion specific effect of a FMRP deletion, increased TE area and distribution along the apical dendrites of CA3 pyramidal neurons appeared in a critical time window during development, supporting the fact that the fragile X syndrome is a developmental disorder. To investigate this critical time window in greater detail, FMRP could be over expressed in *fmr1* KO cells at different developmental stages, to reveal the time point where an over expression of FMRP cannot rescue the exaggerated TE morphology anymore.

A RNA-immunoprecipitation revealed that FMRP binds the mRNAs of cofilin1 and profilin1, two important modulators of the actin network. This is supported by our current study showing that less profilin1 is expressed in *fmr1* KO mice compared to WT

littermates (Michaelsen-Preusse et al., 2016). This provides evidence that FMRP is not only repressing the translation of mRNAs but can as well enhance the expression of proteins. Further should be investigated whether FMRP is regulating the transport and the local translation of cofilin1 and profilin1 mRNAs as well. Therefore, *in situ* hybridization can be used to find altered mRNA location upon the deletion of FMRP. Additionally, by inducing long-term potentiation (LTP) and long-term depression (LTD) in hippocampal tissue the role of FMRP in the activity-dependent regulation of those mRNAs could be studied. The importance of the tight regulation of actin-binding proteins was supported by the fact that an over expression of profilin1 in CA3 pyramidal neurons rescued the actin polymerization deficit found in *fmr1* KO cells compared to WT cells. Still, further experiments have to be performed to prove the role of cofilin1 in the TE and dendritic spine phenotypes found in *fmr1* KO mice. Additionally, the function of the control of profilin1 and cofilin1 by FMRP in synaptic transmission should be investigated in detail, by using over expression or knock-down experiments in CA3 pyramidal neurons followed by a repeated analysis of the synaptic transmission throughout the TE-LMT synapse together with a detailed morphological study of both structures. Additionally, it remains elusive how the dendritic spines at different hippocampal neurons develop different structural phenotypes upon the deletion of FMRP. Most notably, along the same type of neuron an opposed alteration was found. At CA3 pyramidal neurons was revealed both an immature spine morphology in the *stratum radiatum* and a premature TE morphology and function in the *stratum lucidum*. One explanation could be the different contribution of glutamate receptors on both structures. While TEs are mainly AMPA receptor driven, dendritic spines were shown to be more dependent on NMDA receptors. Therefore it should be proven whether the disrupted actin dynamics facilitate the mobility and exocytosis of AMPA receptors, since they are connected to the PSD which is itself connected with the actin network (Allison et al., 1998; Matus, 2000). The regulation of synaptic receptors seems the be especially disrupted in the mouse model of the fragile X syndrome, since dendritic spines of CA1 pyramidal neurons only display morphological alterations upon the induction of cLTP. Here, the actin stabilization in the late phase of LTP is impaired in dendritic spines of CA1 pyramidal neurons which is accompanied by faster relearning in the Morris water maze paradigm. In this thesis, this was studied by a repositioning of the platform, in the future additional weakly probe trials should be performed after the actual training phase to prove this hypothesis. To correlate the structural phenotypes at the TE-LMT synapse found in *fmr1* KO mice to the altered

functionality, mossy fiber LTP experiments should be performed in acute slices of P19 *fmr1* WT and KO mice followed by an additional morphological analysis of both structures.

5. References

Ackermann M, Matus A (2003) Activity-induced targeting of profilin and stabilization of dendritic spine morphology. Nature neuroscience 6:1194-1200.

Acsády L, Kamondi A, Sík A, Freund T, Buzsáki G (1998) GABAergic cells are the major postsynaptic targets of mossy fibers in the rat hippocampus. The Journal of neuroscience 18:3386-3403.

Aimone JB, Wiles J, Gage FH (2006) Potential role for adult neurogenesis in the encoding of time in new memories. Nature neuroscience 9:723-727.

Akins MR, LeBlanc HF, Stackpole EE, Chyung E, Fallon JR (2012) Systematic mapping of fragile X granules in the mouse brain reveals a potential role for presynaptic FMRP in sensorimotor functions. Journal of Comparative Neurology 520:3687-3706.

Allison DW, Gelfand VI, Spector I, Craig AM (1998) Role of actin in anchoring postsynaptic receptors in cultured hippocampal neurons: differential attachment of NMDA versus AMPA receptors. The Journal of neuroscience 18:2423-2436.

Amaral DG, Dent JA (1981) Develoment of the Mossy Fiber of the Dentate Gyrus: A Light and Electron Microscopic Study of the Mossy Fibers and Their Espansions. The Journal of Comparative Neurology 195:51-86.

Amiri A, Sanchez-Ortiz E, Cho W, Birnbaum SG, Xu J, McKay RM, Parada LF (2014) Analysis of FMR1 deletion in a subpopulation of post-mitotic neurons in mouse cortex and hippocampus. Autism research : official journal of the International Society for Autism Research 7:60-71.

Andersen P, Lømo T (1967) Control of hippocampal output by afferent volley frequency. Progress in brain research 27:400-412.

Antar LN, Afroz R, Dictenberg JB, Carroll RC, Bassell GJ (2004) Metabotropic glutamate receptor activation regulates fragile x mental retardation protein and FMR1 mRNA localization differentially in dendrites and at synapses. The Journal of neuroscience : the official journal of the Society for Neuroscience 24:2648-2655.

Antar LN, Li C, Zhang H, Carroll RC, Bassell GJ (2006) Local functions for FMRP in axon growth cone motility and activity-dependent regulation of filopodia and spine synapses. Molecular and cellular neurosciences 32:37-48.

Aou S, Li X-L, Li A-J, Oomura Y, Shiraishi T, Sasaki K, Imamura T, Wayner M (2003) Orexin-A (hypocretin-1) impairs Morris water maze performance and CA1-Schaffer collateral long-term potentiation in rats. Neuroscience 119:1221-1228.

Ashley CT, Wilkinson KD, Reines D, Warren ST (1993) FMR1 protein: conserved RNP family domains and selective RNA binding. SCIENCE-NEW YORK THEN WASHINGTON- 262:563-563.

Bagni C, Greenough WT (2005) From mRNP trafficking to spine dysmorphogenesis: the roots of fragile X syndrome. Nature Reviews Neuroscience 6:376-387.

Bagni C, Oostra BA (2013) Fragile X syndrome: From protein function to therapy. American journal of medical genetics Part A 161A:2809-2821.

Bagni C, Tassone F, Neri G, Hagerman R (2012) Fragile X syndrome: causes, diagnosis, mechanisms, and therapeutics. The Journal of clinical investigation 122:4314-4322.

Baker K, Wray S, Ritter R, Mason S, Lanthorn T, Savelieva K (2010) Male and female Fmr1 knockout mice on C57 albino background exhibit spatial learning and memory impairments. Genes, Brain and Behavior 9:562-574.

Bakker A, Kirwan CB, Miller M, Stark CE (2008) Pattern separation in the human hippocampal CA3 and dentate gyrus. Science 319:1640-1642.

Bakker CE, Verheij C, Willemsen R, van der Helm R, Oerlemans F, Vermey M, Bygrave A, Hoogeveen AT, Oostra BA, Reyniers E, De Boule K, D'Hooge R, Cras P, van Velzen D, Nagels

G, Martin JJ, De Deyn PP, Darby JK, Willems PJ (1994) Fmr1 knockout mice: A model to study fragile X mental retardation. Cell 78:23-33.

Bartesaghi R, Gessi T (2004) Parallel activation of field CA2 and dentate gyrus by synaptically elicited perforant path volleys. Hippocampus 14:948-963.

Bassell GJ, Warren ST (2008) Fragile X syndrome: loss of local mRNA regulation alters synaptic development and function. Neuron 60:201-214.

Bear M (1998) The role of LTD and LTP in development and learning. Mechanistic Relationships between Development and Learning (Carew, TJ et al, eds):205-225.

Bear MF, Huber KM, Warren ST (2004) The mGluR theory of fragile X mental retardation. Trends in neurosciences 27:370-377.

Bhakar AL, Dolen G, Bear MF (2012) The Pathophysiology of Fragile X (and What It Teaches Us about Synapses). AnnuRevNeurosci.

Bilousova TV, Dansie L, Ngo M, Aye J, Charles JR, Ethell DW, Ethell IM (2009) Minocycline promotes dendritic spine maturation and improves behavioural performance in the fragile X mouse model. Journal of medical genetics 46:94-102.

Blackstad TW, Kjaerheim Å (1961) Special axo-dendritic synapses in the hippocampal cortex: Electron and light microscopic studies on the layer of mossy fibers. Journal of Comparative Neurology 117:133-159.

Blanchoin L, Pollard TD, Mullins RD (2000) Interactions of ADF/cofilin, Arp2/3 complex, capping protein and profilin in remodeling of branched actin filament networks. Current Biology 10:1273-1282.

Bosch M, Castro J, Saneyoshi T, Matsuno H, Sur M, Hayashi Y (2014) Structural and molecular remodeling of dendritic spine substructures during long-term potentiation. Neuron 82:444-459.

Bramham CR (2008) Local protein synthesis, actin dynamics, and LTP consolidation. Current opinion in neurobiology 18:524-531.

Braun K, Segal M (2000) FMRP involvement in formation of synapses among cultured hippocampal neurons. CerebCortex 10:1045-1052.

Broekkamp CL, Rijk HW, Joly-Gelouin D, Lloyd KL (1986) Major tranquillizers can be distinguished from minor tranquillizers on the basis of effects on marble burying and swim-induced grooming in mice. European journal of pharmacology 126:223-229.

Brunberg JA, Jacquemont S, Hagerman RJ, Berry-Kravis EM, Grigsby J, Leehey MA, Tassone F, Brown WT, Greco CM, Hagerman PJ (2002) Fragile X premutation carriers: characteristic MR imaging findings of adult male patients with progressive cerebellar and cognitive dysfunction. American Journal of Neuroradiology 23:1757-1766.

Buckmaster PS, Strowbridge BW, Schwartzkroin PA (1993) A comparison of rat hippocampal mossy cells and CA3c pyramidal cells. Journal of Neurophysiology 70:1281-1299.

Chen L, Toth M (2001) Fragile X mice develop sensory hyperreactivity to auditory stimuli. Neuroscience 103:1043-1050.

Chevaleyre V, Siegelbaum SA (2010) Strong CA2 pyramidal neuron synapses define a powerful disynaptic cortico-hippocampal loop. Neuron 66:560-572.

Chicurel ME, Harris KM (1992) Three-dimensional analysis of the structure and composition of CA3 branched dendritic spines and their synaptic relationships with mossy fiber boutons in the rat hippocampus. Journal of Comparative Neurology 325:169-182.

Chierzi S, Stachniak TJ, Trudel E, Bourque CW, Murai KK (2012) Activity maintains structural plasticity of mossy fiber terminals in the hippocampus. Molecular and cellular neurosciences 50:260-271.

Christie SB, Akins MR, Schwob JE, Fallon JR (2009) The FXG: a presynaptic fragile X granule expressed in a subset of developing brain circuits. The Journal of neuroscience : the official journal of the Society for Neuroscience 29:1514-1524.

Cianchetti C, Sannio-Fancello G, Fratta AL, Manconi F, Orano A, Pischedda MP, Pruna D, Spinicci G, Archidiacono N, Filippi G (1991) Neuropsychological, psychiatric, and physical manifestations in 149 members from 18 fragile X families. American journal of medical genetics 40:234-243.

Cohen IL, Fisch GS, Sudhalter V, Wolf-Schein EG, Hanson D, Hagerman R, Jenkins EC, Brown WT (1988) Social gaze, social avoidance, and repetitive behavior in fragile X males: a controlled study. American Journal on Mental Retardation.

Collingridge GL, Peineau S, Howland JG, Wang YT (2010) Long-term depression in the CNS. Nature reviews neuroscience 11:459-473.

Comery TA, Harris JB, Willems PJ, Oostra BA, Irwin SA, Weiler IJ, Greenough WT (1997) Abnormal dendritic spines in fragile X knockout mice: maturation and pruning deficits. ProcNatlAcadSciUSA 94:5401-5404.

Cornish KM, Kogan CS, Li L, Turk J, Jacquemont S, Hagerman RJ (2009) Lifespan changes in working memory in fragile X premutation males. Brain and cognition 69:551-558.

Costa-Mattioli M, Sossin WS, Klann E, Sonenberg N (2009) Translational control of long-lasting synaptic plasticity and memory. Neuron 61:10-26.

Cruz-Martin A, Crespo M, Portera-Cailliau C (2010) Delayed stabilization of dendritic spines in fragile X mice. The Journal of neuroscience : the official journal of the Society for Neuroscience 30:7793-7803.

Cruz-Martin A, Crespo M, Portera-Cailliau C (2012) Glutamate induces the elongation of early dendritic protrusions via mGluRs in wild type mice, but not in fragile X mice. PloS one 7:e32446.

D'Hooge R, Nagels G, Franck F, Bakker CE, Reyniers E, Storm K, Kooy F, Oostra B, Willems PJ, De Deyn PP (1997) Mildly Impaired Water Maze Performance in Male Fmr1 Knockout Mice. Neuroscience 76:367-376.

Darnell JC, Van Driesche SJ, Zhang C, Hung KY, Mele A, Fraser CE, Stone EF, Chen C, Fak JJ, Chi SW, Licatalosi DD, Richter JD, Darnell RB (2011) FMRP stalls ribosomal translocation on mRNAs linked to synaptic function and autism. Cell 146:247-261.

De Boulle K, Verkerk AJ, Reyniers E, Vits L, Hendrickx J, Van Roy B, Van Den Bos F, de Graaff E (1993) A point mutation in the FMR-1 gene associated with fragile X. Nature genetics 3.

De Rubeis S, Bagni C (2010) Fragile X mental retardation protein control of neuronal mRNA metabolism: Insights into mRNA stability. Molecular and Cellular Neuroscience 43:43-50.

de Vrij FM, Levenga J, van der Linde HC, Koekkoek SK, de Zeeuw CI, Nelson DL, Oostra BA, Willemsen R (2008) Rescue of behavioral phenotype and neuronal protrusion morphology in Fmr1 KO mice. NeurobiolDis 31:127-132.

Deacon R (2006) Digging and marble burying in mice: simple methods for in vivo identification of biological impacts. NATURE PROTOCOLS-ELECTRONIC EDITION- 1:122.

Deacon RM, Rawlins JN (2005) Hippocampal lesions, species-typical behaviours and anxiety in mice. Behavioural brain research 156:241-249.

Derek E. Eberhart HEM, Yue Feng and Stephen T. Warren (1996) The fragile X mental retardation protein is a ribonucleoprotein containing both nuclear localization and nuclear export signals. Human Molecular Genetics 5.

Devys D, Lutz Y, Rouyer N, Bellocq J-P, Mandel J-L (1993) The FMR–1 protein is cytoplasmic, most abundant in neurons and appears normal in carriers of a fragile X premutation. Nature genetics 4:335-340.

Dictenberg JB, Swanger SA, Antar LN, Singer RH, Bassell GJ (2008) A direct role for FMRP in activity-dependent dendritic mRNA transport links filopodial-spine morphogenesis to fragile X syndrome. Developmental cell 14:926-939.

Dobkin C, Rabe A, Dumas R, El Idrissi A, Haubenstock H, Brown WT (2000) Fmr1 knockout mouse has a distinctive strain-specific learning impairment. Neuroscience 100:423-429.

Doetsch F, Hen R (2005) Young and excitable: the function of new neurons in the adult mammalian brain. Current opinion in neurobiology 15:121-128.

Eadie B, Zhang W, Boehme F, Gil-Mohapel J, Kainer L, Simpson J, Christie B (2009) Fmr1 knockout mice show reduced anxiety and alterations in neurogenesis that are specific to the ventral dentate gyrus. Neurobiology of disease 36:361-373.

Eberhart DE, Malter HE, Feng Y, Warren ST (1996) The fragile X mental retardation protein is a ribonucleoprotein containing both nuclear localization and nuclear export signals. Human molecular genetics 5:1083-1091.

El-Husseini AE-D, Schnell E, Chetkovich DM, Nicoll RA, Bredt DS (2000) PSD-95 involvement in maturation of excitatory synapses. Science 290:1364-1368.

Feng G, Mellor RH, Bernstein M, Keller-Peck C, Nguyen QT, Wallace M, Nerbonne JM, Lichtman JW, Sanes JR (2000) Imaging neuronal subsets in transgenic mice expressing multiple spectral variants of GFP. Neuron 28:41-51.

Feng Y, Gutekunst CA, Eberhart DE, Yi H, Warren ST, Hersch SM (1997a) Fragile X mental retardation protein: nucleocytoplasmic shuttling and association with somatodendritic ribosomes. JNeurosci 17:1539-1547.

Feng Y, Absher D, Eberhart DE, Brown V, Malter HE, Warren ST (1997b) FMRP associates with polyribosomes as an mRNP, and the I304N mutation of severe fragile X syndrome abolishes this association. Molecular cell 1:109-118.

Ferrari F, Mercaldo V, Piccoli G, Sala C, Cannata S, Achsel T, Bagni C (2007) The fragile X mental retardation protein-RNP granules show an mGluR-dependent localization in the post-synaptic spines. Molecular and cellular neurosciences 34:343-354.

Fischer M, Kaech S, Knutti D, Matus A (1998) Rapid Actin-Based Plasticity in Dendritic Spines. Neuron 20:847-854.

Frankland P, Wang Y, Rosner B, Shimizu T, Balleine B, Dykens E, Ornitz E, Silva A (2004) Sensorimotor gating abnormalities in young males with fragile X syndrome and Fmr1-knockout mice. Molecular psychiatry 9:417-425.

Fridell RA, Benson R, Hua J, Bogerd H, Cullen B (1996) A nuclear role for the Fragile X mental retardation protein. The EMBO journal 15:5408.

Frotscher M (1985) Mossy fibres form synapses with identified pyramidal basket cells in the CA3 region of the guinea-pig hippocampus: a combined Golgi-electron microscope study. Journal of neurocytology 14:245-259.

Frotscher M, Hamori J, Wenzel J (1977) Transneuronal effects of entorhinal lesions in the early postnatal period on synaptogenesis in the hippocampus of the rat. Experimental brain research 30:549-560.

Fujita Y (1962) Synaptic activation of dentate granule cells and its effect upon pyramidal cells in rabbit. Physiologie de Phippocampe Montpellier: Centre National de la Recherche (CNRS).

Fukazawa Y, Saitoh Y, Ozawa F, Ohta Y, Mizuno K, Inokuchi K (2003) Hippocampal LTP is accompanied by enhanced F-actin content within the dendritic spine that is essential for late LTP maintenance in vivo. Neuron 38:447-460.

Gaiarsa J, Beaudoin M, Ben-Ari Y (1992) Effect of neonatal degranulation on the morphological development of rat CA3 pyramidal neurons: inductive role of mossy fibers on the formation of thorny excrescences. Journal of Comparative Neurology 321:612-625.

Galimberti I, Gogolla N, Alberi S, Santos AF, Muller D, Caroni P (2006) Long-term rearrangements of hippocampal mossy fiber terminal connectivity in the adult regulated by experience. Neuron 50:749-763.

Galvez R, Greenough WT (2005) Sequence of abnormal dendritic spine development in primary somatosensory cortex of a mouse model of the fragile X mental retardation syndrome. AmJMedGenetA 135:155-160.

Garber KB, Visootsak J, Warren ST (2008) Fragile X syndrome. European Journal of Human Genetics 16:666-672.

Garthe A, Kempermann G (2013) An old test for new neurons: refining the Morris water maze to study the functional relevance of adult hippocampal neurogenesis. Frontiers in neuroscience 7:63.

Garthe A, Behr J, Kempermann G (2009) Adult-generated hippocampal neurons allow the flexible use of spatially precise learning strategies. PloS one 4:e5464.

Geiger JR, Jonas P (2000) Dynamic control of presynaptic Ca 2+ inflow by fast-inactivating K+ channels in hippocampal mossy fiber boutons. Neuron 28:927-939.

Gieselmann R, Kwiatkowski DJ, Janmey PA, Witke W (1995) Distinct biochemical characteristics of the two human profilin isoforms. European journal of biochemistry 229:621-628.

Godfraind JM, Reyniers E, De BK, D'Hooge R, De Deyn PP, Bakker CE, Oostra BA, Kooy RF, Willems PJ (1996) Long-term potentiation in the hippocampus of fragile X knockout mice. AmJMedGenet 64:246-251.

Gogolla N, Galimberti I, Deguchi Y, Caroni P (2009) Wnt signaling mediates experience-related regulation of synapse numbers and mossy fiber connectivities in the adult hippocampus. Neuron 62:510-525.

Gold AE, Kesner RP (2005) The role of the CA3 subregion of the dorsal hippocampus in spatial pattern completion in the rat. Hippocampus 15:808-814.

Gonzales RB, DeLeon Galvan CJ, Rangel YM, Claiborne BJ (2001) Distribution of thorny excrescences on CA3 pyramidal neurons in the rat hippocampus. Journal of Comparative Neurology 430:357-368.

Grabs D, Bergmann M, Schuster T, Fox P, Brich M, Gratzl M (1994) Differential Expression of Synaptophysin and Synaptoporin During Pre-and Postnatal Development of the Rat Hippocampal Network. European Journal of Neuroscience 6:1765-1771.

Graves AR, Moore SJ, Bloss EB, Mensh BD, Kath WL, Spruston N (2012) Hippocampal pyramidal neurons comprise two distinct cell types that are countermodulated by metabotropic receptors. Neuron 76:776-789.

Greenough WT, Klintsova AY, Irwin SA, Galvez R, Bates KE, Weiler IJ (2001) Synaptic regulation of protein synthesis and the fragile X protein. Proceedings of the National Academy of Sciences 98:7101-7106.

Grosse G, Tapp R, Wartenberg M, Sauer H, Fox PA, Grosse J, Gratzl M, Bergmann M (1998) Prenatal hippocampal granule cells in primary cell culture form mossy fiber boutons at pyramidal cell dendrites. Journal of neuroscience research 51:602-611.

Grossman AW, Elisseou NM, McKinney BC, Greenough WT (2006) Hippocampal pyramidal cells in adult Fmr1 knockout mice exhibit an immature-appearing profile of dendritic spines. Brain research 1084:158-164.

Grossman AW, Aldridge GM, Lee KJ, Zeman MK, Jun CS, Azam HS, Arii T, Imoto K, Greenough WT, Rhyu IJ (2010) Developmental characteristics of dendritic spines in the dentate gyrus of Fmr1 knockout mice. Brain Res 1355:221-227.

Guo W, Murthy AC, Zhang L, Johnson EB, Schaller EG, Allan AM, Zhao X (2012) Inhibition of GSK3β improves hippocampus-dependent learning and rescues neurogenesis in a mouse model of fragile X syndrome. Human molecular genetics 21:681-691.

Hagerman RJ, Hagerman PJ (2002) Fragile X syndrome: Diagnosis, treatment, and research: Taylor & Francis US.

Hagerman RJ, Leehey M, Heinrichs W, Tassone F, Wilson R, Hills J, Grigsby J, Gage B, Hagerman PJ (2001) Intention tremor, parkinsonism, and generalized brain atrophy in male carriers of fragile X. Neurology 57:127-130.

Haglund L, Swanson LW, Köhler C (1984) The projection of the supramammillary nucleus to the hippocampal formation: an immunohistochemical and anterograde transport study with the lectin PHA-L in the rat. Journal of Comparative Neurology 229:171-185.

Hall A (1998) Rho GTPases and the actin cytoskeleton. Science 279:509-514.

Hamlyn LH (1962) The fine structure of the mossy fibre endings in the hippocampus of the rabbit. Journal of anatomy 96:112.

Handley SL (1991) Evaluation of marble-burying behavior as a model of anxiety. Pharmacology Biochemistry and Behavior 38:63-67.

Harlow EG, Till SM, Russell TA, Wijetunge LS, Kind P, Contractor A (2010) Critical period plasticity is disrupted in the barrel cortex of FMR1 knockout mice. Neuron 65:385-398.

He CX, Portera-Cailliau C (2013) The trouble with spines in fragile X syndrome: density, maturity and plasticity. Neuroscience 251:120-128.

Henze DA, Urban NN, Barrionuevo G (2000) The multifarious hippocampal mossy fiber pathway: a review. Neuroscience 98:407-427.

Henze DA, Wittner L, Buzsáki G (2002) Single granule cells reliably discharge targets in the hippocampal CA3 network in vivo. Nature neuroscience 5:790-795.

Hernandez RN, Feinberg RL, Vaurio R, Passanante NM, Thompson RE, Kaufmann WE (2009) Autism spectrum disorder in fragile X syndrome: a longitudinal evaluation. American journal of medical genetics Part A 149A:1125-1137.

Herreras O, Solis JM, Del Río RM, Lerma J (1987) Characteristics of CA 1 activation through the hippocampal trisynaptic pathway in the unanaesthetized rat. Brain research 413:75-86.

Hinton VJ, Brown WT, Wisniewski K, Rudelli RD (1991) Analysis of neocortex in three males with the fragile X syndrome. AmJMedGenet 41:289-294.

Holahan MR, Rekart JL, Sandoval J, Routtenberg A (2006) Spatial learning induces presynaptic structural remodeling in the hippocampal mossy fiber system of two rat strains. Hippocampus 16:560-570.

Holtmaat A, Svoboda K (2009) Experience-dependent structural synaptic plasticity in the mammalian brain. Nature Reviews Neuroscience 10:647-658.

Honkura N, Matsuzaki M, Noguchi J, Ellis-Davies GC, Kasai H (2008) The subspine organization of actin fibers regulates the structure and plasticity of dendritic spines. Neuron 57:719-729.

Hotulainen P, Llano O, Smirnov S, Tanhuanpää K, Faix J, Rivera C, Lappalainen P (2009) Defining mechanisms of actin polymerization and depolymerization during dendritic spine morphogenesis. The Journal of cell biology 185:323-339.

Huber KM, Kayser MS, Bear MF (2000) Role for rapid dendritic protein synthesis in hippocampal mGluR-dependent long-term depression. Science 288:1254-1256.

Huber KM, Roder JC, Bear MF (2001) Chemical induction of mGluR5-and protein synthesis–dependent long-term depression in hippocampal area CA1. Journal of Neurophysiology 86:321-325.

Huber KM, Gallagher SM, Warren ST, Bear MF (2002) Altered synaptic plasticity in a mouse model of fragile X mental retardation. Proceedings of the National Academy of Sciences 99:7746-7750.

Irwin S, Galvez R, Weiler I, Beckel-Mitchener A, Greenough W, Hagerman R, Hagerman P (2002) Brain structure and functions of FMR1 protein. Fragile X syndrome: Diagnosis treatment, and research:191-205.

Irwin SA, Galvez R, Greenough WT (2000) Dendritic spine structural anomalies in fragile-X mental retardation syndrome. Cerebral cortex 10:1038-1044.

Irwin SA, Patel B, Idupulapati M, Harris JB, Crisostomo RA, Larsen BP, Kooy F, Willems PJ, Cras P, Kozlowski PB (2001a) Abnormal dendritic spine characteristics in the temporal and visual cortices of patients with fragile-X syndrome: a quantitative examination. American journal of medical genetics 98:161-167.

Irwin SA, Patel B, Idupulapati M, Harris JB, Crisostomo RA, Larsen BP, Kooy F, Willems PJ, Cras P, Kozlowski PB, Swain RA, Weiler IJ, Greenough WT (2001b) Abnormal dendritic spine characteristics in the temporal and visual cortices of patients with fragile-X syndrome: a quantitative examination. AmJMedGenet 98:161-167.

Ivanco TL, Greenough WT (2002) Altered mossy fiber distributions in adult Fmr1 (FVB) knockout mice. Hippocampus 12:47-54.

Jan Y-N, Jan LY (2010) Branching out: mechanisms of dendritic arborization. Nature Reviews Neuroscience 11:316-328.

Kasai H, Matsuzaki M, Noguchi J, Yasumatsu N, Nakahara H (2003) Structure–stability–function relationships of dendritic spines. Trends in neurosciences 26:360-368.

Kesner RP (2013) A process analysis of the CA3 subregion of the hippocampus. frontiers in cellular neuroscience.

Kesner RP, Gilbert PE, Wallenstein GV (2000) Testing neural network models of memory with behavioral experiments. Current opinion in neurobiology 10:260-265.

Kessels HW, Malinow R (2009) Synaptic AMPA receptor plasticity and behavior. Neuron 61:340-350.

Khandjian EW, Corbin F, Woerly S, Rousseau F (1996) The fragile X mental retardation protein is associated with ribosomes. Nature genetics 12:91.

Kleppisch T, Voigt V, Allmann R, Offermanns S (2001) Gαq-deficient mice lack metabotropic glutamate receptor-dependent long-term depression but show normal long-term potentiation in the hippocampal CA1 region. The Journal of Neuroscience 21:4943-4948.

Kohara K, Pignatelli M, Rivest AJ, Jung H-Y, Kitamura T, Suh J, Frank D, Kajikawa K, Mise N, Obata Y (2014) Cell type-specific genetic and optogenetic tools reveal hippocampal CA2 circuits. Nature neuroscience 17:269-279.

Kooy RF, D'Hooge R, Reyniers E, Bakker CE, Nagels G, De BK, Storm K, Clincke G, De Deyn PP, Oostra BA, Willems PJ (1996) Transgenic mouse model for the fragile X syndrome. AmJMedGenet 64:241-245.

Kopec CD, Li B, Wei W, Boehm J, Malinow R (2006) Glutamate receptor exocytosis and spine enlargement during chemically induced long-term potentiation. The Journal of neuroscience 26:2000-2009.

Lawrence JJ, McBain CJ (2003) Interneuron diversity series: containing the detonation–feedforward inhibition in the CA3 hippocampus. Trends in neurosciences 26:631-640.

Lazarov O, Demars MP, Da Tommy Zhao K, Ali HM, Grauzas V, Kney A, Larson J (2012) Impaired survival of neural progenitor cells in dentate gyrus of adult mice lacking FMRP. Hippocampus 22:1220-1224.

Lee KJ, Queenan BN, Rozeboom AM, Bellmore R, Lim ST, Vicini S, Pak DT (2013) Mossy fiber-CA3 synapses mediate homeostatic plasticity in mature hippocampal neurons. Neuron 77:99-114.

Leutgeb JK, Leutgeb S, Moser M-B, Moser EI (2007) Pattern separation in the dentate gyrus and CA3 of the hippocampus. science 315:961-966.

Leutgeb S, Leutgeb JK, Treves A, Moser M-B, Moser EI (2004) Distinct ensemble codes in hippocampal areas CA3 and CA1. Science 305:1295-1298.

Levenga J, de Vrij FM, Buijsen RA, Li T, Nieuwenhuizen IM, Pop A, Oostra BA, Willemsen R (2011) Subregion-specific dendritic spine abnormalities in the hippocampus of Fmr1 KO mice. NeurobiolLearnMem.

Li XG, Somogyi P, Ylinen A, Buzsaki G (1994) The hippocampal CA3 network: an in vivo intracellular labeling study. Journal of comparative neurology 339:181-208.

Lisman JE (1999) Relating hippocampal circuitry to function: recall of memory sequences by reciprocal dentate–CA3 interactions. Neuron 22:233-242.

Lisman JE, Talamini LM, Raffone A (2005) Recall of memory sequences by interaction of the dentate and CA3: a revised model of the phase precession. Neural Networks 18:1191-1201.

Liu Q, Siomi H, Siomi M, Fischer U, Zhang Y, Wan L, Dreyfuss G (1996) Molecular characterization of the protein products of the fragile X syndrome gene and the survival of motor neurons

gene. In: Cold Spring Harbor symposia on quantitative biology, pp 689-697: Cold Spring Harbor Laboratory Press.

Logue SF, Paylor R, Wehner JM (1997) Hippocampal lesions cause learning deficits in inbred mice in the Morris water maze and conditioned-fear task. Behavioral neuroscience 111:104.

Lorente de Nó R (1934) Studies on the structure of the cerebral cortex. II. Continuation of the study of the ammonic system. Journal für Psychologie und Neurologie.

Maes B, Fryns JP, Van Walleghem M, Van den Berghe H (1994) Cognitive functioning and information processing of adult mentally retarded men with fragile-X syndrome. American journal of medical genetics 50:190-200.

Maglóczky Z, Acsády L, Freund TF (1994) Principal cells are the postsynaptic targets of supramammillary afferents in the hippocampus of the rat. Hippocampus 4:322-334.

Martin JP, Bell J (1943) A pedigree of mental defect showing sex-linkage. Journal of neurology and psychiatry 6:154-157.

Matsuzaki M, Honkura N, Ellis-Davies GC, Kasai H (2004) Structural basis of long-term potentiation in single dendritic spines. Nature 429:761-766.

Matsuzaki M, Ellis-Davies GC, Nemoto T, Miyashita Y, Iino M, Kasai H (2001) Dendritic spine geometry is critical for AMPA receptor expression in hippocampal CA1 pyramidal neurons. Nature neuroscience 4:1086-1092.

Matus A (2000) Actin-based plasticity in dendritic spines. Science 290:754-758.

McKinney BC, Grossman AW, Elisseou NM, Greenough WT (2005) Dendritic spine abnormalities in the occipital cortex of C57BL/6 Fmr1 knockout mice. AmJMedGenetB NeuropsychiatrGenet 136B:98-102.

Melinda B. Kemper RJH, and Debra Altshul-Stark (1988) Cognitive Profiles of Boys With the Fragile X Syndrome. American Journal of medical genetics.

Meredith RM, Holmgren CD, Weidum M, Burnashev N, Mansvelder HD (2007) Increased threshold for spike-timing-dependent plasticity is caused by unreliable calcium signaling in mice lacking fragile X gene FMR1. Neuron 54:627-638.

Merenstein SA, Sobesky WE, Taylor AK, Riddle JE, Tran HX, Hagerman RJ (1996) Molecular-clinical correlations in males with an expanded FMR1 mutation. American journal of medical genetics 64:388-394.

Michaelsen-Preusse K, Kellner Y, Korte M, Zagrebelsky M (2014) Analysis of Actin Turnover and Spine Dynamics in Hippocampal Slice Cultures. Laser Scanning Microscopy and Quantitative Image Analysis of Neuronal Tissue:189-217.

Michaelsen-Preusse K, Zessin S, Grigoryan G, Scharkowski F, Feuge J, Remus A, Korte M (2016a) Neuronal profilins in health and disease: Relevance for spine plasticity and Fragile X syndrome. Proceedings of the National Academy of Sciences of the United States of America 113:3365-3370.

Michaelsen K, Murk K, Zagrebelsky M, Dreznjak A, Jockusch BM, Rothkegel M, Korte M (2010a) Fine-tuning of neuronal architecture requires two profilin isoforms. Proceedings of the National Academy of Sciences 107:15780-15785.

Michaelsen K, Zagrebelsky M, Berndt-Huch J, Polack M, Buschler A, Sendtner M, Korte M (2010b) Neurotrophin receptors TrkB. T1 and p75NTR cooperate in modulating both functional and structural plasticity in mature hippocampal neurons. European Journal of Neuroscience 32:1854-1865.

Mineur YS, Sluyter F, de WS, Oostra BA, Crusio WE (2002) Behavioral and neuroanatomical characterization of the Fmr1 knockout mouse. Hippocampus 12:39-46.

Ming G-l, Song H (2005) Adult neurogenesis in the mammalian central nervous system. Annu Rev Neurosci 28:223-250.

Mori M, Abegg MH, Gähwiler BH, Gerber U (2004) A frequency-dependent switch from inhibition to excitation in a hippocampal unitary circuit. Nature 431:453-456.

Morris R (1984) Developments of a water-maze procedure for studying spatial learning in the rat. Journal of neuroscience methods 11:47-60.

Morris RG (1981) Spatial localization does not require the presence of local cues. Learning and motivation 12:239-260.

Nicoll RA, Schmitz D (2005) Synaptic plasticity at hippocampal mossy fibre synapses. Nature reviews Neuroscience 6:863-876.

Nimchinsky EA, Oberlander AM, Svoboda K (2001) Abnormal Development of Dendritic Spines inFMR1 Knock-Out Mice. The Journal of Neuroscience 21:5139-5146.

O'keefe J, Nadel L (1978) The hippocampus as a cognitive map: Oxford University Press, USA.

Oddi D, Subashi E, Middei S, Bellocchio L, Lemaire-Mayo V, Guzman M, Crusio WE, D'Amato FR, Pietropaolo S (2015) Early social enrichment rescues adult behavioral and brain abnormalities in a mouse model of fragile X syndrome. Neuropsychopharmacology : official publication of the American College of Neuropsychopharmacology 40:1113-1122.

Owen E, Logue S, Rasmussen D, Wehner J (1997) Assessment of learning by the Morris water task and fear conditioning in inbred mouse strains and F 1 hybrids: implications of genetic background for single gene mutations and quantitative trait loci analyses. Neuroscience 80:1087-1099.

Padmashri R, Reiner BC, Suresh A, Spartz E, Dunaevsky A (2013) Altered structural and functional synaptic plasticity with motor skill learning in a mouse model of fragile X syndrome. The Journal of neuroscience : the official journal of the Society for Neuroscience 33:19715-19723.

Pan F, Aldridge GM, Greenough WT, Gan WB (2010) Dendritic spine instability and insensitivity to modulation by sensory experience in a mouse model of fragile X syndrome. ProcNatlAcadSciUSA 107:17768-17773.

Paradee W, Melikian H, Rasmussen D, Kenneson A, Conn P, Warren S (1999) Fragile X mouse: strain effects of knockout phenotype and evidence suggesting deficient amygdala function. Neuroscience 94:185-192.

Park M, Penick EC, Edwards JG, Kauer JA, Ehlers MD (2004) Recycling endosomes supply AMPA receptors for LTP. Science 305:1972-1975.

Park M, Salgado JM, Ostroff L, Helton TD, Robinson CG, Harris KM, Ehlers MD (2006) Plasticity-induced growth of dendritic spines by exocytic trafficking from recycling endosomes. Neuron 52:817-830.

Park S, Park JM, Kim S, Kim JA, Shepherd JD, Smith-Hicks CL, Chowdhury S, Kaufmann W, Kuhl D, Ryazanov AG, Huganir RL, Linden DJ, Worley PF (2008) Elongation factor 2 and fragile X mental retardation protein control the dynamic translation of Arc/Arg3.1 essential for mGluR-LTD. Neuron 59:70-83.

Pasciuto E, Bagni C (2014) SnapShot: FMRP mRNA targets and diseases. Cell 158:1446-1446. e1441.

Perelroizen I, Didry D, Christensen H, Chua N-H, Carlier M-F (1996) Role of nucleotide exchange and hydrolysis in the function of profilin in actin assembly. Journal of Biological Chemistry 271:12302-12309.

Perrot-Sinal TS, Kostenuik MA, Ossenkopp K-P, Kavaliers M (1996) Sex differences in performance in the Morris water maze and the effects of initial nonstationary hidden platform training. Behavioral neuroscience 110:1309.

Pfeiffer BE, Huber KM (2007) Fragile X mental retardation protein induces synapse loss through acute postsynaptic translational regulation. JNeurosci 27:3120-3130.

Pietropaolo S, Guilleminot A, Martin B, D'Amato FR, Crusio WE (2011) Genetic-background modulation of core and variable autistic-like symptoms in Fmr1 knock-out mice. PloS one 6:e17073.

Pleskacheva MG, Wolfer DP, Kupriyanova IF, Nikolenko DL, Scheffrahn H, Dell'Omo G, Lipp HP (2000) Hippocampal mossy fibers and swimming navigation learning in two vole species occupying different habitats. Hippocampus 10:17-30.

Poling A, Cleary J, Monaghan M (1981) Burying by rats in response to aversive and nonaversive stimuli. Journal of the experimental analysis of behavior 35:31-44.

Portera-Cailliau C (2012) Which comes first in fragile X syndrome, dendritic spine dysgenesis or defects in circuit plasticity? The Neuroscientist : a review journal bringing neurobiology, neurology and psychiatry 18:28-44.

Portera-Cailliau C, Pan DT, Yuste R (2003) Activity-regulated dynamic behavior of early dendritic protrusions: evidence for different types of dendritic filopodia. JNeurosci 23:7129-7142.

Qin M, Xia Z, Huang T, Smith CB (2011) Effects of chronic immobilization stress on anxiety-like behavior and basolateral amygdala morphology in Fmr1 knockout mice. Neuroscience 194:282-290.

Ramírez-Amaya V, Balderas I, Sandoval J, Escobar ML, Bermúdez-Rattoni F (2001) Spatial long-term memory is related to mossy fiber synaptogenesis. The Journal of Neuroscience 21:7340-7348.

Rekart JL, Sandoval CJ, Bermudez-Rattoni F, Routtenberg A (2007) Remodeling of hippocampal mossy fibers is selectively induced seven days after the acquisition of a spatial but not a cued reference memory task. Learning & Memory 14:416-421.

Remondes M, Schuman EM (2004) Role for a cortical input to hippocampal area CA1 in the consolidation of a long-term memory. Nature 431:699-703.

Represa A, Dessi F, Beaudoin M, Ben-Ari Y (1991) Effects of neonatal γ-ray irradiation on rat hippocampus—I. Postnatal maturation of hippocampal cells. Neuroscience 42:137-150.

Roberts TF, Tschida KA, Klein ME, Mooney R (2010) Rapid spine stabilization and synaptic enhancement at the onset of behavioural learning. Nature 463:948-952.

Ruan YW, Lei Z, Fan Y, Zou B, Xu ZC (2009) Diversity and fluctuation of spine morphology in CA1 pyramidal neurons after transient global ischemia. Journal of neuroscience research 87:61-68.

Rudelli RD, Brown WT, Wisniewski K, Jenkins EC, Laure-Kamionowska M, Connell F, Wisniewski HM (1985) Adult fragile X syndrome. Clinico-neuropathologic findings. Acta Neuropathol 67:289-295.

Ruediger S, Vittori C, Bednarek E, Genoud C, Strata P, Sacchetti B, Caroni P (2011) Learning-related feedforward inhibitory connectivity growth required for memory precision. Nature 473:514-518.

Sajikumar S, Frey JU (2003) Anisomycin inhibits the late maintenance of long-term depression in rat hippocampal slices in vitro. Neuroscience letters 338:147-150.

Schöpke R, Wolfer D, Lipp HP, Leisinger-Trigona MC (1991) Swimming navigation and structural variations of the infrapyramidal mossy fibers in the hippocampus of the mouse. Hippocampus 1:315-328.

Scotto-Lomassese S, Nissant A, Mota T, Néant-Féry M, Oostra BA, Greer CA, Lledo P-M, Trembleau A, Caillé I (2011) Fragile X mental retardation protein regulates new neuron differentiation in the adult olfactory bulb. The Journal of Neuroscience 31:2205-2215.

Scoville WB, Milner B (1957) Loss of recent memory after bilateral hippocampal lesions. Journal of Neurology, Neurosurgery & Psychiatry 20:11-21.

Segal M, Kreher U, Greenberger V, Braun K (2003) Is fragile X mental retardation protein involved in activity-induced plasticity of dendritic spines? Brain Res 972:9-15.

Shaner NC, Lin MZ, McKeown MR, Steinbach PA, Hazelwood KL, Davidson MW, Tsien RY (2008) Improving the photostability of bright monomeric orange and red fluorescent proteins. Nature methods 5:545-551.

Shinohara Y, Hosoya A, Yahagi K, Ferecskó AS, Yaguchi K, Sík A, Itakura M, Takahashi M, Hirase H (2012) Hippocampal CA3 and CA2 have distinct bilateral innervation patterns to CA1 in rodents. European Journal of Neuroscience 35:702-710.

Siegel M, Gonzales R, Carnevale N, Claiborne B, Brown T (1992) Biophysical model of hippocampal mossy fiber synapses. In: Soc. Neurosci. Abstr., p 1344.

Siomi H, Siomi MC, Nussbaum RL, Dreyfuss G (1993) The protein product of the fragile X gene, FMR1, has characteristics of an RNA-binding protein. Cell 74:291-298.

Siomi H, Choi M, Siomi MC, Nussbaum RL, Dreyfuss G (1994) Essential role for KH domains in RNA binding: impaired RNA binding by a mutation in the KH domain of FMR1 that causes fragile X syndrome. Cell 77:33-39.

Siomi MC, Zhang Y, Siomi H, Dreyfuss G (1996) Specific sequences in the fragile X syndrome protein FMR1 and the FXR proteins mediate their binding to 60S ribosomal subunits and the interactions among them. Molecular and cellular biology 16:3825-3832.

Snyder EM, Philpot BD, Huber KM, Dong X, Fallon JR, Bear MF (2001) Internalization of ionotropic glutamate receptors in response to mGluR activation. Nature neuroscience 4:1079-1085.

Spencer CM, Alekseyenko O, Hamilton SM, Thomas AM, Serysheva E, Yuva-Paylor LA, Paylor R (2011) Modifying behavioral phenotypes in Fmr1KO mice: genetic background differences reveal autistic-like responses. Autism research 4:40-56.

Squire LR (1992) Memory and the hippocampus: a synthesis from findings with rats, monkeys, and humans. Psychological review 99:195.

Star EN, Kwiatkowski DJ, Murthy VN (2002) Rapid turnover of actin in dendritic spines and its regulation by activity. Nature neuroscience 5:239-246.

Stoppini L, Buchs P-A, Muller D (1991) A simple method for organotypic cultures of nervous tissue. Journal of neuroscience methods 37:173-182.

Strehl A, Lenz M, Itsekson-Hayosh Z, Becker D, Chapman J, Deller T, Maggio N, Vlachos A (2014) Systemic inflammation is associated with a reduction in Synaptopodin expression in the mouse hippocampus. Experimental neurology 261:230-235.

Su T, Fan H-X, Jiang T, Sun W-W, Den W-Y, Gao M-M, Chen S-Q, Zhao Q-H, Yi Y-H (2011) Early continuous inhibition of group 1 mGlu signaling partially rescues dendritic spine abnormalities in the Fmr1 knockout mouse model for fragile X syndrome. Psychopharmacology 215:291-300.

Swanger SA, Yao X, Gross C, Bassell GJ (2011) Automated 4D analysis of dendritic spine morphology: applications to stimulus-induced spine remodeling and pharmacological rescue in a disease model. MolBrain 4:38.

Tamanini F, Meijer N, Verheij C, Willems PJ, Galjaard H, Oostra BA, Hoogeveen AT (1996) FMRP is associated to the ribosomes via RNA. Human molecular genetics 5:809-813.

The-Dutch-Belgian-Fragile-X-Consortium (1994) Fmr1 Knockout Mice: A Model to Study Fragile X Mental Retardation. Cell 78:23-33.

Thomas AM, Bui N, Graham D, Perkins JR, Yuva-Paylor LA, Paylor R (2011) Genetic reduction of group 1 metabotropic glutamate receptors alters select behaviors in a mouse model for fragile X syndrome. Behavioural brain research 223:310-321.

Tonnesen J, Katona G, Rózsa J, Nagerl U (2014) Spine neck plasticity regulates compartmentalization of synapses. Nature neuroscience 17:678-685.

Travaglia A, Bisaz R, Sweet ES, Blitzer RD, Alberini CM (2016) Infantile amnesia reflects a developmental critical period for hippocampal learning. Nature Neuroscience.

Tsiouris JA, Brown WT (2004) Neuropsychiatric symptoms of fragile X syndrome. CNS drugs 18:687-703.

Turrigiano GG (2008) The self-tuning neuron: synaptic scaling of excitatory synapses. Cell 135:422-435.

Tyler WJ, Pozzo-Miller LD (2001) BDNF enhances quantal neurotransmitter release and increases the number of docked vesicles at the active zones of hippocampal excitatory synapses. The Journal of Neuroscience 21:4249-4258.

Urban NN, Henze DA, Barrionuevo G (2001) Revisiting the role of the hippocampal mossy fiber synapse. Hippocampus 11:408-417.

Van Dam D, D'Hooge R, Hauben E, Reyniers E, Gantois I, Bakker CE, Oostra BA, Kooy RF, De Deyn PP (2000) Spatial learning, contextual fear conditioning and conditioned emotional response in Fmr1 knockout mice. Behavioural brain research 117:127-136.

Verhelj C, de Graaff E, Bakker CE, Willemsen R, Willems PJ, Meijer N, Galjaard H, Reuser AJ, Oostra BA, Hoogeveen AT (1995) Characterization of FMR1 proteins isolated from different tissues. Human molecular genetics 4:895-901.

Verkerk AJMH et al. (1991) Identification of a Gene (FMR-1) Containing a CGG Repeat Coincident with a Breakpoint Cluster Region Exhibiting Length Variation in Fragile X Syndrome. Cell 65:905-914.

Volk LJ, Pfeiffer BE, Gibson JR, Huber KM (2007) Multiple Gq-coupled receptors converge on a common protein synthesis-dependent long-term depression that is affected in fragile X syndrome mental retardation. The Journal of Neuroscience 27:11624-11634.

Webster DG, Williams MH, Owens RD, Geiger VB, Dewsbury DA (1981) Digging behavior in 12 taxa of muroid rodents. Animal Learning & Behavior 9:173-177.

Wegiel J, Flory M, Kuchna I, Nowicki K, Ma SY, Imaki H, Wegiel J, Frackowiak J, Kolecka BM, Wierzba-Bobrowicz T, London E, Wisniewski T, Hof PR, Brown WT (2015) Neuronal nucleus and cytoplasm volume deficit in children with autism and volume increase in adolescents and adults. Acta neuropathologica communications 3:2.

Wilke SA, Antonios JK, Bushong EA, Badkoobehi A, Malek E, Hwang M, Terada M, Ellisman MH, Ghosh A (2013) Deconstructing complexity: serial block-face electron microscopic analysis of the hippocampal mossy fiber synapse. The Journal of neuroscience : the official journal of the Society for Neuroscience 33:507-522.

Willemsen R, Bontekoe C, Tamanini F, Galjaard H, Hoogeveen A, Oostra B (1996) Association of FMRP with ribosomal precursor particles in the nucleolus. Biochemical and biophysical research communications 225:27-33.

Wisniewski K, French J, Fernando S, Brown W, Jenkins E, Friedman E, Hill A, Miezejeski C (1985) Fragile X syndrome: associated neurological abnormalities and developmental disabilities. Annals of neurology 18:665-669.

Wisniewski KE, Segan SM, Miezejeski CM, Sersen EA, Rudelli RD (1991) The Fra(X) syndrome: neurological, electrophysiological, and neuropathological abnormalities. AmJMedGenet 38:476-480.

Witke W (2004) The role of profilin complexes in cell motility and other cellular processes. Trends in cell biology 14:461-469.

Yoshihara Y, Mizuno T, Nakahira M, Kawasaki M, Watanabe Y, Kagamiyama H, Jishage K-i, Ueda O, Suzuki H, Tabuchi K (1999) A genetic approach to visualization of multisynaptic neural pathways using plant lectin transgene. Neuron 22:33-41.

Yun SH, Trommer BL (2011) Fragile X mice: Reduced long-term potentiation and N-Methyl-D-Aspartate receptor-mediated neurotransmission in dentate gyrus. Journal of neuroscience research 89:176-182.

Yuste R (2010) Dendritic spines: MIT Press.

Yuste R, Bonhoeffer T (2001) Morphological changes in dendritic spines associated with long-term synaptic plasticity. Annual review of neuroscience 24:1071-1089.

Zagrebelsky M, Holz A, Dechant G, Barde Y-A, Bonhoeffer T, Korte M (2005) The p75 neurotrophin receptor negatively modulates dendrite complexity and spine density in hippocampal neurons. The Journal of neuroscience 25:9989-9999.

Zagrebelsky M, Lonnemann N, Fricke S, Kellner Y, Preuß E, Michaelsen-Preusse K, Korte M (2016) Nogo-A regulates spatial learning as well as memory formation and modulates structural plasticity in the adult mouse hippocampus. Neurobiology of Learning and Memory.

Zalfa F, Giorgi M, Primerano B, Moro A, Di Penta A, Reis S, Oostra B, Bagni C (2003) The fragile X syndrome protein FMRP associates with BC1 RNA and regulates the translation of specific mRNAs at synapses. Cell 112:317-327.

Zalfa F, Eleuteri B, Dickson KS, Mercaldo V, De Rubeis S, di Penta A, Tabolacci E, Chiurazzi P, Neri G, Grant SG, Bagni C (2007) A new function for the fragile X mental retardation protein in regulation of PSD-95 mRNA stability. Nature neuroscience 10:578-587.

Zang JB, Nosyreva ED, Spencer CM, Volk LJ, Musunuru K, Zhong R, Stone EF, Yuva-Paylor LA, Huber KM, Paylor R (2009) A mouse model of the human Fragile X syndrome I304N mutation. PLoS genetics 5:e1000758.

Zhang J, Hou L, Klann E, Nelson DL (2009) Altered hippocampal synaptic plasticity in the FMR1 gene family knockout mouse models. Journal of neurophysiology 101:2572-2580.

Zhang Y, Brown MR, Hyland C, Chen Y, Kronengold J, Fleming MR, Kohn AB, Moroz LL, Kaczmarek LK (2012) Regulation of neuronal excitability by interaction of fragile X mental retardation protein with slack potassium channels. The Journal of neuroscience : the official journal of the Society for Neuroscience 32:15318-15327.

Zhao S, Studer D, Chai X, Graber W, Brose N, Nestel S, Young C, Rodriguez EP, Saetzler K, Frotscher M (2012) Structural plasticity of hippocampal mossy fiber synapses as revealed by high-pressure freezing. The Journal of comparative neurology 520:2340-2351.

Zito K, Knott G, Shepherd GM, Shenolikar S, Svoboda K (2004) Induction of spine growth and synapse formation by regulation of the spine actin cytoskeleton. Neuron 44:321-334.

6. List of Abbreviations

AMPA	α-amino-3-hydroxy-5-methyl-4-isoxazolepropionic acid
ARC	activity regulated cytoskeletal-associated protein
ASD	autism spectrum disorder
CA	*cornu ammonis*
CFL1	cofilin1
DG	dentate gyrus
DIV	days of *in vitro*
DNA	deoxyribonucleic acid
ERK	extracellular signal-related kinase
eGFP	enhanced green fluorescent protein
fEPSC	field excitatory postsynaptic current
FMRP	fragile X mental retardation protein
FRAP	fluorescence recovery after photobleaching
FXG	fragile X granules
FXS	fragile X syndrome
GluR1	glutamate receptor subunit 1
KO	knockout
KH	K homology
LMT	large mossy fiber terminal
LTD	long-term depression
LTP	long-term potentiation
mEPSC	miniature excitatory postsynaptic current
mGluR	metabotropic glutamate receptor
mRNA	messenger ribonucleic acid
mRNP	messenger ribonucleoprotein particles

NMDA	N-methyl-D-aspartate
OHC	organotpyic hippocampal cultures
P	postnatal day
PCR	polymerase chain reaction
PFN1	profilin1
PFN2a	profilin2a
PSD	postsynaptic density
RIP	RNA immunoprecipitation
RNA	ribonucleic acid
RT	room temperature
SEP	super ecliptic pHluorin
SUM	supramammillary nucleus
SynPo	synaptoporin
SynPoD	synaptopodin
TE	thorny excrescence
WT	wild type

7. Danksagung

Ich möchte mich an dieser Stelle bei allen Menschen bedanken, ohne die diese Arbeit nicht möglich und die Zeit deutlich weniger schön gewesen wäre.

Zuerst möchte ich mich bei meinem Doktorvater Prof. Dr. Martin Korte bedanken. Martin hat mich immer gefordert und gefördert, wobei ich mich immer auf seine Unterstützung verlassen konnte. Außerdem hat er mir in seiner Arbeitsgruppe alle Ressourcen zur Verfügung gestellt, um das spannende Thema meiner Doktorarbeit von diversen methodischen Aspekten anzugehen.

Prof. Dr. Reinhard Köster möchte ich für die Übernahme des Koreferates danken. Zudem habe ich nicht vergessen, dass er bereits während meines Masterstudiums ein extra Seminar darüber geben hat, wie man sich in der Wissenschaft bewirbt, wofür ich ihm zutiefst dankbar bin.

Des Weiteren danke ich Prof. Dr. Florian Bittner für die Leitung meiner Promotionskommission. Ich habe mich immer gefreut, wenn wir uns im Gang begegnet sind und wir uns unterhalten haben.

Bei Dr. Kristin Michaelsen-Preusse muss ich mich besonders bedanken. Du hattest immer ein offenes Ohr für mich, hast mit mir immer angeregt über meine Arbeit diskutiert und mich im wissenschaftlichen Schreiben, Arbeiten und Leben sehr weit voran gebracht. Ich habe unsere Meetings immer sehr genossen, vor allem auch weil du ein wunderbarer Mensch bist.

Vielen Dank auch an Dr. Marta Zagrebelsky für ihre wissenschaftliche Weitsicht und Diskussionsfreudigkeit. Zudem möchte ich auch Dr. Martin Rothkegel für seine unendliche Expertise in der Biochemie und sein Fürsorglichkeit danken.

Nicht zu vergessen ist Diane Mundil, die beste TA und Kulturpartnerin der Welt. Danke für die tollen Kulturen, die Gespräche und danke, dass du so ein toller Mensch bist.

Des Weiteren möchte ich mich bei allen Doktoranden und mittlerweile Freunden bedanken die mich auf meinem Weg begleitet haben: **Dr. Marianna Beyer, Dr. Stefanie Schweinhuber, Dr. Sabine Zessin,** Dr. Ulrike Herrmann, Dr. Nina Gödecke, Der Lonnemann, Jan Kleveman, Susann Ludewig, Jonas Feuge und Shirin Hosseini. Ihr seid die Besten.

Ohne die besten Eltern der Welt wäre es nicht möglich gewesen. Ihr habt mich immer unterstützt und an mich geglaubt. Ihr seid meine größten Vorbilder. Dazu mein Opa Manfred der viel zu dem Menschen beigetragen hat der ich heute bin. Ich liebe euch.

Und zu allerletzt gilt mein tiefster Dank Steffen, du bist mein Fels in der Brandung. Du machst mein Leben bunter und gibst mir so viel Geborgenheit jeden Tag und bedingungslos. **Du bist fantastisch.**

8. Curriculum Vitae

Franziska Scharkowski

Current Address	Wabestraße 2
	38106 Braunschweig
	Germany
Mobile	+49 (0)176 30325240
E-Mail	f.scharkowski@tu-bs.de

EDUCATION

Since 06/2013	University of Braunschweig Department of cellular neurobiology, research group of Martin Korte PhD thesis ("Spine development & activity-dependent plasticity in the hippocampus of a mouse model of the Fragile X syndrome")
04/2011- 05/2013	Technical University Braunschweig Master of Science in Biology (Thesis: "The role of cortactin in hippocampus-dependent memory formation and synaptic plasticity") Specialization: Cell Biology and Biochemistry with focus on cellular and biochemical neurobiology
10/2008 - 03/2011	Technical University Braunschweig Bachelor of Science in Biology (Thesis: "The biochemical characterization of profiline and formin interactions") Specializations: biochemical neurobiology
08/2002 – 07/2008	Gymnasium Oschersleben, Oschersleben, Germany A-Levels

WORK EXPERIENCE

06/2012-10/2012 Internship at the Netherlands Institute for Neuroscience

(Research group of Dr. Christian Lohmann)

"Morphology & activity of pyramidal CA3 neurons is influenced by its culturing treatments"

- Research in the field of cellular neurobiology
- Participation/preparation of seminars
- Working with Matlab/ImageJ

10/2011 - 12/2011 Internship at the Department of Cellular Neurobiology

(Research group of Prof. Dr. Martin Korte, department cellular neurobiology, Zoological Institute, Technical University of Braunschweig)

- Research in the field of biochemical neurobiology
- Participation and preparation of seminars
- Working with Microsoft office

01/2011 and 09/2011 Student Assistant at the Department of Cellular Neurobiology (Zoological Institute, Technical University of Braunschweig)

- Assisting with preparing and performing an practical term for students
- Support of the students with experiments and analyses

07/2008 – 10/2008 Internship at IPK Gatersleben, Germany

- Internship in the field of seed studies
- technical support for the publication: "Seed conservation in *ex situ* genebanks-genetics studies on longevity in barley" (by Manuela Nagel *et al.*, 2009) and as part of the doctor thesis of Manuela Nagel

COMPETENCIES

Languages German (native)

English (fluent)

French (basic)

Dutch (basic)

Technical Skills	MS Office
	Image J
	Photoshop, Illustrator
	Microscopes (confocal laser scanning microscope; binocular, fluorescence Microscopes, light microscopes)
Social Skills	Ability to work autonomous as well as in a team on challenging and complex tasks during projects for internships and during my theses (description above). Comfortable with taking a leadership role during teamwork and ability to motivate team members.
	Good contribution to teamwork as well as great organizational skills. Additionally to supervising students; I am able to mediate complex relationships and mechanism.
Scholarships	ERASMUS placement
	Mobility scholarship (department of biology, TU Braunschweig)
Additional Qualifications	Participation in the summer school Utrecht 2014 – Neuronal Circuit Development and Plasticity, Utrecht 2014
	Participation in the workshop: Erfolgreich Drittmittel einwerben (Success in grant application), Braunschweig 2014
	Qualification in working with experimental animal models, including core modules (functions A, B, C & D) function specific modules for function A and modules 20 for species mouse. Asked by **FELASA**